Cranial endocast of *Anagale gobiensis* (Anagalidae) and its implications for early brain evolution in Euarchontoglires

Sergi López-Torres[1,2,3,4], Ornella C. Bertrand[5], Madlen M. Lang[6], Łucja Fostowicz-Frelik[7,8], Mary T. Silcox[6], Jin Meng[1,4]

[1]Division of Paleontology, American Museum of Natural History, 10024-5192, New York, NY, United States of America. JM ORCiD: 0000-0002-3385-8383

[2]Richard Gilder Graduate School, American Museum of Natural History, 10024-5192, New York, NY, United States of America.

[3]University of Warsaw, Faculty of Biology, Biological and Chemical Research Centre, Institute of Evolutionary Biology, Warsaw, Poland. SLT ORCiD: 0000-0002-0046-1013

[4]New York Consortium in Evolutionary Primatology, New York, NY, United States of America.

[5]Institut Català de Paleontologia Miquel Crusafont, Universitat Autònoma de Barcelona, Edifici ICTA-ICP, c/ Columnes s/n, Campus de la UAB, 08193 Cerdanyola del Vallès. Barcelona, Spain. OCB ORCiD: 0000-0003-3461-3908

[6]Department of Anthropology, University of Toronto Scarborough, M1C 1A4, Toronto, ON, Canada. MML ORCiD: 0000-0003-2604-4733. MTS ORCiD: 0000-0002-4174-9435

[7]Department of Organismal Biology and Anatomy, The University of Chicago, Chicago, IL, United States of America. ŁFF ORCiD: 0000-0002-1266-1178

[8]Institute of Paleobiology, Polish Academy of Sciences, Warsaw, Poland.

Corresponding author: Sergi López-Torres. Postal address: Żwirki i Wigury 101, Warsaw 02-089, Poland. Telephone: +48-730-980-445. E-mail: s.lopez-torres@uw.edu.pl.

Short running title: Cranial endocast of an anagalid

ABSTRACT

Anagalids are an extinct group of primitive mammals from the Asian Palaeogene thought to be possible basal members of Glires. Anagalid material is rare, with only a handful of crania known. Here we describe the first virtual endocast of an anagalid, based on the holotype of *Anagale gobiensis* (AMNH 26079; late Eocene, China), which allows for comparison with published endocasts from fossil members of modern euarchontogliran lineages (i.e. primates, rodents, lagomorphs). The endocast displays traits often observed in fossorial mammals, such as relatively small petrosal lobules and a low neocortical ratio, which would be consistent with previous inferences about use of subterranean food sources based on heavy dental wear. In fact, *Anagale gobiensis* has the lowest neocortical ratio yet recorded for a euarchontogliran. This species was olfaction-driven, based on the relatively large olfactory bulbs and laterally expansive palaeocortex. The endocast supports previous inferences that relatively large olfactory bulbs, partial midbrain exposure and low encephalisation quotient are ancestral for Euarchontoglires, although the likely fossorial adaptations of *Anagale gobiensis* may also partly explain these traits. While *Anagale gobiensis* is a primitive mammal in many aspects, some of its derived endocranial traits point towards a new, different trajectory of brain evolution within Euarchontoglires.

Keywords: Anagalidae, Eocene, China, endocast, brain evolution

INTRODUCTION

Anagalidae is an enigmatic and poorly studied group of primitive mammals known from the Palaeogene of China and Mongolia (Hu, 1993; Li, 2016; López-Torres & Fostowicz-Frelik, 2018a). Although anagalids were never common in the fossil record, their species diversity drops substantially after the middle Palaeocene (Nongshangian Asian Land Mammal Age [ALMA]), with only *Anagale gobiensis* Simpson, 1931 and *Zofiagale ergilinensis* López-Torres & Fostowicz-Frelik, 2018a being known from the late Eocene (Ulangochuian and Ergilian Asian Land Mammal Ages, respectively; López-Torres & Fostowicz-Frelik, 2018a) and *Anagalopsis kansuensis* Bohlin, 1951, possibly coming from the earliest Oligocene (Bohlin, 1951; but see Zhang & Wang [2016] for an earlier estimate). No anagalids have been reported from the late Palaeocene (Gashatan ALMA) and most of the Eocene (Bumbanian to Sharamurunian ALMAs) (Li *et al*., 2016; López-Torres & Fostowicz-Frelik, 2018a).

There has been considerable debate about which genera should be included in Anagalidae, which relates to the question of the group's broader affinities. On the one hand, workers have used Anagalidae as a convenient taxonomic label for a diversity of forms that seem to share some similarities to Glires without clearly pertaining to one of its modern lineages (Szalay & McKenna, 1971; Wang, 1975; Xu, 1976a, b; Huang & Zheng, 1983). Glires is comprised of the extant orders of Rodentia and Lagomorpha, and both comprehensive morphological (e.g. Li *et al*., 1989; Meng *et al*., 2003; Marivaux *et al*., 2004; Meng, 2004) and molecular (e.g. Murphy *et al*., 2001; Huchon *et al*., 2002; Poux *et al*., 2006) analyses have established the monophyly of this group. In turn, Glires belongs, together with Euarchonta (Dermoptera, Scandentia and Primates; Archonta of Asher and Helgen, 2010), in the higher-level clade Euarchontoglires (Springer *et al*., 2004; O'Leary *et al*., 2013). On the other hand, a more restrictive sense

was used by Hu (1993), who considered just seven of the 15 genera often included in the group to be unquestionable anagalids (McKenna & Bell, 1997; Li, 2016). Here we employ Hu's (1993) more restrictive sense of anagalids.

In terms of their relationships to modern groups, historically anagalids had been suggested to be closely related to Scandentia (Simpson, 1931), to Glires (Bohlin, 1951), and later to Macroscelidea and Lagomorpha (McKenna, 1975). In modern cladistic contexts, a diversity of possible relationships have been recovered. Meng et al. (2003), included both *Anagale* and *Anagalopsis* in their phylogenetic analysis, in which Anagalidae was recovered as sister to Glires. Similarly, Meng (2004) and Fostowicz-Frelik (2017) placed Anagalidae as sister to Glires. In contrast, work by Asher and colleagues (Asher et al., 2003, 2005, 2019; Asher, 2007) have recovered a diversity of possible resolutions to the phylogenetic position of the group, including relationships to Scandentia, a position on the lagomorph stem, a position at the base of Rodentia, as sister group to the order Macroscelidea (elephant shrews), as an early diverging placental lineage, or as unresolved. One factor likely contributing to this diversity of results is the fact that most analyses have sampled only a small subset of the anagalids known (even if the group is restricted to the subset included by Hu, 1993), and are based on character matrices that were not designed to address the question of anagalid relationships specifically. López-Torres and Fostowicz-Frelik (2018b) sampled the entire group (including both Hu's [1993] unquestionable anagalids, and anagalids *sensu lato*) and employed characters that were specifically designed to tease apart anagalid relationships. Their preliminary results placed most anagalid species on the Glires stem (including *Anagale*), except for some species that were nested within Euarchonta. So, while questions still remain about anagalid relationships, the evidence currently available points to relationships with Euarchontoglires. As such, anagalids have the

potential to be informative about primitive states in both Glires and Euarchontoglires. In particular, *Anagale gobiensis* is one of the most basal anagalids according to López-Torres and Fostowicz-Frelik's (2018a) phylogenetic analysis, making it of particular relevance to that perspective, in spite of its fairly late age (late Eocene).

The palaeoecology of anagalids remains largely unknown. *Anagale gobiensis* has significantly worn-down cheek teeth and powerful forelimbs, which led McKenna (1963) to suggest that they may have obtained fairly abrasive food below the surface of the ground. This view is consistent with Bohlin's (1951) suggestion that anagalids were potentially fossorial animals. Also, the high degree of dental wear observed in anagalids is similar to that observed in some extinct fossorial rodents such as *Tsaganomys* and *Cyclomylus* (Bryant & McKenna, 1995; Wang, 2001).

This current paper presents the first endocranial data for any anagalid, deriving from a virtual endocast of *Anagale gobiensis* (AMNH 26079; holotype) from the late Eocene of Nei Mongol, China. In the last decade, numerous descriptions of virtual endocasts of fossil euarchontogliran taxa have been published, in particular those of primates (Silcox *et al*., 2009, 2010a; Kirk *et al*., 2014; Orliac *et al*., 2014; Harrington *et al*., 2016, 2020; Ramdarshan & Orliac, 2016) and rodents (Bertrand & Silcox, 2016; Bertrand *et al*., 2016a, 2017, 2018, 2019), but cranial endocasts have also been generated for lagomorphs (López-Torres *et al*., 2020) and apatemyids (von Koenigswald *et al*., 2009; Silcox *et al*., 2011). These studies have shed light on the early brain evolution of modern mammalian lineages. For example, "plesiadapiform" endocasts provide some data relevant to the earliest phases of primate brain evolution (Silcox *et al*., 2009, 2010a, 2020; Orliac *et al*., 2014; Long *et al*., 2015), *Rhombomylus turpanensis* Zhai, 1978 and "ischyromyids" are relevant to rodent brain evolution (Meng *et al*., 2003; Bertrand & Silcox, 2016; Bertrand *et al*., 2016a, 2017, 2018, 2019)

and *Megalagus turgidus* Cope, 1873 to lagomorph brain evolution (López-Torres *et al*., 2020). These endocasts have also been used to make broader-based inferences about what might have been primitive in the form of the brain for Euarchonta, Glires and Euarchontoglires (Silcox *et al*., 2010a; Bertrand *et al*., 2016a; López-Torres *et al*., 2020). However, groups that branched off nearer to the base of Euarchontoglires have the potential to offer particularly salient insights into these earlier evolutionary stages (Silcox *et al*., 2011). Therefore, the study of the anagalid brain is key for a holistic understanding of the evolution of the brain in Euarchontoglires, and particularly Glires (see Fig. 1).

MATERIALS AND METHODS

Specimen AMNH 26079 includes an almost complete cranium with a portion of the right parietal missing and damaged premaxilla (Fig. 2). The specimen was described by Simpson (1931) as the holotype of the new genus and species *Anagale gobiensis* and it was later re-described by McKenna (1963), together with a fragmentary rostrum (AMNH 26141). The cranium of *Anagale gobiensis* comes from the Ulan Gochu Formation of Twin Oboes, Nei Mongol, China (Simpson, 1931) and is dated to the Ulangochuian Asian Land Mammal Age. Early work considered the Ulangochuian to be early Oligocene (Simpson, 1931; McKenna, 1963; Romer, 1966; Li & Ting, 1983; Tong *et al*., 1995), but later work correlated it to the Chadronian North American Land Mammal Age, reaching a consensus that the Ulangochuian is late Eocene in age (Wang, 1997; Meng & McKenna, 1998; Zhang & Li, 2000; Luterbacher *et al*., 2004; Wang *et al*., 2007, 2019; Zhang & Wang, 2016), between 37.2 and 39.9 Ma (Wang *et al*., 2019).

The cranium of *Anagale gobiensis* (AMNH 26079) was scanned at the X-ray computed tomography scanner at the American Museum of Natural History. The specimen was scanned with an 85.80 mm distance from the source. The energy settings were 155 kv and 135 μA. A total of 1800 projections were generated, with a voxel size of 0.021118 mm. The digital specimen was captured in 2905 slices, each 1371 by 1758 pixels.

The endocranial cavity of *Anagale gobiensis* was manually segmented in Avizo 9.0.1 (Visualization Science Group, 1995-2015) with a WACOM Cintiq 21UX tablet. A new labelfield module was created in the segmentation editor and the inside of the endocranial cavity was isolated using the pen tool for approximately every five slices, with the intervening slices segmented with the interpolating tool. In all cases, interpolation was checked to ensure it accurately followed the endocranial shape with edits made when needed. When bone was missing, a straight line was traced from the two nearest pieces of preserved bone. The cranium is practically undistorted, making the resulting quantitative measurements highly reliable.

The endocast of *Anagale gobiensis* (Fig. 3) is compared to the sample of previously published endocasts pertaining to early members of Euarchontoglires. In particular, the comparative sample includes early Glires, that is, "ischyromyids" (*Paramys*, *Pseudotomus*, *Reithroparamys*, *Rapamys*, and *Ischyromys*; Bertrand & Silcox, 2016; Bertrand *et al*., 2016a, 2019), fossil sciuroids (Bertrand *et al*., 2017, 2018), *Rhombomylus* (Meng *et al*., 2003) and a stem lagomorph (López-Torres *et al*., 2020); Primates, including "plesiadapiforms" (Silcox *et al*., 2009, 2010a; Orliac *et al*., 2014) and early Tertiary fossil euprimates (Kirk *et al*., 2014; Harrington *et al*., 2016, 2020; Ramdarshan and Orliac, 2016); and the most primitive apatemyid known from endocranial data (*Labidolemur kayi*; Silcox *et al*., 2011). A sample of extant rodents

(Bertrand & Silcox, 2016; Bertrand *et al*., 2017, 2018, 2019) and extant lagomorphs (López-Torres *et al*., 2020) were used to provide context to the fossil data in the quantitative analyses. Also, a high-quality 1:1 cast of the endocast of *Anagale gobiensis* was 3D-printed to facilitate examination and to validate our observations on the computer screen.

Surface area, length and volumetric measurements were taken on the endocasts to calculate several ratios using Avizo 9.0.1 (Table 1). The volume of the endocast of *Anagale gobiensis* was obtained by isolating the more complete half of the endocast using the 'volume edit' module and doubling its volume. The volume of the olfactory bulbs was obtained by isolating the two olfactory bulbs, also using volume edit. The petrosal lobules were re-segmented in the transverse plane (XZ dimension) using a distinct labelfield module and the volume measured from the resulting reconstruction. The term petrosal lobule is used here rather than alternatives like "paraflocculus", following Lang et al. (2022). The homology of the cerebellar structures that are housed in the subarcuate fossa can vary between orders, which has implications for their nomenclature and how we understand their functions between taxa. In Glires (Tan et al., 1995; Panezai et al., 2020) and Scandentia (Ni et al., 2018) the lobules are formed by the paraflocculi, which are divided into the ventral and dorsal paraflocculus (Tan et al., 1995). In contrast, the petrosal lobules of primates are formed by only a portion of the paraflocculi (Voogd and Barmack, 2006). While the dorsal and the ventral paraflocculi are functionally linked to the petrosal lobules (Voogd et al., 2012), they sit within the endocranial cavity adjacent to the flocculus and subarcuate fossa (Xiong et al., 2010). As we are using endocasts and not neural tissue, any measurements obtained represent the potential maximum volume of the tissue occupying the subarcuate fossa of the petrosal bone and consequently, the term "petrosal lobule" is more accurate in

describing what can be measured (Lang et al., 2022). To obtain the neocortical surface area, the area above the rhinal fissure was selected, whereas the circular fissure and the confluence of sinuses were excluded. We followed Jerison (2012) and Long *et al*. (2015), who measured only one side of the neocortex (the more complete hemisphere), excluding the superior sagittal sinus, and then doubled the area of the hemisphere. The resulting data on relative neocortical surface area, relative olfactory bulb and petrosal lobule volumes are presented in Table 1. The surface renderings of the endocasts described in this paper are available from MorphoSource (Boyer *et al*., 2014).

We generated a series of bivariate plots as well as boxplots based on the data in Table 1, combined with values collected from the literature (endocranial volume and surface area, olfactory bulb volume, petrosal lobule volume, neocortical surface areas; Gingerich & Gunnell, 2005; Silcox *et al*., 2009, 2010a, 2011; Kirk *et al*., 2014; Orliac *et al*., 2014; Harrington *et al*., 2016, 2020; Ramdarshan & Orliac, 2016; Bertrand *et al*., 2019, 2021; López-Torres *et al*., 2020; see data in Table 1 and in López-Torres et al., 2022, tables S1-S4) using the software PAST (Hammer *et al*., 2001). Because the specimen of *Anagale gobiensis* is the only specimen for which we have data (n = 1), it is impossible to use statistical hypothesis testing. Instead, we follow a descriptive and heuristic approach for our quantitative data.

Body mass estimation

For comparative purposes, we calculated the encephalisation quotient (EQ) using equations from Jerison (1973) and Eisenberg (1981). For the calculation of EQs, it is important to have an accurate estimation of the body mass of the animal in question. López-Torres & Fostowicz-Frelik (2018a) reconstructed a body mass for *Anagale*

gobiensis of 1756 g based on Conroy's (1987) prosimian equation using M_1 area. They argued that even though Conroy's equation uses a prosimian primate sample, this equation has been used to estimate body masses in "plesiadapiforms" in the past literature (e.g. Conroy, 1987; Rose *et al*. 1993; Bloch & Gingerich, 1998; Gingerich & Gunnell, 2005; Fox *et al*., 2015; Silcox *et al*., 2017; Silcox & López-Torres, 2017) and analagids have a similar generalized morphotype to other primitive euarchontoglirans, such as "plesiadapiforms". Our estimates based on cranial length (305.76 g—using Kielan-Jaworowska's [1983] equation; 444.99 g—using Thewissen & Gingerich's [1989] equation; 531.39 g—using Bertrand et al.'s [2016b] equation; 649.31 g—using Millien & Bovy's [2010] equation), are notably much lower than the dental estimate, which highlights the challenge in finding the most appropriate equation for body mass estimation for an extinct animal with no clear modern homologue.

Body masses based on the postcranial elements that actually support the body weight of the animal could be argued to be more directly connected to an animal's mass than equations based on cranial or dental measurements (Hylander, 1985; Grabowski *et al*., 2015; Yapuncich *et al*., 2015). However, the fragmentary nature of the postcranial skeleton of *Anagale gobiensis* limits the number of equations that could be used. From a phylogenetic standpoint, postcranial equations based on samples of rodents (Moncunill-Solé *et al*., 2014) and lagomorphs (Moncunill-Solé *et al*., 2015) should be relevant, because *Anagale gobiensis* has been suggested to be closely related to Glires. From Moncunill-Solé *et al*.'s (2014) rodent equation using the transversal width of the distal end of the femur, *Anagale gobiensis* has an estimated body mass of 1464.68 g. A lagomorph equation using the transversal width of the proximal end of the tibia (Moncunill-Solé *et al*., 2015) gives a similar result, 1311.26 g. Although somewhat lower, a similar value (1122.77 g) is yielded by Tsubamoto's (2014) mammalian

equation using trochlear width of the astragalus. Another comparable estimate (1430.89 g) was calculated from an equation based on tibial midshaft diameter of several mammalian groups ("Insectivora", Primates, Lagomorpha, Rodentia, Carnivora, Proboscidea, and Artiodactyla) from Gingerich (1990). Because the tibia of *Anagale gobiensis* has a very prominent tibial crest (Simpson, 1931), the tibial midshaft diameter was measured immediately distal to the end of the tibial crest, where the cross-section of the bone shaft is more circular. It is worth noting that similar estimates are obtained when using Glires-specific equations (Moncunill-Solé *et al.*, 2015) and more generalized mammalian equations (Gingerich, 1990; Tsubamoto, 2014). Whereas all the mentioned postcranial equations yield body mass estimates over 1 kg, Gingerich (1990) also provides an equation based on tibial length (with a lower r^2) which gives an estimated body mass of 520.24 g, making it similar to the cranial length estimates. However, long bone circumference has been found to be more strongly related to body mass than length (Campione & Evans, 2012), so we consider tibial diameter to likely better reflect how the animal distributes the weight through its limbs rather than the length of the bone (or the length of the cranium); the r^2 values from Gingerich (1990) support this reasoning. Therefore, we have employed the estimates based on tibial midshaft diameter (Gingerich, 1990), proximal tibial width (Moncunill-Solé *et al*., 2015), distal femoral width (Moncunill-Solé *et al*., 2014) and astragalar trochlear width (Tsubamoto, 2014) in our discussion of relative brain size. Bertrand *et al*.'s (2016b) rodent equation based on cheektooth (P4-M3) length actually provides similar values (1311.48 g—left toothrow; 1348.56 g—right toothrow) to the mentioned postcranial equations. However, Bertrand *et al*.'s (2016) cheektooth area equation gives much higher body mass estimates (2235.59 g—left toothrow; 2374.41 g—right toothrow) than the cheektooth length equation. This might be explained by the significantly wider M1

in *Anagale gobiensis* with respect to the other cheek teeth than typically seen in modern rodents, making cheektooth length probably more appropriate for estimating body mass in *Anagale gobiensis*. It is also possible that the molar area increases with wear; a common effect seen in fossil rodents and lagomorphs with high crowned teeth. The teeth of AMNH 26079 are deeply worn, making estimates based on molar area not completely reliable. On these bases, we consider the best estimate for a range of body masses for AMNH 26079 to be 1122.77—1464.68 g. See Table 2 for a detailed list of body mass estimates.

Institutional abbreviations

AMNH—American Museum of Natural History, New York, NY; AMNH F:AM—Frick collection, American Museum of Natural History, New York; UW—University of Wyoming, Laramie, WY.

RESULTS: DESCRIPTION AND COMPARISONS

Olfactory bulbs

Anagale gobiensis has pedunculated olfactory bulbs that are well separated from the frontal lobes by a clearly demarcated circular fissure. The bulbs reach their full length close to the midline (Fig. 3a). The olfactory bulbs account for at least 18.96% of the total endocast length (Table 1). That proportion is greater than in early Oligocene *Ischyromys* and sciuroid rodents (15.16-17.85%; Bertrand & Silcox, 2016; Bertrand *et al*., 2017), within the range of early and middle Eocene *Paramys*, *Pseudotomus*,

Reithroparamys, and *Rapamys* (15.58-22.06%; Bertrand & Silcox, 2016; Bertrand *et al*., 2019), Eocene euprimates (11.7%-19.9%; calculated from data in Harrington *et al*., 2020) and Oligo—Miocene sciuroids (18.62-20.30%; Bertrand *et al*., 2018), and similar to that of Palaeocene—Eocene "plesiadapiforms" (19.39-22.30%; Silcox *et al*., 2009, 2010; Orliac *et al*., 2014). The olfactory bulb length proportion is lower than in the early Eocene rodent *Paramys copei* (22.06%; Bertrand *et al*., 2016a), the early Oligocene lagomorph *Megalagus turgidus* (22.03%; López-Torres *et al*., 2020) and the apatotherian *Labidolemur kayi* (31%; Silcox *et al*., 2011). With respect to the width of the olfactory bulbs, *Anagale gobiensis* has the highest olfactory bulbs-to-cerebrum width ratio (62.47%) compared to fossil rodents, stem lagomorphs, fossil euprimates and "plesiadapiforms", and comparable to those in *Labidolemur* (62.08%; Silcox *et al*., 2011).

The cribriform plate is damaged in AMNH 26079 (see Fig. 4a), so an accurate reconstruction of the ventral aspect of the olfactory bulbs is impossible. However, for the sake of acquiring a better estimate of the olfactory bulb volume, we reconstructed the ventral aspect of the bulbs by placing straight lines between preserved bony landmarks. When olfactory bulb volume is plotted against body mass, *Anagale gobiensis* falls slightly above the fossil rodent morphospace, whereas *Labidolemur* falls much higher than *Anagale gobiensis* (Fig. 5). The olfactory bulbs of *Anagale gobiensis* account for 7.15% of the overall volume of the endocast (Table 1), which should be considered a conservative estimate because they are clearly somewhat truncated ventrally (Fig. 3c, d). This percentage is higher than in any fossil rodent or lagomorph (Fig. 6). Among early Tertiary primates, only *Plesiadapis cookei* Jepsen, 1930 has been reported to have a higher relative olfactory bulb volume (7.8%; Orliac *et al*., 2014) than in *Anagale gobiensis* and that value probably represents an overestimate because the

ventral aspect of the cerebrum is missing from the reconstruction (see Orliac *et al*., 2014: fig. S2). The apatotherian *Labidolemur* also shows a higher ratio (12.18-14.75%; Silcox *et al*., 2011).

The olfactory bulbs in *Anagale gobiensis* are located above the M^1 (Fig. 2), similar to what is observed in *Ischyromys typus* (Bertrand and Silcox, 2016) and *Me. turgidus* (López-Torres *et al*., 2020). In *Cedromus wilsoni* the olfactory bulbs are located above the P4 (Bertrand *et al*., 2017) and in *Paramys* spp. above the M^2 (Bertrand *et al*., 2016a). The location varies amongst primates, with their rostral extent being over the molars in fossil euprimates (Harrington *et al*., 2016, 2020; Ramdarshan & Orliac, 2016), above the M^3 in *Microsyops annectens* and *Plesiadapis tricuspidens*, but above the premolars in *Ignacius graybullianus* (Silcox *et al*., 2009, 2010a; Orliac *et al*., 2014).

Cerebrum and midbrain

The presence of a well demarcated circular fissure, with no coverage of the olfactory peduncles by the cerebrum, is consistent with little expansion of the frontal lobes in *Anagale gobiensis* rostrally. In fact, the rhinal fissure can be traced rostrally and is well separated from the circular fissure, so the anterior edges of the frontal lobes of the neocortex are not even the anteriormost structure of the cerebrum, as they usually are in other fossil euarchontoglirans (Fig. 3a). Uncovered olfactory peduncules also occur in “ischyromyids” (Scott & Osborn, 1890; Bertrand and Silcox, 2016; Bertrand *et al*., 2016a, 2019), the pseudosciurid *Adelomys vaillanti* (Dechaseaux, 1958), the theridomyid *Theridomys bonduelli* (Dechaseaux, 1958) and the stem lagomorph *Me. turgidus* (López-Torres *et al*., 2020). This observation has been made for

"plesiadapiforms" as well (Silcox *et al*., 2009; Orliac *et al*., 2014). Early Eocene euprimates (Kirk *et al*., 2014; Harrington *et al*., 2016, 2020; Ramdarshan & Orliac, 2016), the basal member of Glires *Rh. turpanensis* (Meng *et al*., 2003), the sciurid *C. wilsoni* (Bertrand *et al*., 2017), the aplodontiid *Altasciurus relictus* (= *Prosciurus relictus* in Bertrand *et al*., 2018), the sciurin *Protosciurus* cf. *rachelae* (Bertrand *et al*., 2018) and the apatotherian *L. kayi* (Silcox *et al*., 2011) all have a very short circular fissure, so the cerebrum is closer to the olfactory bulbs (Fig. 7).

The rhinal fissure marks the separation between the palaeocortex and the neocortex and provides information on the degree of development of the latter (Jerison, 2012; Long *et al*., 2015). The orbitotemporal canal has been used as a proxy landmark for the rhinal fissure in some fossil taxa (e.g. Gurche, 1982; Novacek, 1982; Martin, 1990; Silcox *et al*., 2009, 2010a, 2011; Bertrand & Silcox, 2016), based on its relationship to the rhinal fissure in lemurs (Martin, 1990) and at least some rodents (Bertrand *et al*., 2017). When present on the endocast, the orbitotemporal canal is a raised structure that runs along its lateral aspect (see Bertrand et al. [2019: fig. 4C-D]). An orbitotemporal canal is not observable on the endocast of *Anagale gobiensis* (Fig. 8); based on the CT data it does not have an intraosseous path either (i.e., it is not visible in cross-section in Fig. 4b). In *Anagale gobiensis*, the rhinal fissure is visible as a weak sulcus running longitudinally, but positioned quite far dorsally, on both sides of the endocast (Fig. 3a, d; Fig. 9). The position of the rhinal fissure in *Anagale gobiensis* is more dorsal than in any other Palaeogene euarchontogliran for which the braincase is known (Silcox *et al*., 2009, 2010a, 2011; Orliac *et al*., 2014; Bertrand and Silcox, 2016; Bertrand *et al*., 2016a, 2017, 2018, 2019; López-Torres *et al*., 2020), making the neocortex very limited in its extension. The neocortical surface area ratio for *Anagale gobiensis* (10.98%) represents the lowest ever recorded in a fossil euarchontogliran

(Fig. 10), with neocortical surface area ratios in other Palaeogene euarchontoglirans, ranging between 16.25% (in *Paramys delicatus*; Bertrand *et al*., 2019) and 31.71% (*Protosciurus* cf. *rachelae*; Bertrand *et al*., 2018, 2019). Although, these values are very low, other Eocene mammals appear to have similar neocortical ratios such as the taeniodont *Ectoganus copei* (8%) and the tillodont *Trogosus hillsi* (10%; see Bertrand *et al.*, 2022). On the other hand, notably higher values have been calculated for early fossil euprimates (e.g. 44-46% for *Rooneyia viejaensis*; 41-43% for *Microchoerus erinaceus*; Ramdarshan and Orliac, 2016; Harrington *et al*., 2020), making this group of mammals the most neocorticalised among primitive euarchontoglirans (Fig. 7; Jerison, 2012; Long *et al*., 2015).

The development of neocortical sulci is related to absolute brain size, with the brain generally being lissencephalic (i.e., without infoldings) in species with brain masses of less than 5 g (Macrini *et al*., 2007). With an endocast volume of 7798.04 mm^3 and using a brain mass/cranial capacity ratio of 1.05:1 (Jerison, 1973), *Anagale gobiensis* would have had an estimated brain mass of 7.43 g. Therefore, the brain of *Anagale gobiensis* would have been large enough to be expected to exhibit some infoldings. There are three weakly developed sulci that can be observed (Fig. 3a). One is the lateral sulcus (Fig. 9), which runs parallel to the superior sagittal sinus/sulcus, a feature generally also found in other fossil euarchontoglirans whose brains would have weighed more than 5 g (Silcox *et al*., 2010b, 2011; Orliac *et al*., 2014; Bertrand *et al*., 2016, 2019; Harrington *et al*., 2016; López-Torres *et al*., 2020). Another weak sulcus is located caudolateral to the frontal lobes, running obliquely caudolaterally, joining the ventral neocortical edge in the rostral third of the neocortex. This is tentatively identified as a presylvian sulcus. There is also a weak, convexly curved sulcus, lateral to the lateral sulcus. This is tentatively identified as a suprasylvian sulcus. The last two

sulci are identified based on their relative position in the endocast, and we acknowledge that complex sulcal morphology and variation makes it difficult to establish meaningful homologies. Finally, there is no Sylvian sulcus in *Anagale gobiensis*, making it similar in this way to other fossil euarchontoglirans that are not euprimates (Harrington *et al*., 2016). Interestingly, the sulcal pattern observed in *Anagale gobiensis* is similar to that seen in the endocast of the extant macroscelidean *Rhynchocyon* (Benoit et al., 2013, fig. 2e). Whereas this could potentially support phylogenetic proximity between anagalids and macroscelideans, a hypothesis suggested by McKenna (1975) and Asher et al. (2005), as noted above, we the balance of evidence to support a closer relationship to Euarchontoglires. Alternatively, the similarity in sulcal pattern between *Anagale gobiensis* and *Rhynchocyon* might reflect evolutionary convergence if anagalids lived in a similar habitat (i.e. montane and lowland forests and closed-canopy woodlands; Kingdon et al., 2013) or had a similar ecology (i.e. digging for food sources; Kingdon et al., 2013) to macroscelideans.

Because the edge of the neocortex is located fairly far dorsally, the lateral aspect of the endocast is mostly made up of exposed palaeocortex (i.e. piriform cortex, olfactory cortex). The palaeocortex is inflated, expanding laterally beyond the neocortical edge and overhanging ventrally. On the ventral side of the endocast, between the olfactory bulbs and the optic chiasm, there is a pair of olfactory tubercles. They are well-defined and ventrally protruding.

Caudally, the cerebrum does not cover the cerebellum in *Anagale gobiensis* at all (Fig. 3a, Fig. 9). A pair of colliculi is exposed. One hypothesis is that these could be the caudal (= inferior) colliculi, with the rostral (= superior) colliculi covered by the transverse sinuses. Caudal colliculi that are visible on the surface of the endocast are also observed in some specimens of *Ischyromys* (A. E. Wood no. 221 and AMNH

F:AM 144638); *Reithroparamys delicatissimus*; *Reithroparamys sciuroides*; *Rapamys atramontis*; *Ad. vaillanti*; the cylindrodontid *Dolocylindrodon texanus*; *Plesiadapis cookei*; *Pl. tricuspidens*; *Microsyops* cf. *elegans*; one specimen of *Microsyops annectens* (UW 14559); *Ig. graybullianus*; *L. kayi*, and in the extant sengi *Rhynchocyon* (Wood, 1937; Gingerich & Gunnell, 2005; Silcox *et al*., 2009, 2010a, 2011, 2020; Benoit et al., 2013; Orliac *et al*., 2014; Bertrand & Silcox, 2016; Bertrand *et al*., 2019). Alternatively, it is possible that the visible colliculi in *Anagale gobiensis* are the rostral colliculi and the caudal colliculi are not visible. In other primitive euarchontoglirans (e.g. *Me. turgidus*, *Paramys*, *C. wilsoni*, *Altasciurus* aff. *saskatchewaensis*, one specimen of *Microsyops annectens*; Silcox *et al*., 2010; Bertrand *et al*., 2016, 2017, 2018; López-Torres *et al*., 2020) the colliculi are not visible, but a patch of midbrain is apparent between the transverse sinuses and the cerebellum. In *Rh. turpanensis* the midbrain is very broadly exposed (Meng *et al*., 2003), but the colliculi are not apparent, although this may be a product of preservation. This contrasts with the condition of Eocene euprimates, in which the midbrain is never exposed (Kirk *et al*., 2014; Harrington *et al*., 2016, 2020; Ramdarshan & Orliac, 2016).

Finally, the hypophyseal fossa (for the pituitary gland) is apparent as a clear, nearly circular bulge on the ventral surface of the endocast, approximately in line horizontally with the stem of the pathway for cranial nerve V_3 (Fig. 3b).

Cerebellum and petrosal lobules

The cerebrum of *Anagale gobiensis* does not overlap onto the cerebellum, so the dorsal surface of the cerebellum is broadly exposed on the endocast, exhibiting a vermis that is separated from the lateral lobes by paramedian fissures (Fig. 3a, Fig. 9). The

vermis has two clear fissures running coronally. Rostral to the lobe of the vermis is the fissura prima (Dow, 1942). In lateral view (Fig. 3d), between the fissura prima and the summit of the vermis, there is another sulcus that has not been identified. Caudoventral to the summit of the vermis is the prepyramidal fissure (fissura suprapyramidalis in Dow, 1942; Fig. 9). This fissure is continuous with the fissura paraflocculari s (Larsell and Dow, 1935; Dow, 1942; Maugoust and Orliac, 2021), which defines the rostral edge of the petrosal lobules. No other fissure ventral to the prepyramidal fissure is observable (Fig. 9), suggesting there is no visible fissura secunda. Excluding the petrosal lobules, the cerebrum is clearly wider than the cerebellum.

The petrosal lobules are rounded with very short stems attaching them to the rest of the cerebellum (see Figs. 3, 4c; Fig. 9). They are more anteriorly located than the lateral lobes and vermis in dorsal view (Fig. 3a). When petrosal lobule volume is plotted against body mass, *Anagale gobiensis* appears close to the "ischyromyid" morphospace and just above *Aplodontia rufa*, an extant aplodontiid rodent (Fig. 11). The percentage of petrosal lobule volume relative to the volume of the total endocast in *Anagale gobiensis* (1.01%) is within the range of "ischyromyids" (Fig. 12; 0.62-2.05%; Bertrand & Silcox, 2016; Bertrand *et al*., 2016a, 2019), but lower than in *Me. turgidus* (2.31 %; López-Torres *et al*., 2020), *Al. relictus* (3.35%; Bertrand *et al*., 2018), *C. wilsoni* (2.96%; Bertrand *et al*., 2017) and *Protosciurus* cf. *rachelae* (3.65-4.82%; Bertrand *et al*., 2018). Comparing the percentage of petrosal lobule volume with "plesiadapiforms" and apatemyids is not possible, because quantitative measures for the relative size of the petrosal lobule have not yet been published for these groups.

Brainstem and cranial nerves

Various casts of the openings for the cranial nerves can be seen on the ventral surface of AMNH 26079 (Fig. 3b). The cast of the optic chiasm is visible on AMNH 26079, located just rostral to the level of the sphenorbital fissure. The sphenorbital fissure in *Anagale gobiensis* serves as a passage for the ophthalmic veins and cranial nerves III, IV, V_1 and VI. The casts of these nerves show a faint contour and based on the typical branching pattern of cranial nerves, the most medial cranial nerve in the sphenorbital fissure would likely be the oculomotor nerve (CN III). Of the two other casts, the more medial one may pertain to the trochlear nerve (CN IV), while the largest and most lateral cast likely contained part of the trigeminal nerve (CN V) and abducens nerve (CN VI) (Fig. 3b). *Anagale gobiensis* lacks a foramen rotundum or any evidence of a separate passageway for V_2, which means it also presumably passed through the sphenorbital fissure, as observed in *L. kayi* (Silcox *et al*., 2011). This contrasts with the situation in "ischyromyids", *C. wilsoni*, and extant squirrels, in which there is a distinct passageway for V_2 on the endocast even though it ultimately does lead to the sphenorbital fissure rather than to a distinct foramen rotundum (Bertrand *et al*., 2017; 2019). In *Ap. Rufa,* the sphenorbital fissure is not confluent with the foramen rotundum, whereas in fossil aplodontiids, they are merged with each other (Bertrand *et al.*, 2018). With respect to stem lagomorphs, there is no separate foramen rotundum in *Palaeolagus haydeni* (Wolniewicz and Fostowicz-Frelik, 2021). The foramen rotundum is variable in its presence in primates; there is a separate passageway for V_2 leading to a distinct opening on the endocast of adapoids (Harrington *et al*., 2016) and *Microsyops annectens* (Silcox *et al*., 2010), but not *Ig. graybullianus* or *Microchoerus erinaceus* (Silcox *et al*., 2009; Ramdarshan & Orliac, 2016). The condition in *Plesiadapis* is a matter of continuing debate (Bloch & Silcox, 2006; Orliac *et al*., 2014). Gurche (1978)

considered the presence of a distinct foramen rotundum to be variable in *Necrolemur antiquus* (see discussion in Harrington *et al*., 2020), which highlights the lability of this character.

AMNH 26079 has a foramen ovale (Simpson, 1931) as is typical of mammals, but unlike some rodents lacks a separate foramen ovale (Wahlert, 1974; Bertrand *et al*., 2018: Table S14). Casts of the internal auditory meatus, with passageways for cranial nerves VII (facial) and VIII (vestibulocochlear), are visible on both sides located rostroventral to the petrosal lobules (Fig. 3b-d). A cast of the jugular foramen, through which the internal jugular vein and cranial nerves IX (glossopharyngeal), X (vagus) and XI (accessory) would have run, is positioned directly ventral to the petrosal lobule (Fig. 3b, c; Fig. 9), in a similar position to the one seen in fossil rodents (Bertrand & Silcox, 2016; Bertrand *et al*., 2016a, 2017, 2018, 2019), early euprimates (Harrington *et al*., 2016, 2020; Ramdarshan & Orliac, 2016), "plesiadapiforms" (Silcox *et al*., 2009, 2010a; Orliac *et al*., 2014) and *Labidolemur* (Silcox *et al*., 2011). In *Me. turgidus*, the jugular foramen is shifted more rostrally (López-Torres *et al*., 2020). Finally, there is a cast of a single hypoglossal foramen for cranial nerve XII (hypoglossal) on each side of the brainstem (Fig. 3b; Fig. 9), as seen in some "ischyromyids" (e.g. *Paramys copei*; *Pa. delicatus*; *Notoparamys costilloi*; *Pseudotomus horribilis*; *Pseudotomus petersoni*; *Ra. atramontis*; *Re. delicatissimus*; *Re. sciuroides*; Bertrand *et al*., 2016, 2019), *C. wilsoni* (Bertrand *et al*., 2017); *Al. relictus*, *Protosciurus* cf. *rachelae* (Bertrand *et al*., 2018); stem lagomorphs (*Me. turgidus* and *P. haydeni*; López-Torres *et al*., 2020; Wolniewicz and Fostowicz-Frelik, 2021); early euprimates (Harrington *et al*., 2016, 2020; Ramdarshan and Orliac, 2016), "plesiadapiforms" (Bloch and Silcox, 2006; Silcox *et al*., 2009, 2010a; Orliac *et al*., 2014) and *L. kayi* (Silcox *et al*., 2011). However, casts for two hypoglossal nerves (per side) are observed in some

"ischyromyids" (e.g. *Pseudotomus robustus* [= *Pseudotomus oweni* in Bertrand *et al*., 2019], *Is. Typus*; Wahlert, 1974; Bertrand and Silcox, 2016; Bertrand *et al*., 2019).

Blood vessels

Anagale gobiensis has a pattern of venous sinuses on the endocast that is basically similar to the arrangement inferred as primitive for therian mammals (Wible & Rougier, 2004). The superior sagittal sinus is most prominent around the level of the cerebral frontal lobes and fades away more caudally. This suggests that this sinus would have partially been located deep in the meninges (Macrini *et al*., 2007). The superior sagittal sinus is continuous with the transverse sinus. In *Anagale gobiensis* the transverse sinus connects with the sigmoid sinus, which is continuous with the internal jugular vein as observed for rodents (Fig. 9; Bertrand & Silcox, 2016; Bertrand *et al*., 2016a, 2017, 2018, 2019), early euprimates (Harrington *et al*., 2016, 2020; Ramdarshan & Orliac, 2016), "plesiadapiforms" (Silcox *et al*., 2009, 2010a, 2020) and apatemyids (Silcox *et al*., 2011). The jugular foramen is continuous with the cast of the inferior petrosal sinus in *Anagale gobiensis*. This is also observed in early euprimates (Kirk *et al*., 2014; Harrington *et al*., 2016, 2020; Ramdarshan & Orliac, 2016), fossil rodents, *Me. turgidus* and *Microsyops annectens* (Silcox *et al*., 2010a; Bertrand & Silcox, 2016; Bertrand *et al*., 2017, 2018, 2019; López-Torres *et al*., 2020). The inferior petrosal sinus is not well marked in *Ig. graybullianus* (Silcox *et al*., 2009) and it is not preserved in *Pl. tricuspidens* or *L. kayi* (Silcox *et al*., 2011; Orliac *et al*., 2014). There is a large postglenoid foramen present (Simpson, 1931). However, the cast of the postglenoid vein was not traced when reconstructing the endocast, because the vein would have been very large and would have significantly affected the volume and surface area

calculations. The orbitotemporal canal is not observable on the endocast, and as noted above did not run intraosseously.

With respect to arteries, a small cast on the surface of the endocast lateral to the pituitary gland is here identified as the cast for the carotid foramen (Fig. 3b), but it is not clearly related to a pathway for a vessel on the endocast which makes interpreting its contents somewhat ambiguous. Lateral to the carotid foramen, there is a larger cast that corresponds to the piriform fenestra (posterior lacerate foramen of Simpson, 1931; pyriform fenestra of McDowell, 1958). The piriform fenestra transmits various neurovascular structures, including the postglenoid vein (Wible and Shelley, 2020). The alisphenoid canal, which transmits the ramus infraorbitalis of the stapedial artery (Wible, 1987), is visible and merges with the sphenorbital fissure (Fig. 3b-d). As Wible (1987) discussed, there is a significant amount of variability among mammals in the presence or absence of an alisphenoid canal, suggesting that it is a feature that arose multiple times (see also Asher, 2001). Within Euarchontoglires it is present in lagomorphs (Wible, 1987; Wolniewicz and Fostowicz-Frelik, 2021) and scandentians (Wible, 1987), but absent in dermopterans (associated with the complete involution of the internal carotid artery; Wible, 1993). In rodents, it is variably present (Wible, 1987), but has been identified in the most primitive forms (Wahlert, 1974; Bertrand & Silcox, 2016). Although missing in "plesiadapiforms" (Silcox *et al*., 2009, 2010; Orliac *et al*., 2014), a clear alisphenoid canal is present in *Labidolemur* (Silcox *et al*., 2011) and has been identified in the early euprimate *Microchoerus erinaceus* (Ramdarshan & Orliac, 2016). These various lines of evidence suggest that *Anagale*'s condition (presence of the canal) is likely primitive for Glires, and possibly for Euarchontoglires.

Relative brain size and encephalisation quotient

Figure 13 shows a bivariate plot of logarithmic endocranial volume against logarithmic body mass. The range of body masses for *Anagale gobiensis* places this species within the shared morphospace between extinct euprimates and extinct rodents.

The EQ estimates of *Anagale gobiensis* are calculated based on the range of body mass estimates given above (Fig. 14). *Anagale gobiensis* has a range of EQs (Eisenberg, 1981) of 0.61—0.74 (Table 3). Compared to other early members of Euarchontoglires (Fig. 14), *Anagale gobiensis* has EQ values within the range of "ischyromyids" (0.36—0.76; Bertrand and Silcox, 2016; Bertrand *et al*., 2016a, 2019), Oligocene sciuroids (0.99—1.33; Bertrand *et al*., 2017, 2018) and Eocene euprimates (0.37—1.53; Kirk *et al*., 2014; Harrington *et al*., 2016, 2020; Ramdarshan & Orliac, 2016). *Anagale gobiensis* has higher EQ values than Palaeocene and early Eocene "plesiadapiforms" (0.14—0.61; Silcox *et al*., 2009, 2010a; Orliac *et al*., 2014; Long *et al*., 2015), the Oligocene stem lagomorph *Megalagus* (0.39; López-Torres *et al*., 2020) and the late Palaeocene—early Eocene apatemyid *Labidolemur* (0.36; Silcox *et al*., 2011). However, *Anagale gobiensis* has a lower EQ than Oligocene sciuroids (0.99—1.33; Bertrand *et al*., 2017, 2018) and the late Eocene apatemyid *Carcinella* (1.28; von Koenigswald *et al*., 2009).

DISCUSSION

The EQ results and the plot of endocranial volume and body mass show that *Anagale gobiensis* had a level of encephalisation similar to that of "ischyromyids" and Eocene euprimates (Figs. 12 and 13). However, the endocast of *Anagale gobiensis* differs considerably in the proportions of the subregions from the endocasts of fossil euprimates in having much better developed regions related to olfaction (such as the

palaeocortex, olfactory bulbs and olfactory tubercles), but a much smaller neocortex (Fig. 7). Indeed, probably the most surprising feature of the endocranial morphology of *Anagale gobiensis* is its extremely low degree of neocorticalisation, which is particularly surprising in light of its late Eocene age and the trend of increasing neocorticalisation in both Glires and Primates. At 10.98% of neocortical surface area relative to the total endocranial surface area, *Anagale gobiensis* is the least neocorticalised euarchontogliran known to date, although there are other Eocene mammals that do also exhibit a low neocortical surface ratio (Fig. 8; see Bertrand *et al.*, 2022). The neocortex in *Anagale gobiensis* is almost entirely restricted to the dorsal face of the endocast, with very little ventral projection on the sides. The neocortex encompasses regions responsible for the primary processing of visual, auditory, somatosensory, motor, sensorimotor and prefrontal sensory information (Martin, 1990; Kaas, 2012; Long *et al*., 2015), and for these reasons may be impacted based on aspects of a species' ecology, such as its lifestyle. The locomotor behaviour of *Anagale gobiensis* is largely unknown. The high degree of dental wear, tendency towards hypsodonty and the inference of adaptations for forelimb digging (McKenna, 1963) could be interpreted as evidence that anagalids sourced their food from underground. A smaller neocortex has been suggested to be linked to fossorial lifestyle (Bertrand *et al*., 2018; 2021), likely because of reduced visual requirements, so perhaps this low degree of neocorticalisation could be an indication that *Anagale gobiensis* was actually fossorial. This inferred pattern of behaviour could also help to explain the similarities in the form of the endocast to the macroscelidean *Rhynchocyon* (Benoit et al., 2013). However, this idea requires further testing based on assessment of the postcranial material.

Anagale gobiensis has complete exposure of one set of colliculi, tentatively identified as the caudal colliculi (see discussion in the section '*Cerebrum and midbrain*' above). Whereas this is often seen as a primitive trait, it has been argued that an expansion of this region could be associated with increased auditory acuity (Edinger, 1964). This may be critical in semi-fossorial species to avoid predators or when visibility is reduced in subterranean environments (Begall *et al*., 2007).

Compared to other fossil euarchontoglirans, *Anagale gobiensis* has a proportionally large volume of the brain dedicated to olfaction. The olfactory bulb volume ratio in *Anagale gobiensis* is higher than in any fossil member of Glires and within the upper range for plesiadapiforms (Fig. 6). Only apatemyids have proportionately much larger olfactory bulbs. This pattern is also seen in the analysis relative to body mass (Fig. 5), in which *Labidolemur* and *Anagale gobiensis* both sit above the range of variation for other euarchontoglirans. Therefore, *Anagale gobiensis* was likely an animal that was largely olfaction driven. This is also consistent with *A. gobiensis* having a laterally and ventrally inflated palaeocortex (also known as olfactory cortex) and well-defined, ventrally protruding olfactory tubercles; a greater emphasis in olfaction is supported by larger palaeocortical structures (Barton et al., 1995).

The petrosal lobule volume ratio in *Anagale gobiensis* is much lower than that observed in *Megalagus* and modern lagomorphs, within the rodent range (Fig. 12). When considered in relation to body mass *Anagale gobiensis* is just below "ischyromyid" morphospace, near the aplodontiid rodent *Ap. rufa* (Fig. 11). The petrosal lobules play a role in the stabilisation of eye movements necessary for accurate visual tracking (Rambold *et al*., 2002; Hiramatsu *et al*., 2008), suggesting that *Anagale gobiensis* was probably living in an environment in which quick visual tracking was not a selective pressure. Following McKenna's (1963) observation that *Anagale gobiensis*

was probably a forelimb scratching digger, this species might have spent some time in burrows, where there is a lack of visual cues, or might have had a relatively slow mode of locomotion in which quick visual tracking was not critical for survival. Bertrand *et al*. (2018; 2021) deduced that a low petrosal lobule ratio might be linked to fossoriality in aplodontiid rodents, which is consistent with the idea that *Anagale gobiensis* might have been a digger. Additionally, Lang et al. (2022) found that fossorial taxa have significantly smaller petrosal lobules relative to body mass compared to other locomotor groups across Euarchontoglires.

As a potential outgroup to Glires and a lineage branching off a deep node in Euarchontoglires, *Anagale gobiensis* has the potential to be crucially informative to the brain evolution of these clades, with the proviso that its own patterns of behaviour may have shaped certain aspects of its brain anatomy, particularly if it was fossorial. *Anagale gobiensis* shares features with other primitive groups in the lineages of Rodentia, Lagomorpha and Primates, which may therefore be relevant for reconstructing ancestral stages in Euarchontoglires. As observed in all these groups, *Anagale gobiensis* has a partially exposed midbrain and a relatively low EQ. However, it is not entirely clear if these traits are symplesiomorphies inherited from the euarchontogliran ancestor or if *Anagale gobiensis* has gone through a secondary reversal of these traits due to fossorial adaptations. *Anagale gobiensis* has a higher relative volume of the olfactory bulbs than in fossil members of Glires, or "plesiadapiforms", but smaller than in *Labidolemur*; this could suggest that large olfactory bulbs may be ancestral for Euarchontoglires but could also reflect adaptations in Apatemyidae and Anagalidae. *Anagale gobiensis* also displays small petrosal lobules, comparable proportionally to those of modern and extinct fossorial rodents (see Bertrand *et al.*, 2021; Lang *et al*., 2022), suggesting that the reduction in petrosal lobule size in *Anagale gobiensis* might reflect some degree of

fossorial behaviour. As the petrosal lobule (and the flocculus) has been classically interpreted as being used for gaze stabilisation (Rambold *et al*., 2002; Hiramatsu *et al*., 2008), it is expected that animals that live in subterranean or low-light environments would have small floccular fossae. There is still some uncertainty in determining whether Glires ancestrally had small or large petrosal lobules, since "ischyromyids" are fairly variable in this character (Bertrand *et al*., 2019). Based on a recent study, the petrosal lobules were reconstructed as being small at the base of Euarchontoglires and then increasing in proportion through time (Bertrand et *al.*, 2021). As a late Eocene taxon, this would lead one to expect that the petrosal lobule relative volume would be higher than the value reconstructed for primitive Rodentia (there is insufficient data to reconstruct the primitive lagomorph node) but is actually lower, consistent with the inference about fossoriality. Finally, *Anagale gobiensis* is uniquely less neocorticalised compared to other euarchontoglirans of similar age and even compared to Palaeocene euarchontoglirans (Fig. 7). This suggests that *Anagale gobiensis* may have secondarily decreased its neocortical area due to fossoriality or other ecological aspects and therefore the ancestor of Glires and Euarchontoglires might have been more neocorticalised than *Anagale gobiensis*. Low neocorticalisation is likely primitive for Euarchontoglires as the Eocene "ischyromyids" and "plesiadapiforms" have less expanded neocortices than more derived rodents and primates.

CONCLUSION

The present study reconstructs the first virtual endocast of an anagalid, a poorly known group of Palaeogene euarchontoglirans from Asia, argued to be closely related to modern members of Glires. The endocast of *Anagale gobiensis* sheds some new light on the reconstruction of the palaeoecology and behaviour of the animal, which has

remained largely unknown. *Anagale gobiensis* displays relatively small petrosal lobules, and the lowest neocortical ratio recorded for a euarchontogliran. These traits might be expected if anagalids were fossorial, which would be consistent with indications that they may have sourced their food from below ground (McKenna, 1963). The evidence from the endocast shows that *Anagale gobiensis* was likely very olfaction driven, based on the relatively large olfactory bulbs and olfactory tubercles, and a laterally expansive palaeocortex (= olfactory cortex; piriform cortex). This suite of traits means that *Anagale gobiensis* does not follow the trend in other euarchontogliran lineages of having significantly increased their degree of neocorticalisation by the end of the Eocene. The expansion of the palaeocortex in *Anagale gobiensis* represents a different pattern than seen in other fossil members of Euarchontoglires.

Despite its likely specialisation for fossoriality, *Anagale gobiensis* pertains to a very primitive lineage of euarchontoglirans and its endocast may be informative with respect to some aspects of the earliest stages of brain evolution in Euarchontoglires. The endocast further supports relatively large olfactory bulbs, partial midbrain exposure, and a relatively low EQ as ancestral traits for Euarchontoglires. The petrosal lobule volume ratio falls within the fairly broad range of "ischyromyid" rodents, which is consistent with previous studies showing that an increase in petrosal lobules occurred through time in Euarchontoglires including rodents (Bertrand et al., 2022). However, the low ratio of the petrosal lobules of *Anagale gobiensis* could be related to an adaptation to fossoriality as previously hypothesised for rodents (Bertrand et al., 2021). Ultimately, the relative size of the petrosal lobules has not been explored in other key early euarchontoglirans, such as "plesiadapiforms" or apatemyids, which would be fundamental to constrain what the ancestral state would be.

The palaeoecological diversity of anagalids is currently unknown. Future work on other known anagalid crania, such as those of *Anagalopsis kansuensis* (Bohlin, 1951), *Eosigale gujingensis* (Hu, 1993), and *Linnania lofoensis* (Chow *et al*., 1973), will help augment our understanding of the behaviour and endocranial morphology of this family. Additionally, an in-depth study of the postcranial skeleton of *Anagale gobiensis* would also be key to have the full picture of the locomotor ecology of this species and provide further insight into this enigmatic group of mammals.

Author contributions. SLT, OCB, MTS, ŁFF and JM contributed to the conception and design of the study. OCB and JM acquired the CT data, SLT and MML segmented out the virtual specimen and collected the data. All authors interpreted the data. SLT drafted the article. All authors revised it critically for important intellectual content and gave final approval before submission.

Acknowledgements. The authors would like to thank Mao Fangyuan (Institute of Vertebrate Paleontology and Paleoanthropology) for facilitating access to data. We also thank Morgan Hill from the Microscopy and Imaging Facility (MIF) at the AMNH for facilitating the scanning of specimens. We are grateful to Rémi Allemand and Gabriela San Martin-Flores for help during the segmentation process, to Keegan Selig for 3D printing of the endocast, and Peggy Brady for relevant discussions on the cranial anatomy of *Anagale gobiensis*. We would also like to thank Robert Asher, Sally Thomas, and three anonymous reviewers for helpful comments that significantly improved this paper. This study was supported by a Kalbfleisch Postdoctoral Research Fellowship to SLT, a Marie Skłodowska-Curie Actions: Individual Fellowship (H2020-

MSCA-IF-2018-2020; No. 792611) to OCB, an NSERC CGS grant to MML, and an NSERC Discovery Grant to MTS. The authors have no conflicts of interest to declare.

DATA AVAILABILITY

A 3D surface model of the endocast of *Anagale gobiensis* (AMNH 26079) is available in MorphoSource: http://morphosource.org/permalink/?PXXX [login username: anagale.reviewer@gmail.com; password: 12345]. Other data for this study are available in the Dryad Digital Repository: https://datadryad.org/stash/share/XXXX [please note that the data for this paper are not yet published and these temporary links should not be shared without the express permission of the author]

REFERENCES

ASHER, R. J. 2001. Cranial anatomy in tenrecid insectivorans: Character evolution across competing phylogenies. *American Museum Novitates*, **3352**, 1-53.

ASHER, R. J. 2007. A web-database of mammalian morphology and a reanalysis of placental phylogeny. *BMC Evolutionary Biology*, **7**, 108.

ASHER, R. J. and HELGEN, K. M. 2010. Nomenclature and placental mammal phylogeny. *BMC Evolutionary Biology*, **10**, 102.

ASHER, R. J., MENG, J., WIBLE, J. R., MCKENNA, M. C., ROUGIER, G. W., DASHZEVEG, D. and NOVACEK, M. J. 2005. Stem Lagomorpha and the antiquity of Glires. *Science*, **307**, 1091–1094.

ASHER, R. J., NOVACEK, M. J. and GEISLER, J. H. 2003. Relationships of endemic African mammals and their fossil relatives based on morphological and molecular evidence. *Journal of Mammalian Evolution*, **10**, 131–194.

ASHER, R. J., SMITH, M. R., RANKIN, A. and EMRY, R. J. 2019. Congruence, fossils and the evolutionary tree of rodents and lagomorphs. *Royal Society Open Science*, **6**, 190387.

BARTON, R. A., PURVIS, A., and HARVEY, P. H. 1995. Evolutionary radiation of visual and olfactory brain systems in primates, bats and insectivores. *Philosophical Transactions of the Royal Society of London B*, **348**, 381–392.

BEGALL, S., BURDA, H. and SCHLEICH, C. E. 2007. *Subterranean rodents: News from underground*. Springer Science & Business Media, 398 pp.

BENOIT, J., CRUMPTON, N., MÉRIGEAUD, S. and TABUCE, R. 2013. A memory already like an elephant's? The advanced brain morphology of the last common ancestor of Afrotheria. *Brain, Behavior and Evolution*, **81**, 154–169.

BERTRAND, O. C., AMADOR-MUGHAL, F., LANG, M. M. and SILCOX, M. T. 2018. Virtual endocasts of fossil Sciuroidea: brain size reduction in the evolution of fossoriality. *Palaeontology*, **61**, 919–948.

BERTRAND, O. C., AMADOR-MUGHAL, F., LANG, M. M. and SILCOX, M. T. 2019. New virtual endocasts of Eocene Ischyromyidae and their relevance in evaluating neurological changes occurring through time in Rodentia. *Journal of Mammalian Evolution*, **26**, 345–371.

BERTRAND, O. C., AMADOR-MUGHAL, F. and SILCOX, M. T. 2016a. Virtual endocasts of Eocene *Paramys* (Paramyinae): oldest endocranial record for

Rodentia and early brain evolution in Euarchontoglires. *Proceedings of the Royal Society B: Biological Sciences*, **283**, 20152316.

BERTRAND, O. C., AMADOR-MUGHAL, F. and SILCOX, M. T. 2017. Virtual endocast of the early Oligocene *Cedromus wilsoni* (Cedromurinae) and brain evolution in squirrels. *Journal of Anatomy*, **230**, 128–151.

BERTRAND, O. C., PÜSCHEL, H.P., SCHWAB, J.A., SILCOX, M.T. and BRUSATTE, S.L. 2021. The impact of locomotion on the brain evolution of squirrels and close relatives. *Communications Biology*, **4**, 1–15.

BERTRAND, O. C., SCHILACI, M. A. and SILCOX, M. T. 2016b. Cranial dimensions as estimators of body mass and locomotor habits in extant and fossil rodents. *Journal of Vertebrate Paleontology*, **36**, e1014905.

BERTRAND, O. C., SHELLEY, S. L., WILLIAMSON, T. E., WIBLE, J. R., CHESTER, S. G. B., FLYNN, J. J., HOLBROOK, L. T., LYSON, T. R., MENG, J., MILLER, I. M., PÜSCHEL, H. P., SMITH, T., SPAULDING, M., TSENG, Z. J. and BRUSATTE, S. L. 2022. Brawn before brains in placental mammals after end-Cretaceous extinction. *Science*, **376**, 80–85.

BERTRAND, O. C. and SILCOX, M. T. 2016. First virtual endocasts of a fossil rodent: *Ischyromys typus* (Ischyromyidae, Oligocene) and brain evolution in rodents. *Journal of Vertebrate Paleontology*, **36**, e1095762.

BLOCH, J. I. and GINGERICH, P. D. 1998. *Carpolestes simpsoni*, new species (Mammalia, Proprimates) from the late Paleocene of the Clarks Fork Basin, Wyoming. *Contributions of the Museum of Paleontology at the University of Michigan*, **30**, 131–162.

BLOCH, J. I. and SILCOX, M. T. 2006. Cranial anatomy of the Paleocene plesiadapiforms *Carpolestes simpsoni* (Mammalia, Primates) using ultra high-resolution X-ray computed tomography, and the relationship of plesiadapiforms to Euprimates. *Journal of Human Evolution*, **50**, 1–35.

BOHLIN, B. 1951. Some mammalian remains from Shih-her-ma-ch'eng, Hui-hui-p'u area, Western Kansu. Reports from the Scientific Expedition to the North-Western Provinces of China under the Leadership of Dr Sven Hedin. The Sino-Swedish Expedition Publication 35, VI. *Vertebrate Paleontology*, **5**, 1–48 + 7 pl.

BOYER, D. M., KAUFMAN, S., GUNNELL, G. F., ROSENBERGER, A. L. and DELSON, E. 2014. Managing 3D digital data sets of morphology: MorphoSource is a new project-based data archiving and distribution tool. *American Journal of Physical Anthropology*, **153**, 84.

BRYANT, J. D. and MCKENNA, M. C. 1995. Cranial anatomy and phylogenetic position of *Tsaganomys altaicus* (Mammalia: Rodentia) from the Hsanda Gol Formation (Oligocene), Mongolia. *American Museum Novitates*, **3156**, 1–42.

CAMPIONE, N. E. and EVANS, D. C. 2012. A universal scaling relationship between body mass and proximal limb bone dimensions in quadrupedal terrestrial tetrapods. *BMC Biology*, **10**, 60.

CHOW, M. M., CHANG, Y., WANG, B. and TING, S. 1973. New mammalian genera and species from the Paleocene of Nanhsiung, N. Kwangtung. *Vertebrata PalAsiatica*, **11**, 31–35. [in Chinese]

CONROY, G. C. 1987. Problems of body-weight estimation in fossil primates. *International Journal of Primatology*, **8**, 115–137.

COPE, E. D. 1873. Third notice of extinct Vertebrata from the Tertiary of the Plains. *Paleontological Bulletin*, **16**, 1–8.

DECHASEAUX, C. 1958. Encéphales de Simplicidentés fossils. 819–821. *In* PIVETEAU, J. (ed.) *Traité de Paléontologie, Vol 6: L'origine des mammifères et les aspects fondamentaux de leur évolution*. Masson et Cie, 1135 pp.

DOW, R. S. 1942. The evolution and anatomy of the cerebellum. *Biological Reviews*, **17**, 179–220.

EDINGER, T. 1964. Midbrain exposure and overlap in mammals. *American Zoologist*, **4**, 5–19.

FERREIRA-CARDOSO, S., ARAÚJO, R., MARTINS, N. E., MARTINS, G. G., WALSH, S., MARTINS, R. M. S., KARDJILOV, N., MANKE, I., HILGER, A. and CASTANHINHA, R. 2017. Floccular fossa size is not a reliable proxy of ecology and behaviour in vertebrates. *Scientific Reports*, **7**, 2005.

FOSTOWICZ-FRELIK, Ł. 2017. Convergent and parallel evolution in early Glires (Mammalia). 199–216. *In* PONTAROTTI, P. (ed.) *Evolutionary biology: Self/nonself evolution, species and complex traits evolution, methods and concepts*. Springer Verlag, 395 pp.

FOX, R. C., SCOTT, C. S. and BUCKLEY, G. A. 2015. A 'giant' purgotoriid (Plesiadapiformes) from the Paleocene of Montana, USA: mosaic evolution in the earliest primates. *Palaeontology*, **58**, 277–291.

GINGERICH, P. D. 1990. Prediction of body mass in mammalian species from long bone lengths and diameters. *Contributions from the Museum of Paleontology, The University of Michigan*, **28**, 79–92.

GINGERICH, P. D. and GUNNELL, G. F. 2005. Brain of *Plesiadapis cookei* (Mammalia, Proprimates): surface morphology and encephalization compared to those of Primates and Dermoptera. *Contributions from the Museum of Paleontology, The University of Michigan*, **31**, 185–195.

GRABOWSKI, M. W., HATALA, K. G., JUNGERS, W. L. and RICHMOND, B. G. 2015. Body mass estimates of hominin fossils and the evolution of human body size. *Journal of Human Evolution*, **85**, 75–93.

GURCHE, J. A. 1978. Early primate brain evolution. Unpublished Master's thesis, University of Kansas, Lawrence.

GURCHE, J. A. 1982. Early primate brain evolution. 227–246. *In* ARMSTRONG, E. and FALK, D. (eds.) *Primate brain evolution: Methods and concepts*. Plenum Press, 346 pp.

HARRINGTON, A. R., SILCOX, M. T., YAPUNCICH, G. S., BOYER, D. M. and BLOCH, J. I. 2016. First virtual endocasts of adapiform primates. *Journal of Human Evolution*, **99**, 52–78.

HIRAMATSU, T., OHKI, M., KITAZAWA, H., XIONG, G., KITAMURA, T., YAMADA, J. and NAGAO, S. 2008. Role of primate cerebellar lobulus petrosus of paraflocculus in smooth pursuit eye movement control revealed by chemical lesion. *Neuroscience Research*, **60**, 250–258.

HU, Y. 1993. Two new genera of Anagalidae (Anagalida, Mammalia) from the Paleocene of Qianshan, Anhui and the phylogeny of anagalids. *Vertebrata PalAsiatica*, **31**, 153–182. [in Chinese]

HUANG, X. and ZHENG, J. 1983. A new anagalid from Upper Paleocene of Nanxiong Basin, Guangdong. *Vertebrata PalAsiatica*, **21**, 59–63.

HUCHON, D., MADSEN, O., SIBBALD, M. J. J. B., AMENT, K., STANHOPE, M., CATZEFLIS, F., DE JONG, W. W., DOUZERY, E. J. P. 2002. Rodent phylogeny and timescale for the evolution of Glires: evidence from an extensive taxon sampling using three nuclear genes. *Molecular Biology and Evolution*, **19**, 1053–1065.

HYLANDER, W. L. 1985. Mandibular function and biomechanical stress and scaling. *American Zoologist*, **25**, 315–330.

JEPSEN, G. L. 1930. New vertebrate fossils from the lower Eocene of the Bighorn Basin, Wyoming. *Proceedings of the American Philosophical Society*, **69**, 117–131.

JERISON, H. J. 1973. *Evolution of the brain and intelligence*. Academic Press, 482 pp.

JERISON, H. J. 2012. Digitized fossil brains: neocroticalization. *Biolinguistics*, **6**, 383–392.

KAAS, J. H. 2012. The evolution of the neocortex in primates. 91–102. *In* HOFMAN, M. A. and FALK, D. (eds.) *Evolution of the primate brain*. Elsevier, 496 pp.

KIELAN-JAWOROWSKA, Z. 1983. Multituberculate endocranial casts. *Palaeovertebrata*, **13**, 1–12.

KINGDON, J., HAPPOLD, D., HOFFMANN, M., BUTYNSKI, T., HAPPOLD, M. and KALINA, J. 2013. *Mammals of Africa. Volume I: Introductory Chapters and Afrotheria*. Bloomsbury, 352 pp.

KIRK, E. C., DAGHIHI, P., MACRINI, T. E., BHULLAR, B. A. S. and ROWE, T. B. 2014. Cranial anatomy of the Duchesnean primate *Rooneyia viejaensis*: new insights from high resolution computed tomography. *Journal of Human Evolution*, **74**, 82–95.

LANG, M. M., BERTRAND, O. C., SAN MARTIN-FLORES, G., LAW, C. J., ABDUL-SATER, J., SPAKOWSKI, S. and SILCOX, M. T. 2022. Scaling patterns of cerebellar petrosal lobules in Euarchontoglires: Impacts of ecology and phylogeny. *Anatomical Record*, **305**, 3472–3503.

LARSELL, O. and DOW, R. S. 1935. The development of the cerebellum in the bat (*Corynorhinus* sp.) and certain other mammals. *Journal of Comparative Neurology*, **62**, 443–468.

LI, C. K. 2016. Order Anagalida. 390–411. *In* LI, C. K and QIU, Z. (eds.) *Basal synapsids and mammals, Volume III, Eulipotyphlans, proteutheres, chiropterans, euarchontans, and anagalids*. Palaeovertebrata Sinica, **3**, 488 pp. [in Chinese]

LI, C. K. and TING, S. Y. 1983. The Paleogene mammals of China. *Bulletin of the Carnegie Museum of Natural History*, **21**, 1–93.

LI, C. K., WILSON, R. W., DAWSON, M. R. and KRISHTALKA, L. 1989. The origin of rodents and lagomorphs. 97–108. *In* GENOWAYS, H. H. (ed.) *Current mammalogy*. Plenum Press, 512 pp.

LI, Q., WANG, Y.-Q., FOSTOWICZ-FRELIK, Ł. 2016. Small mammal fauna from Wulanhuxiu (Nei Mongol, China) implies faunal turnover across the Irdinmanhan-Sharamurunian boundary. *Acta Palaeontologica Polonica*, **61**, 759–776.

LONG, A., BLOCH, J. I. and SILCOX, M. T. 2015. Quantification of neocortical ratios in stem primates. *American Journal of Physical Anthropology*, **157**, 363–373.

LÓPEZ-TORRES, S., BERTRAND, O. C., LANG, M. M., SILCOX, M. T. and FOSTOWICZ-FRELIK, Ł. 2020. Cranial endocast of the stem lagomorph *Megalagus* and brain structure of basal Euarchontoglires. *Proceedings of the Royal Society B*, **287**, 20200665.

LÓPEZ-TORRES, S., BERTRAND, O. C., LANG, M. M., FOSTOWICZ-FRELIK, Ł., SILCOX, M. T. and MENG, J. 2022. Cranial endocast of *Anagale gobiensis* (Anagalidae) and its implications for early brain evolution in Euarchontoglires. Dryad Digital Repository. https://datadryad.org/stash/share/XXXX

LÓPEZ-TORRES, S. and FOSTOWICZ-FRELIK, Ł. 2018a. A new Eocene anagalid (Mammalia: Euarchontoglires) from Mongolia and its implications for the group's phylogeny and dispersal. *Scientific Reports*, **8**, 13955.

LÓPEZ-TORRES, S. and FOSTOWICZ-FRELIK, Ł. 2018b. The phylogenetic position of the Anagalidae within Euarchontoglires and its implications for the evolution of Glires and Euarchonta. *Society of Vertebrate Paleontology 2018 Program and Abstracts*, 170.

LUTERBACHER, H. P., ALI, J. R., BRINKHUIS, H., GRADSTEIN, F. M., HOOKERI, J. J., MONECHI, S., OGG, J. G., POWELL, J., RÖHL, U., SANFILIPPO, A. and SCHMITZ, B. 2004. The Paleogene Period. 384–408. *In* GRADSTEIN, F. M., OGG, J. G. and SMITH, A. (eds.) *A geologic time scale 2004*. Cambridge University Press, 589 pp.

MACRINI, T. E., ROUGIER, G. W. and ROWE, T. 2007. Description of a cranial endocast from the fossil mammal *Vincelestes neuquenianus* (Theriiformes) and

its relevance to the evolution of endocranial characters in therians. *Anatomical Record*, **290**, 875–892.

MARIVAUX, L., VIANEY-LIAUD, M. and JAEGER, J. J. 2004. High-level phylogeny of early Tertiary rodents: dental evidence. *Zoological Journal of the Linnean Society*, **142**, 105–133.

MARTIN, R. D. 1990. *Primate origins and evolution: A phylogenetic reconstruction*. Chapman and Hall, 840 pp.

MAUGOUST, J., ORLIAC, M. J. 2021. Endocranial cast anatomy of the extinct hipposiderid bats *Palaeophyllophora* and *Hyposideros* (*Pseudorhinolophus*) (Mammalia: Chiroptera). *Journal of Mammalian Evolution*, doi: 10.1007/s10914-020-09522-9.

MCDOWELL, S. B. JR. 1958. The Greater Antillean insectivores. *Bulletin of the American Museum of Natural History*, **115**, 113–214.

MCKENNA, M. C. 1963. New evidence against tupaioid affinities of the mammalian family Anagalidae. *American Museum Novitates*, **2158**, 1–16.

MCKENNA, M. C. 1975. Toward a phylogenetic classification of the Mammalia. 21–46. *In* LUCKETT, W. P. and SZALAY, F. S. (eds.) *Phylogeny of the Primates: A multidisciplinary approach*. Plenum Press, 480 pp.

MCKENNA, M. C. and BELL, S. 1997. *Classification of Mammals Above the Species Level*. Columbia University Press, 640 pp.

MENG, J. 2004. Phylogeny and divergence of basal Glires. *Bulletin of the American Museum of Natural History*, **285**, 93–109.

MENG, J., HU, Y. and LI, C. K. 2003. The osteology of *Rhombomylus* (Mammalia, Glires): implications for phylogeny and evolution. *Bulletin of the American Museum of Natural History*, **275**, 1–247.

MENG, J. and MCKENNA, M. C. 1998. Faunal turnovers of Palaeogene mammals from the Mongolian Plateau. *Nature*, **394**, 364–367.

MILLIEN, V. and BOVY, H. 2010. When teeth and bones disagree: body mass estimation of a giant rodent. *Journal of Mammalogy*, **91**, 11–18.

MONCUNILL-SOLÉ, B., JORDANA, X., MARÍN-MORATALLA, N., MOYÀ-SOLÀ, S. and KÖHLER, M. 2014. How large are the extinct giant insular rodents? New body mass estimations from teeth and bones. *Integrative Zoology*, **9**, 197–212.

MONCUNILL-SOLÉ, B., QUINTANA, J., JORDANA, X., ENGELBREKTSSON, P. and KÖHLER, M. 2015. The weight of fossil leporids and ochotonids: body mass estimation models for the order Lagomorpha. *Journal of Zoology*, **295**, 269–278.

MURPHY, W. J., EIZIRIK, E., JOHNSON, W. E., ZHANG, Y. P., RYDER, O. A. and O'BRIEN, S. J. 2001. Molecular phylogenetics and the origins of placental mammals. *Nature*, **409**, 614–618.

NI, R. J., HUANG, Z. H., LUO, P. H., MA, X. H., Li, T. and ZHOU, J. N. 2018. The tree shrew cerebellum atlas: Systematic nomenclature, neurochemical characterization, and afferent projections. *Journal of Comparative Neurology*, **526**, 2744–2775.

NOVACEK, M. J. 1982. The brain of *Leptictis dakotensis*, an Oligocene leptictid, Eutheria, Mammalia, from North America. *Journal of Paleontology*, **56**, 1177–1186.

NOVACEK, M. J. 1986. The skull of leptictid insectivorans and the higher-level classification of eutherian mammals. *Bulletin of the American Museum of Natural History*, **183**, 1–112.

O'LEARY, M. A., BLOCH, J. I., FLYNN, J. J., GAUDIN, T. J., GIALLOMBARDO, A., GIANNINI, N. P., GOLDBERG, S. L., KRAATZ, B. P., LUO, Z.-X., MENG, J., NOVACEK, M. J., PERINI, F. A., RANDALL, Z. S., ROUGIER, G. W., SARGIS, E. J., SILCOX, M. T., SIMMONS, N. B., SPAULDING, M., VELAZCO, P. M., WEKSLER, M., WIBLE, J. R. and CIRRANELLO, A. 2013. The placental mammal ancestor and the post-K-Pg radiation of placentals. *Science*, **339**, 662–667.

ORLIAC, M. J., LADEYÉZE, S., GINGERICH, P. D., LEBRUN, R. and SMITH, T. 2014. Endocranial morphology of Palaeocene *Plesiadapis tricuspidens* and evolution of the early primate brain. *Proceedings of the Royal Society B: Biological Sciences*, **281**, 20132792.

PANEZAI, S. K., LUO, Y., VIBULYASECK, S., SARPONG, G. A., NGUYEN-MINH, V. T., NEDELESCU, H., HIRANO, S. and SUGIHARA, I. 2020. Reorganization of longitudinal compartments in the laterally protruding paraflocculus of the postnatal mouse cerebellum. *Journal of Comparative Neurology*, **528**, 1725–1741.

PILLERI, G., GIHR, M. and KRAUS, C. 1984. Cephalization in rodents with particular reference to the Canadian beaver (*Castor canadensis*). 11–102. *In* PILLERI, G. (ed.) *Investigations on Beavers*. Brain Anatomy Institute, 113 pp.

POUX, C., CHEVRET, P., HUCHON, D., DE JONG, W. W. and DOUZERY, E. J. P. 2006. Arrival and diversification of caviomorph rodents and platyrrhine primates in South America. *Systematic Biology*, **55**, 228–244.

RAMBOLD, H., CHURCHLAND, A., SELIG, Y., JASMIN, L. and LISBERGER, S. G. 2002. Partial ablations of the flocculus and ventral paraflocculus in monkeys cause linked deficits in smooth pursuit eye movements and adaptive modification of the VOR. *Journal of Neurophysiology*, **87**, 912–924

RAMDARSHAN, A. and ORLIAC, M. J. 2016. Endocranial morphology of *Microchoerus erinaceus* (Euprimates, Tarsiiformes) and early evolution of the Euprimates brain. *American Journal of Physical Anthropology*, **159**, 5–16.

ROMER, A. S. 1966. *Vertebrate Paleontology*. University of Chicago Press, 478 pp.

ROSE, K. D., BEARD, K. C. and HOUDE, P. 1993. Exceptional new dentitions of the diminutive plesiadapiforms *Tinimomys* and *Niptomomys* (Mammalia), with comments on the upper incisors of plesiadapiforms. *Annals of the Carnegie Museum*, **62**, 351–361.

SCOTT, W. B. and OSBORN, H. F. 1890. The Mammalia of the Uinta Formation. *Transactions of the American Philosophical Society*, **16**, 461–572.

SILCOX, M. T., BENHAM, A. E. and BLOCH, J. I. 2010a. Endocasts of *Microsyops* (Microsyopidae, Primates) and the evolution of the brain in primitive primates. *Journal of Human Evolution*, **58**, 505–521.

SILCOX, M. T., BLOCH, J. I., BOYER, D. M. and HOUDE, P. 2010b. Cranial anatomy of Paleocene and Eocene *Labidolemur kayi* (Mammalia: Apatotheria), and the relationships of the Apatemyidae to other mammals. *Zoological Journal of the Linnean Society*, **160**, 773–825.

SILCOX, M. T., DALMNYN, C. K. and BLOCH, J. I. 2009. Virtual endocast of *Ignacius graybullianus* (Paromomyidae, Primates) and brain evolution in early Primates. *Proceedings of the National Academy of Sciences of the United States of America*, **106**, 10987–10992.

SILCOX, M. T., DALMNYN, C. K., HRENCHUK, A., BLOCH, J. I., BOYER, D. M. and HOUDE, P. 2011. Endocranial morphology of *Labidolemur kayi* (Apatemyidae, Apatotheria) and its relevance to the study of brain evolution in Euarchontoglires. *Journal of Vertebrate Paleontology*, **31**, 1314–1325.

SILCOX, M. T., GUNNELL, G. F. and BLOCH, J. I. 2020. Cranial anatomy of *Microsyops annectens* (Microsyopidae, Euarchonta, Mammalia) from the middle Eocene of Northwestern Wyoming. *Journal of Paleontology*, **94**, 979–1006.

SIMPSON, G. G. 1931. A new insectivore from the Oligocene, Ulan Gochu Horizon, of Mongolia. *American Museum Novitates*, **505**, 1–22.

SPRINGER, M. S., STANHOPE, M. J., MADSEN, O. and DE JONG, W. W. 2004. Molecules consolidate the placental mammal tree. *Trends in Ecology and Evolution*, **19**, 430–438.

SZALAY, F. S. and MCKENNA, M. C. 1971. Beginning of the age of mammals in Asia: the late Paleocene Gashato fauna, Mongolia. *Bulletin of the American Museum of Natural History*, **144**, 273–317.

TAN, J., SIMPSON, J. I. and VOOGD, J. 1995. Anatomical compartments in the white matter of the rabbit flocculus. *Journal of Comparative Neurology*, **356**, 1–22.

THEWISSEN, J. G. M. and GINGERICH, P. D. 1989. Skull and endocranial cast of *Eoryctes melanus*, a new palaeoryctid (Mammalia: Insectivora) from the early Eocene of western North America. *Journal of Vertebrate Paleontology*, **9**, 459–470.

TONG, Y. S., ZHENG, S. H. and QIU, Z. D. 1995. Cenozoic mammal ages of China. *Vertebrata PalAsiatica*, **33**, 290–314. [in Chinese]

TSUBAMOTO, T. 2014. Estimating body mass from the astragalus in mammals. *Acta Palaeontologica Polonica*, **59**, 259–265.

VON KOENIGSWALD, W., RUF, I. and GINGERICH, P. D. 2009. Cranial morphology of a new apatemyid, *Carcinella sigei* n. gen. n. sp. (Mammalia, Apatotheria) from the late Eocene of southern France. *Palaeontographica Abteilung A*, **288**, 53–91.

VOOGD, J. and BARMACK, N. H. 2006. Oculomotor cerebellum. *Progress in Brain Research*, **151**, 231–268.

VOOGD, J., SCHRAA-TAM, C. K., VAN DER GEEST, N. and DE ZEEUW, C. I. 2012. Visuomotor cerebellum in human and nonhuman primates. *The Cerebellum*, **11**, 392–410.

VISUALIZATION SCIENCES GROUP. 1995-2015. Avizo ® *9.0.1*. Konrad-Zuse-Zentrum für Informationstechnik, Berlin, Germany.

WAHLERT, J. H. 1974. The cranial foramina of protrogomorphous rodents; an anatomical and phylogenetic study. *Bulletin of the Museum of Comparative Zoology*, **146**, 363–410.

WANG, B. Y. 1975. Paleocene mammals from the Chaling Basin, Hunan. *Vertebrata PalAsiatica*, **13**, 154–162. [in Chinese]

WANG, B. Y. 1997. Problems and recent advances in the division of the continental Oligocene. *Journal of Stratigraphy*, **21**, 81–90.

WANG, B. Y. 2001. On Tsaganomyidae (Rodentia, Mammalia) of Asia. *American Museum Novitates*, **3317**, 1–50.

WANG, Y. Q., LI, Q., BAI, B., JIN, X., MAO, F. Y. and MENG, J. 2019. Paleogene integrative stratigraphy and timescale of China. *Science China Earth Sciences*, **62**, 287–309.

WANG, Y. Q., MENG, J., NI, X. J. and LI, C., K. 2007. Major events of Paleogene mammal radiation in China. *Geological Journal*, **42**, 415–430.

WIBLE, J. R. 1987. The eutherian stapedial artery: character analysis and implications for superordinal relationships. *Zoological Journal of the Linnean Society*, **91**, 107–135.

WIBLE, J. R. 1993. Cranial circulation and relationships of the colugo *Cynocephalus* (Dermoptera, Mammalia). *American Museum Novitates*, **3072**, 1–27.

WIBLE, J. R. and ROUGIER, G. W. 2000. Cranial anatomy of *Kryptobaatar dashzevegi* (Mammalia, Multituberculata), and its bearing on the evolution of mammalian characters. *Bulletin of the American Museum of Natural History*, **247**, 1–120.

WIBLE, J. R. and SHELLEY, S. L. 2020. Anatomy of the petrosal and middle ear of the brown rat, *Rattus norvegicus* (Berkenhout, 1769) (Rodentia, Muridae). *Annals of Carnegie Museum*, **86**, 1–35.

WOLNIEWICZ, A. S. and FOSTOWICZ-FRELIK, Ł. 2021. CT-informed skull osteology of *Palaeolagus haydeni* (Mammalia: Lagomorpha) and its bearing on the reconstruction of the early lagomorph body plan. *Frontiers in Ecology and Evolution*, **9**, 634757.

WOOD, A. E. 1937. The mammalian fauna of the White River Oligocene. Part II. Rodentia. *Transactions of the American Philosophical Society*, **28**, 157–269.

XIONG, G., NAGAO, S. and KITAZAWA, H. 2010. Mossy and climbing fiber collateral inputs in monkey cerebellar paraflocculus lobulus petrosus and hemispheric lobule VII and their relevance to oculomotor functions. *Neuroscience Letters*, **468**, 282–286.

XU, Q. 1976a. New materials of Anagalidae from the Palaeocene of Anhui (A). *Vertebrata PalAsiatica*, **14**, 174–184. [in Chinese]

XU, Q. 1976b. New materials of Anagalidae from the Palaeocene of Anhui (B). *Vertebrata PalAsiatica*, **14**, 242–251. [in Chinese]

YAPUNCICH, G. S., GLADMAN, J. T., BOYER, D. M. 2015. Predicting euarchontan body mass: A comparison of tarsal and dental variables. *American Journal of Physical Anthropology*, **157**, 472–506.

ZHAI, R.-J. 1978. More fossil evidence favouring an Early Eocene connection between Asia and Neoarctic. *Institute of Vertebrate Paleontology and Paleoanthropology Beijing Memoir*, **13**, 107–115.

ZHANG, Y. Y. and LI, J. G. 2000. The Tertiary chronostratigraphic researches and Tertiary chronostratigraphic chart of China. *Journal of Stratigraphy*, **24**, 120–125.

ZHANG, Z. Q. and WANG, J. 2016. On the geological age of mammalian fossils from Shanmacheng, Gansu Province. *Vertebrata PalAsiatica* 54: 351–357.

FIGURE CAPTIONS

Figure 1. Phylogenetic hypothesis of euarchontogliran relationships. Based on Korth & Emry (1991), Meng *et al*. (2003) and Silcox *et al*. (2010b); modified. Only groups represented by fossil endocasts discussed in the manuscript are included. Scandentia and Dermoptera are excluded because they are unknown from fossil skulls.

Figure 2. Transparent cranium with endocast of *Anagale gobiensis* (AMNH 26079) from the Ulan Gochu Formation at Twin Oboes, Nei Mongol, China. (a) dorsal, (b) left lateral, (c) right lateral and (d) ventral views. Scale bar represents: 1 cm.

Figure 3. Virtual endocast of *Anagale gobiensis* (AMNH 26079) in (a) dorsal, (b) ventral, (c) right lateral and (d) left lateral views. Scale bar represents: 5 mm.

Figure 4. Coronal slices of the cranium of *Anagale gobiensis* (AMNH 26079) at the level of the a) olfactory bulbs, b) main body of the cerebrum, and c) the petrosal lobules. Scale bar represents: 1 cm.

Figure 5. Bivariate plot of logarithmic olfactory bulb volume against logarithmic body mass for fossil Euarchontoglires. BM = Body mass. Data are given in Table S1.

Figure 6. Boxplot of olfactory bulb volume ratio of fossil Euprimates, Plesiadapiformes, fossil Rodentia, extant Rodentia, stem Lagomorpha (represented by *Megalagus*

turgidus), extant Lagomorpha, Apatemyidae (represented by *Labidolemur kayi*) and *Anagale gobiensis*. Data are given in Table S4.

Figure 7. Endocast morphology and relationships for Euarchontoglires. The topology of the tree is based on Fig. 1.

Figure 8. Interior of the cranium of *Anagale gobiensis* (AMNH 26079) sliced in the sagittal plane. Scale bar represents: 1 cm.

Figure 9. Virtual endocast of *Anagale gobiensis* (AMNH 26079) in oblique caudal view. Scale bar represents: 5 mm.

Figure 10. Boxplot of neocortical ratio of fossil Euprimates, plesiadapiforms, fossil Rodentia, extant Sciuroidea, stem Lagomorpha (represented by *Megalagus turgidus*), extant Lagomorpha and *Anagale gobiensis*. Data are given in Table S4.

Figure 11. Bivariate plot of logarithmic petrosal lobule volume against logarithmic body mass for selected Euarchontoglires. BM = Body mass. Data are given in Table S2.

Figure 12. Boxplot of petrosal lobule volume ratio of fossil Euprimates, Ischyromyidae, fossil Aplodontiidae (represented by *Mesogaulus paniensis* [*] and *Altasciurus relictus* [**]), extant Aplodontiidae (represented by the only living species, *Aplodontia rufa*),

fossil Sciuridae, extant Sciuridae, stem Lagomorpha (represented by *Megalagus turgidus*), extant Lagomorpha and *Anagale gobiensis*. Data are given in Table S4.

Figure 13. Bivariate plot of logarithmic endocranial volume against logarithmic body mass for fossil Euarchontoglires. BM = Body mass. Data are given in Table S1.

Figure 14. Encephalisation quotients (EQs) for *Anagale gobiensis* (AMNH 26079) compared to fossil Euarchontoglires. EQs based on Eisenberg (1981). Abbreviations: BoM↑, high body mass estimate used; BoM↓, low body mass estimate used; BrM↑, high brain mass estimate used; BrM↓, low brain mass estimate used. Data are given in Table S3.

TABLE CAPTIONS

Table 1. Quantitative measurements of the endocast of *Anagale gobiensis* (AMNH 26079). Calculations of EQ based on an estimated body mass of *Anagale gobiensis* of 1122.77—1464.68 g (see Tables 2 and 3). The total endocranial volume (TV) was calculated by doubling the volume of the more complete left side. The neocortical surface area (NS) was measured by doubling the area of the neocortex for the more complete left hemisphere.

Table 2. Body mass estimations for *Anagale gobiensis*, AMNH 26079. The body mass estimates indicated with an asterisk are argued to be the most likely to be correct (see discussion in the text).

Table 3. Calculation of encephalisation quotients (EQ) for *Anagale gobiensis*, AMNH 26079. For details on the body mass equations see Table 2.

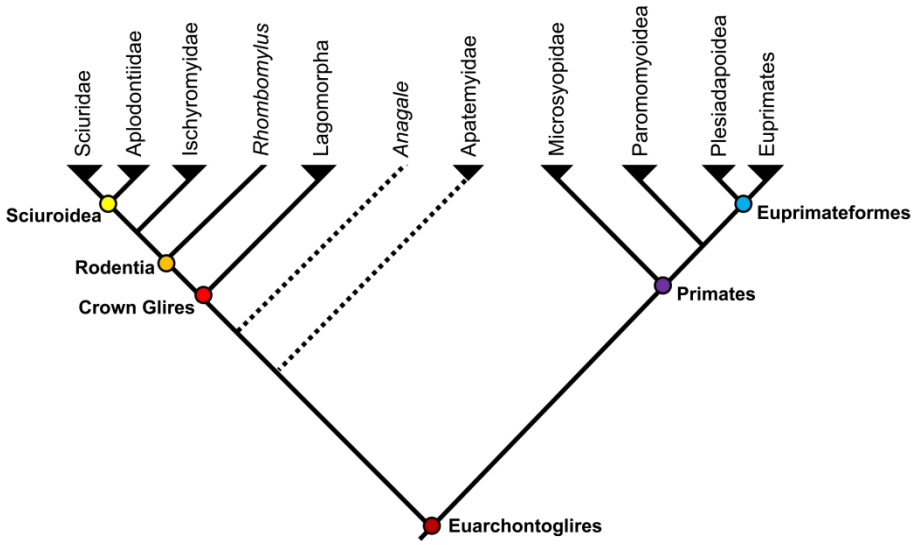

Figure 1. Phylogenetic hypothesis of euarchontogliran relationships. Based on Korth & Emry (1991), Meng et al. (2003) and Silcox et al. (2010b); modified. Only groups represented by fossil endocasts discussed in the manuscript are included. Scandentia and Dermoptera are excluded because they are unknown from fossil skulls.

338x190mm (300 x 300 DPI)

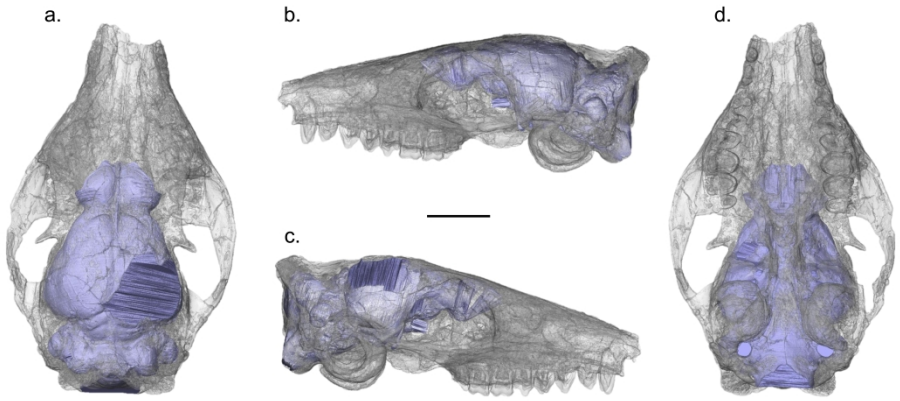

Figure 2. Translucid cranium with endocast of *Anagale gobiensis* (AMNH 26079) from the Ulan Gochu Formation at Twin Oboes, Nei Mongol, China. (a) dorsal, (b) left lateral, (c) right lateral and (d) ventral views. Scale bar represents: 1 cm.

338x190mm (600 x 600 DPI)

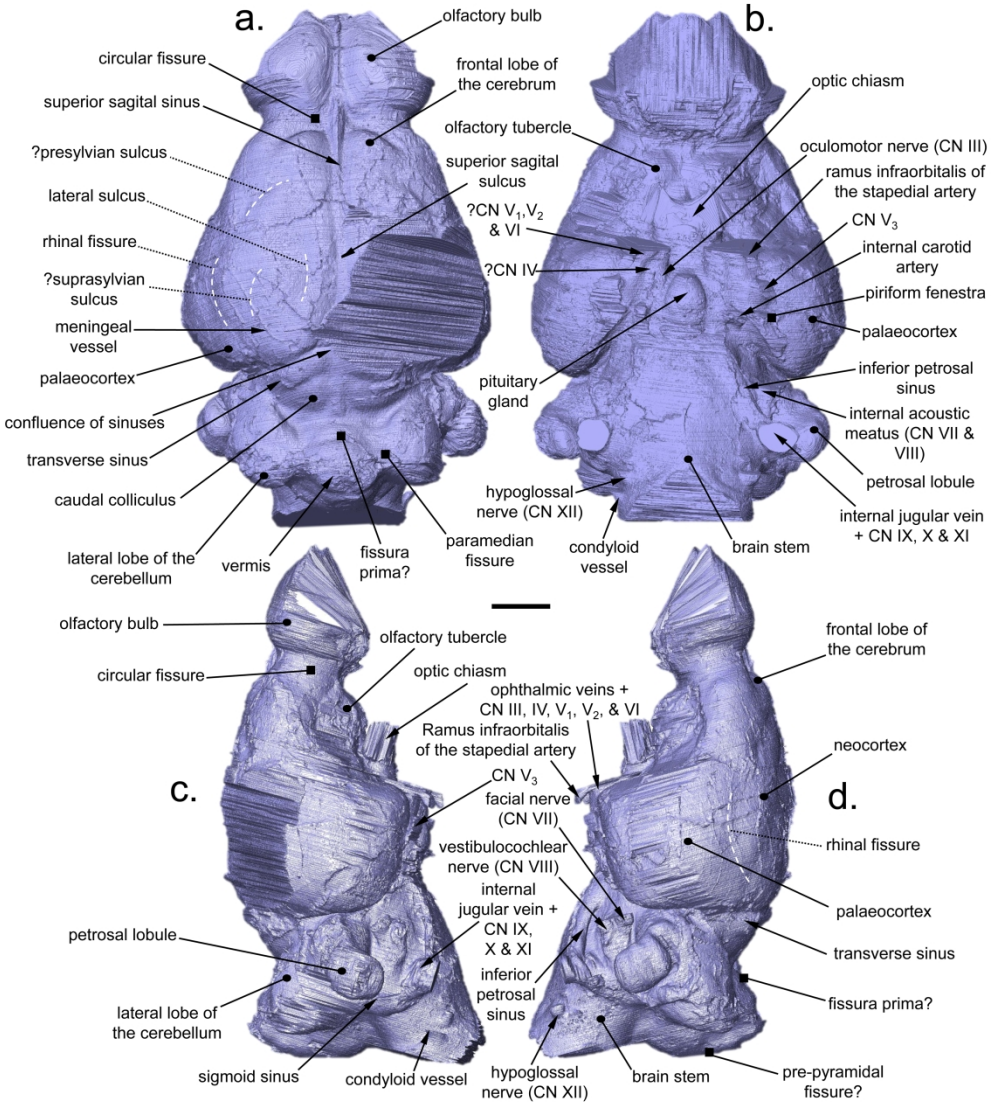

Figure 3. Virtual endocast of *Anagale gobiensis* (AMNH 26079) in (a) dorsal, (b) ventral, (c) right lateral and (d) left lateral views. Scale bar represents: 5 mm.

165x186mm (600 x 600 DPI)

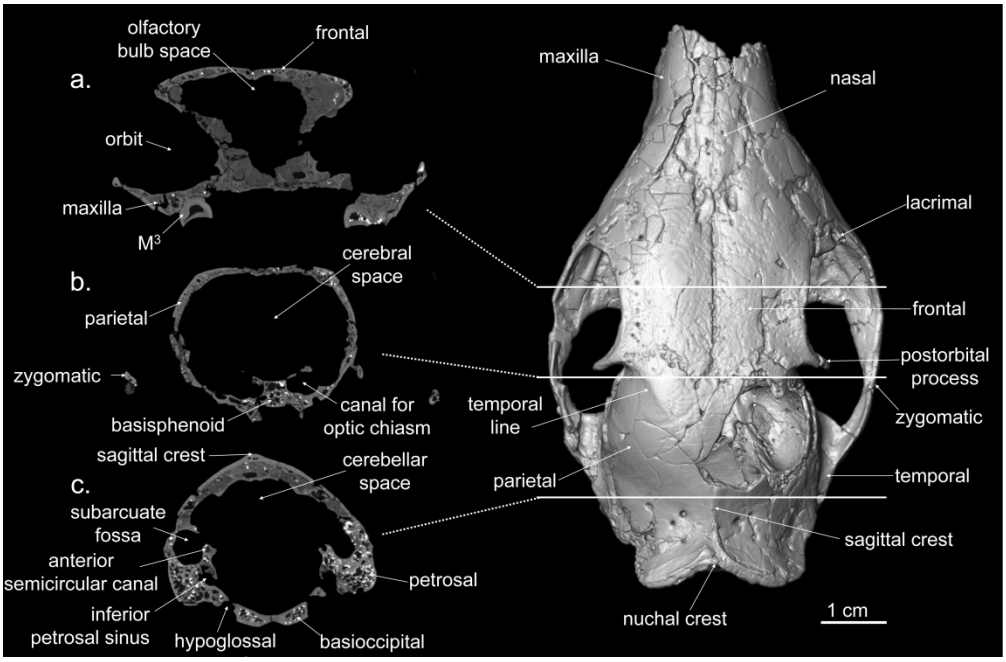

Figure 4. Coronal slices of the cranium of *Anagale gobiensis* (AMNH 26079) at the level of the a) olfactory bulbs, b) main body of the cerebrum, and c) the petrosal lobules. Scale bar represents: 1 cm.

165x108mm (600 x 600 DPI)

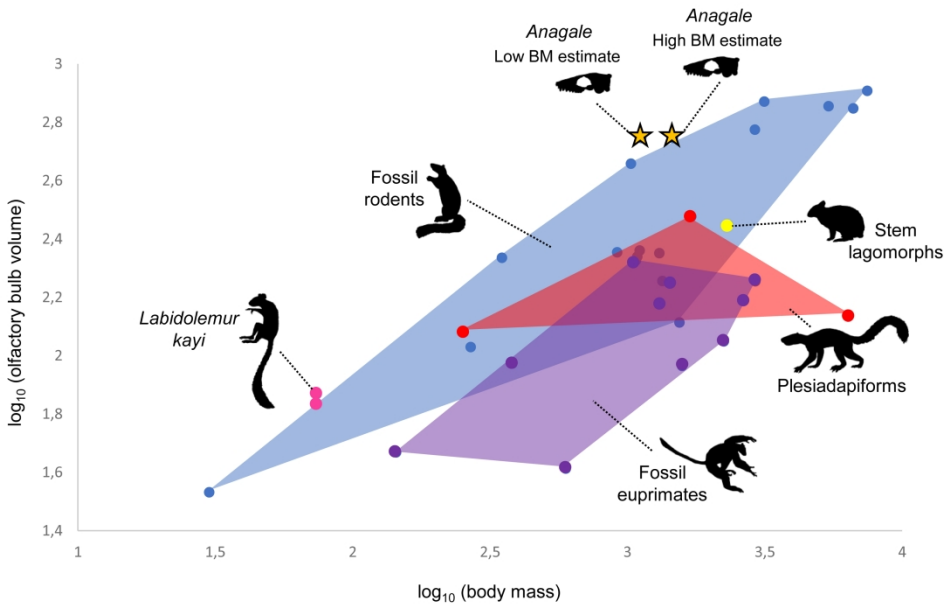

Figure 5. Bivariate plot of logarithmic olfactory bulb volume against logarithmic body mass for fossil Euarchontoglires. BM = Body mass. Data are given in Table S1.

165x101mm (600 x 600 DPI)

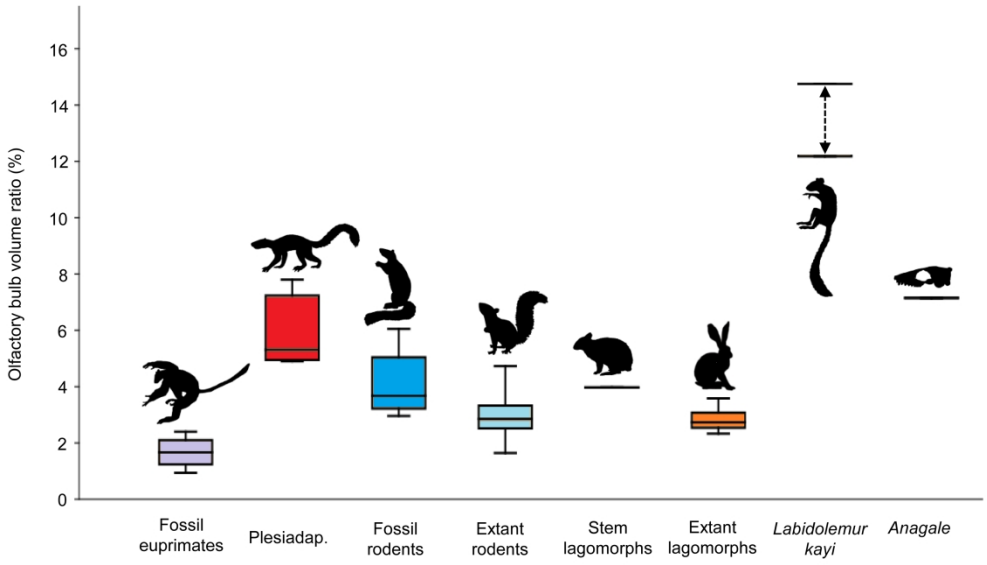

Figure 6. Boxplot of olfactory bulb volume ratio of fossil Euprimates, Plesiadapiformes, fossil Rodentia, extant Rodentia, stem Lagomorpha (represented by *Megalagus turgidus*), extant Lagomorpha, Apatemyidae (represented by *Labidolemur kayi*) and *Anagale gobiensis*. Data are given in Table S4.

165x98mm (600 x 600 DPI)

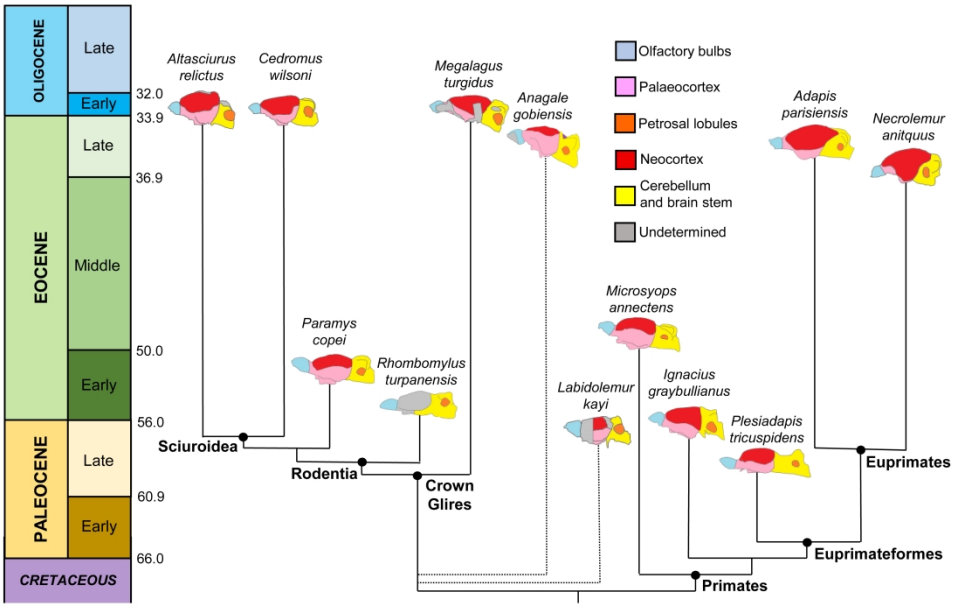

Figure 7. Endocast morphology and relationships for Euarchontoglires. The topology of the tree is based on Fig. 1.

165x103mm (600 x 600 DPI)

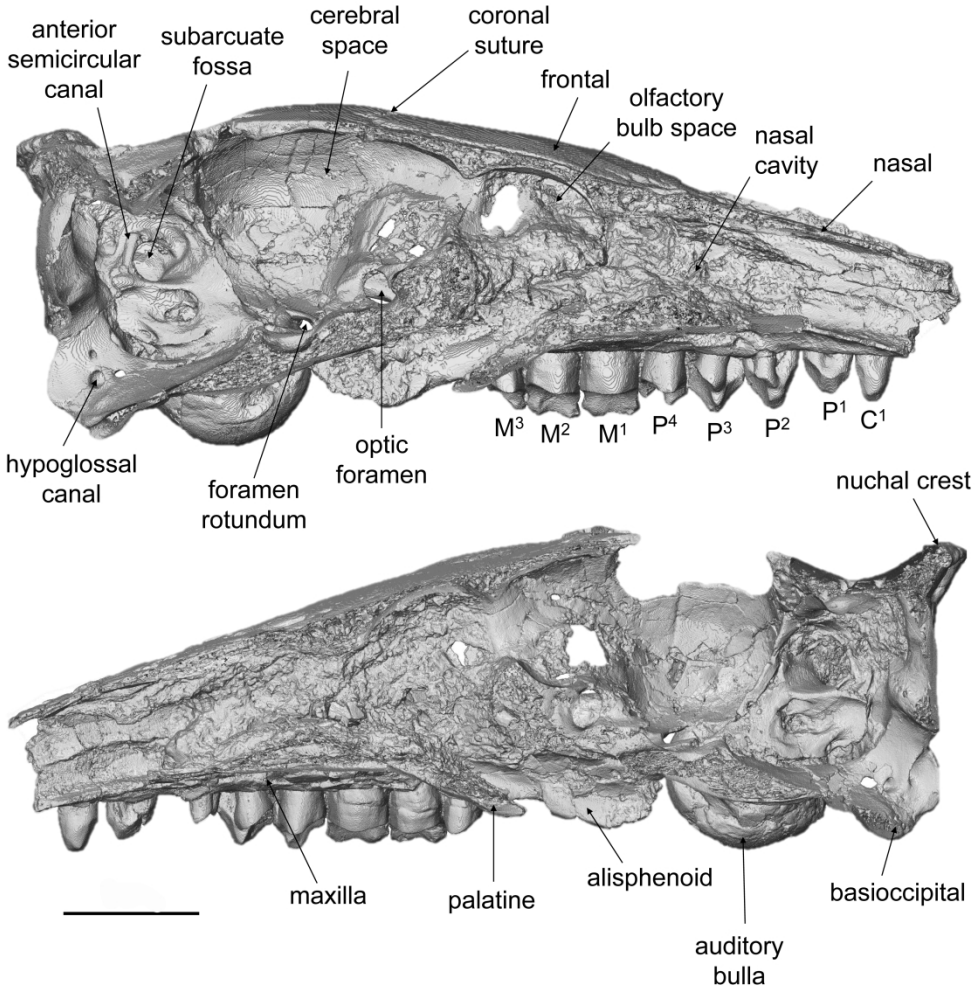

Figure 8. Interior of the cranium of *Anagale gobiensis* (AMNH 26079) sliced in the sagittal plane. Scale bar represents: 1 cm.

165x170mm (600 x 600 DPI)

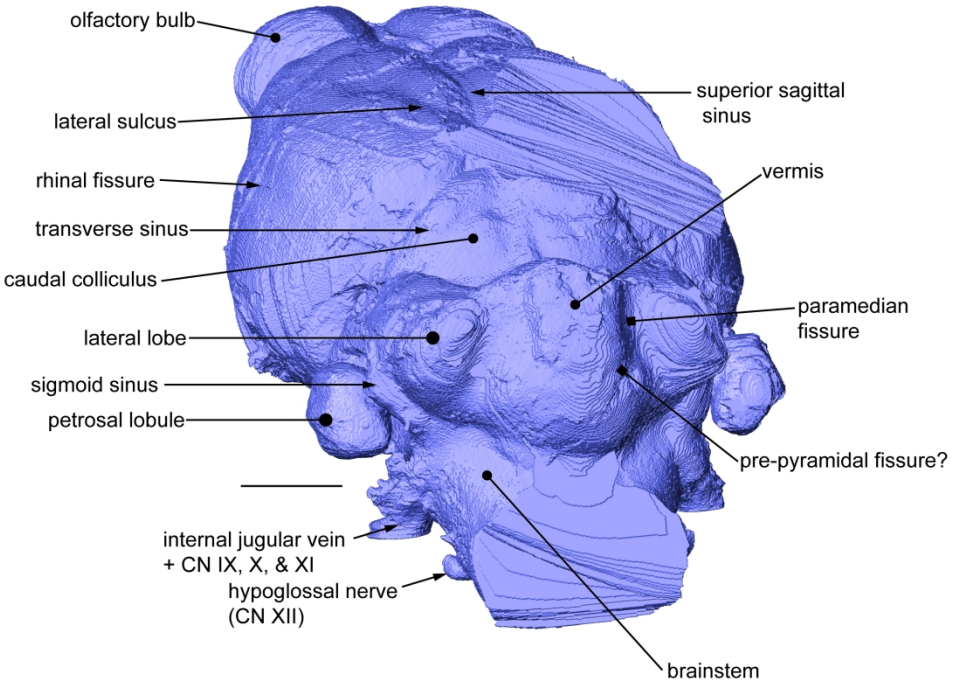

Figure 9. Virtual endocast of *Anagale gobiensis* (AMNH 26079) in oblique caudal view. Scale bar represents: 5 mm.

200x147mm (300 x 300 DPI)

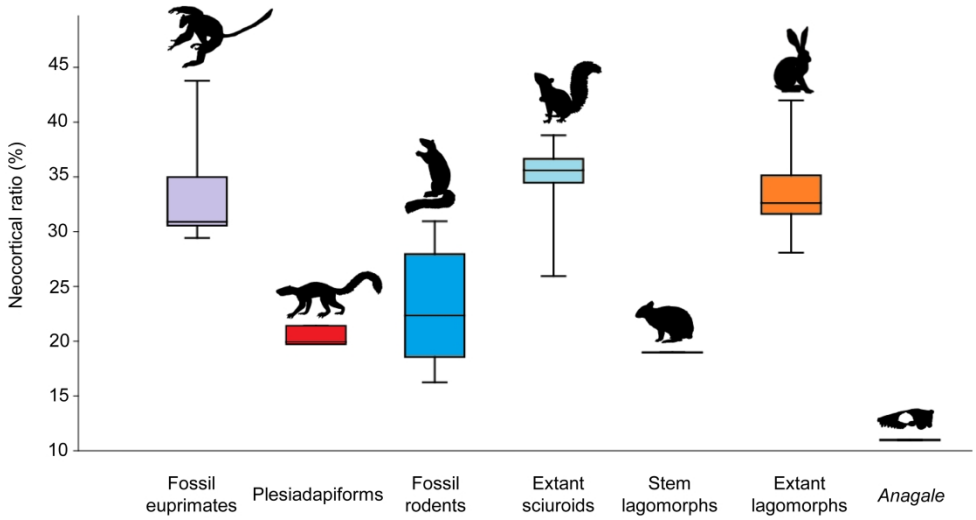

Figure 10. Boxplot of neocortical ratio of fossil Euprimates, plesiadapiforms, fossil Rodentia, extant Sciuroidea, stem Lagomorpha (represented by *Megalagus turgidus*), extant Lagomorpha and *Anagale gobiensis*. Data are given in Table S4.

165x93mm (600 x 600 DPI)

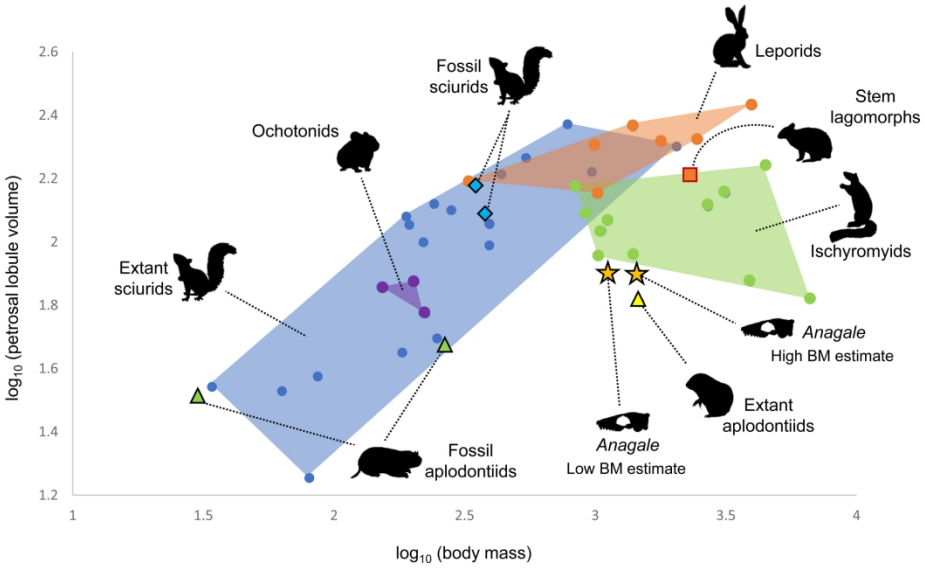

Figure 11. Bivariate plot of logarithmic petrosal lobule volume against logarithmic body mass for selected Euarchontoglires. BM = Body mass. Data are given in Table S2.

203x127mm (300 x 300 DPI)

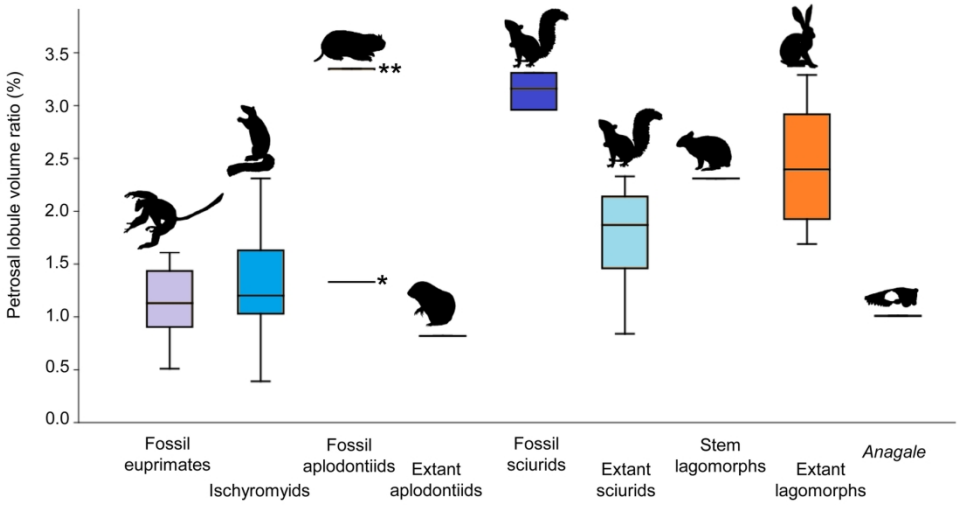

Figure 12. Boxplot of petrosal lobule volume ratio of fossil Euprimates, Ischyromyidae, fossil Aplodontiidae (represented by Mesogaulus paniensis [*] and Altasciurus relictus [**]), extant Aplodontiidae (represented by the only living species, Aplodontia rufa), fossil Sciuridae, extant Sciuridae, stem Lagomorpha (represented by Megalagus turgidus), extant Lagomorpha and Anagale gobiensis. Data are given in Table S4.

165x88mm (300 x 300 DPI)

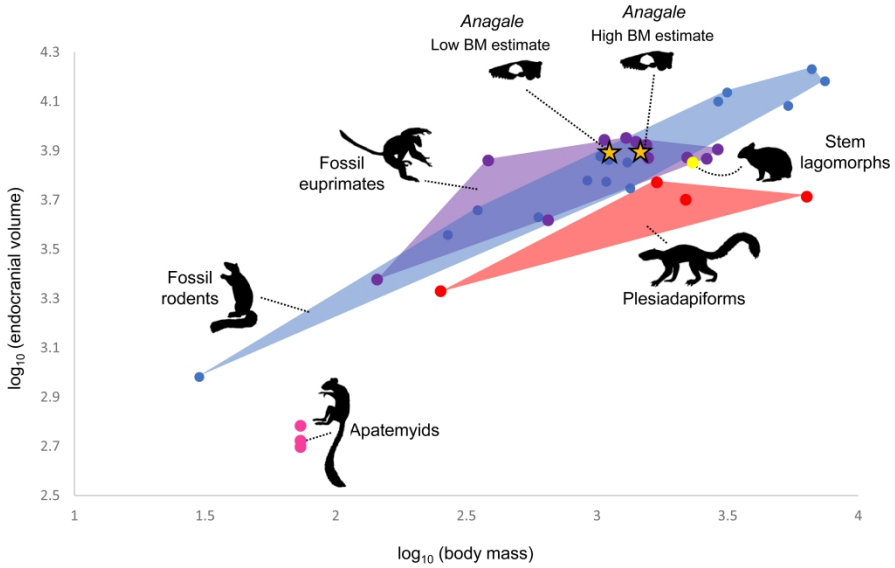

Figure 13. Bivariate plot of logarithmic endocranial volume against logarithmic body mass for fossil Euarchontoglires. BM = Body mass. Data are given in Table S1.

203x127mm (600 x 600 DPI)

Table 1.

Measurement (abbreviation); values in mm	
Total length (TL)	41.14
Olfactory bulb length (OL)	7.80
Olfactory bulb width (OW)	15.38
Olfactory bulb height (OH)	8.42
Maximum neocortex height (NMH)	5.17
Cerebrum total length (CRML)	19.92
Cerebrum maximal width (CRMW)	24.62
Cerebrum maximal height (CRMH)	17.38
Cerebellum length (vermis) (CLML)	12.35
Cerebellum width (without petrosal lobules) (CLW)	17.42
Length ratios; values in %	
OL/TL	18.96
CRML/TL	48.42
CLML/TL	30.02
CLW/CRMW	70.76
OW/CRMW	62.47
OW/CLW	88.29
NMH/CRMH	32.07
Surfaces (abbreviation); values in mm^2	
Total endocast area (TS)	3827.58
Neocortical surface area (NS)	420.24
Neocortical surface area (one side) (NS1)	210.12
Volumes (abbreviation); values in mm^3	
Total endocast (TV)	7798.04
Olfactory bulbs (right and left sides; OV)	557.78
Petrosal lobules (right and left sides; PLV)	79.11
Surface and volume ratios; values in %	
NS/TS	10.98
OV/TV	7.15
PLV/TV	1.01
Mass; values in mg	
Olfactory bulb mass	531.22
Petrosal lobule mass	75.34
Encephalization quotients	
Jerison's EQ	0.47-0.56
Eisenberg's EQ	0.61-0.74

Table 2.

Equation	Group	Anatomical landmark	Measurement	Body mass (g)	Source
Postcranial equations					
Gingerich (1990)	Mammalia	Tibial midshaft diameter[1]	5.39 mm	1430.89*	This paper
		Tibial length	58.60 mm	520.04	This paper
Tsubamoto (2014)	Mammalia	Trochlear width of astragalus	5.89 mm	1122.77*	This paper
Moncunill-Solé *et al*. (2014)	Rodentia	Distal femoral transversal diameter	13.17 mm	1464.68*	This paper
Moncunill-Solé *et al*. (2015)	Lagomorpha	Proximal tibial transversal diameter	13.33 mm	1311.26*	This paper
Cranial equations					
Kielan-Jaworowska (1983)	Mammalia	Cranial length	57.6 mm	305.76	This paper
Thewissen & Gingerich (1989)	Insectivora + Tupaiidae	Cranial length	57.6 mm	444.99	This paper
Millien & Bovy (2010)	Rodentia	Cranial length	57.6 mm	649.31	This paper
Bertrand *et al*. (2016a)	Rodentia	Cranial length	57.6 mm	531.39	This paper
Dental equations					
Conroy (1986)	Prosimii	M_1 area	19.58 mm^2	1756.11	López-Torres & Fostowicz-Frelik (2018)
Bertrand *et al*. (2016a)	Rodentia	Left toothrow length[2]	15.52 mm	1311.48*	This paper
		Right toothrow length[2]	15.66 mm	1348.56*	This paper

[1]The tibial shaft diameter in *Anagale gobiensis* was measured immediately distal to the tibial crest.

[2]Toothrow length in *Anagale gobiensis* is treated as P4-M3 toothrow length to be comparable to rodents.

Table 3.

Body mass equation	Jerison's (1973) EQ	Eisenberg's (1981) EQ
Gingerich (1990)	0.48	0.62
Tsubamoto (2014)	0.56	0.74
Moncunill-Solé *et al*. (2014)	0.47	0.61
Moncunill-Solé *et al*. (2015)	0.50	0.66
Bertrand *et al*. (2016a)	0.50	0.66

Order	Superfamily	Family	Species	Specimen number	Total Endocranial Volume (mm3)	Log Endocr Vol	Olfactory bulb volume (mm3)	Log OB Vol	Body mass (g)	Log Body Mass	Type of body mass equation used	Source
-	-	Anagalidae	*Anagale gobiensis* (low body mass estimate)	AMNH 26079	7798.04	3.891985459	557.78	2.746462938	1122.77	3.0502908	Trocheal width of astragalus (Tsubamoto, 2014)	This paper
-	-	Anagalidae	*Anagale gobiensis* (high body mass estimate)	AMNH 26079	7798.04	3.891985459	557.78	2.746462938	1464.67	3.165739786	Distal femoral transversal diameter (Moncunill-Solé et al., 2014)	This paper
Lagomorpha	-	Megalagidae	*Megalagus turgidus*	FMNH UC 1642	7052.78	3.848360337	280.1	2.447313109	2325.01	3.366424825	Width of occipital condyles (Moncunill-Solé et al., 2015)	López-Torres et al. (2020)
Rodentia	Sciuroidea	Aplodontiidae	*Altasciurus relictus*	USNM 437793	957.45	2.981113836	34	1.531478917	30.07	1.478133428	Cranial length (Bertrand et al., 2016)	Bertrand et al (2019)
Rodentia	Sciuroidea	Sciuridae	*Protosciurus* cf. *rachelae*	YPM 14736	4546.82	3.657707762	216.41	2.335277325	349.62	2.543596268	Cranial length (Bertrand et al., 2016)	Bertrand et al (2019)
Rodentia	Sciuroidea	Sciuridae	*Cedromus wilsoni*	USNM 256584	3609.87	3.557491562	106.97	2.029257936	268.89	2.429574651	Cranial length (Bertrand et al., 2016)	Bertrand et al (2019)
Rodentia	-	Ischyromyidae	*Paramys copei*	AMNH 4756	7526.65	3.876601721	455.45	2.65844166	1029.89	3.012790841	Cheektooth area (Bertrand et al., 2016)	Bertrand et al (2019)
Rodentia	-	Ischyromyidae	*Paramys delicatus*	AMNH 12506	12565.40	4.099176318	595.51	2.7748876	2913.82	3.46446272	Cranial length (Bertrand et al., 2016)	Bertrand et al (2019)
Rodentia	-	Ischyromyidae	*Pseudotomus horribilis*	USNM 17159	15188.20	4.181506307	808.92	2.907905573	7466.70	3.873128748	Cranial length (Bertrand et al., 2016)	Bertrand et al (2019)
Rodentia	-	Ischyromyidae	*Pseudotomus robustus*	USNM 17161	12063.00	4.081455328	717.06	2.855553074	5396.00	3.732071693	Cranial length (Bertrand et al., 2016)	Bertrand et al (2019)
Rodentia	-	Ischyromyidae	*Pseudotomus petersoni*	AMNH 2018	17014.90	4.230829401	704.34	2.847784203	6644.56	3.822466227	Cranial length (Bertrand et al., 2016)	Bertrand et al (2019)
Rodentia	-	Ischyromyidae	*Pseudotomus hians*	AMNH 5025	13679.10	4.136057524	743.20	2.871105117	3153.50	3.498792835	Cranial length (Bertrand et al., 2016)	Bertrand et al (2019)
Rodentia	-	Ischyromyidae	*Reithroparamys delicatissimus*	AMNH 12561	6433.98	4.136057524	206.31	2.314511859	843.33	3.498792835	Cranial length (Bertrand et al., 2016)	Bertrand et al (2019; 2021)
Rodentia	-	Ischyromyidae	*Rapamys atramontis*	AMNH 128706	7109.97	3.851867768	224.62	2.351444556	1307.61	3.116477912	Cranial length (Bertrand et al., 2016)	Bertrand et al (2019)
Rodentia	-	Ischyromyidae	*Rapamys atramontis*	AMNH 128704	6006.47	3.778619312	226.06	2.354219881	918.93	2.96328243	Cheektooth area (Bertrand et al., 2016)	Bertrand et al (2019)
Rodentia	-	Ischyromyidae	*Ischyromys typus*	ROMV 1007	5578.07	3.74648396	180.09	2.255489598	1342.23	3.127826941	Cranial length (Bertrand et al., 2016)	Bertrand et al (2019)
Rodentia	-	Ischyromyidae	*Ischyromys typus*	AMNH 12252	5934.55	3.773387793	218.46	2.339367953	1086.42	3.035997752	Cheektooth area (Bertrand et al., 2016)	Bertrand et al (2019)
Rodentia	-	Ischyromyidae	*Ischyromys typus*	AMNH F:AM 144638	7276.91	3.861947004	229.12	2.360063001	1109.01	3.044935462	Cheektooth area (Bertrand et al., 2016)	Bertrand et al (2019)
Primates	-	Microsyopidae	*Microsyops annectens*	UW 12362	5900	3.770852012	300.00	2.477121255	1710	3.23299611	Cranial length (Silcox et al., 2009a)	Silcox et al (2010)
Primates	Paromomyoidea	Paromomyidae	*Ignacius graybullianus*	USNM 421608	2140	3.330413773	120	2.079181246	253	2.403120521	Cranial length (Silcox et al., 2009a)	Silcox et al (2009b)
Primates	Plesiadapoidea	Plesiadapidae	*Plesiadapis tricuspidens*	MNHN CR 125	5210	3.716837723	136	2.133538908	6372	3.804275767	Cranial length (Martin, 1990)	Orliac et al. (2014)
Primates	Plesiadapoidea	Plesiadapidae	*Plesiadapis cookei*	UM 87990	5000	3.698970004	-	-	2239	3.342422681	Long bone lengths and diameters (Gingerich & Gunnell, 2005)	Gingerich & Gunnell (2005)
Primates	Adapoidea	Notharctidae	*Notharctus tenebrosus*	AMNH 127167	7380	3.868056362	155	2.190331698	2641	3.421768401	M1 area (Dagosto & Terranova, 1992)	Harrington et al. (2016)
Primates	Adapoidea	Notharctidae	*Notharctus tenebrosus*	USNM V 23277	8060	3.906335042	180	2.255272505	2923	3.465828815	M1 area (Dagosto & Terranova, 1992)	Harrington et al. (2016)
Primates	Adapoidea	Notharctidae	*Notharctus tenebrosus*	USNM V 23278	7430	3.870988814	112	2.049218023	2244	3.351022853	M1 area (Dagosto & Terranova, 1992)	Harrington et al. (2016)
Primates	Adapoidea	Notharctidae	*Smilodectes gracilis*	USNM V 17994	8630	3.936010796	178	2.250420002	1420	3.152288344	M1 area (Dagosto & Terranova, 1992)	Harrington et al. (2016)
Primates	Adapoidea	Notharctidae	*Smilodectes gracilis*	USNM V 17996	8990	3.953759692	150	2.176091259	1303	3.114944416	M1 area (Dagosto & Terranova, 1992)	Harrington et al. (2016)
Primates	Adapoidea	Notharctidae	*Smilodectes gracilis*	USNM V 21815	7440	3.871572936	92.2	1.964730921	1582	3.199206479	M1 area (Dagosto & Terranova, 1992)	Harrington et al. (2016)
Primates	Adapoidea	Notharctidae	*Smilodectes gracilis*	UM 32773	8420	3.925312091	130	2.113943352	1547	3.189490314	M1 area (Dagosto & Terranova, 1992)	Harrington et al. (2016)
Primates	Adapoidea	Adapidae	*Adapis parisiensis*	NHM M 1345	8810	3.944975908	212	2.326335861	1074	3.031004281	M1 area (Dagosto & Terranova, 1992)	Harrington et al. (2016)
Primates	-	-	*Rooneyia viejaensis*	TMM 40688-7	7234	3.859378504	94	1.973127854	381	2.580924976	Cranial length (Silcox et al., 2009a)	Kirk et al. (2014); Harrington et al. (2020)
Primates	Omomyoidea	Microchoeridae	*Microchoerus erinaceus*	UM-PRR 1771	4260	3.629409599	41	1.612783857	597	2.775974331	m1 area (Conroy, 1987)	Ramdarshan & Orliac (2016)
Primates	Omomyoidea	Microchoeridae	*Necrolemur antiquus*	MaPhQ 289	2360	3.372912003	46.6	1.668385917	144	2.158362492	Cranial length (Martin, 1990)	Harrington et al. (2020)
Apatotheria	-	Apatemyidae	*Labidolemur kayi* (assumption set 1)	USNM 530208/530221	607.79	2.78375355	74.05	1.869525063	74	1.86923172	Postcranial measurements (Armstrong et al., 2011)	Silcox et al (2011)
Apatotheria	-	Apatemyidae	*Labidolemur kayi* (assumption set 2)	USNM 530208/530221	605.52	2.782128492	74.05	1.869525063	74	1.86923172	Postcranial measurements (Armstrong et al., 2011)	Silcox et al (2011)
Apatotheria	-	Apatemyidae	*Labidolemur kayi* (assumption set 3)	USNM 530208/530221	501.88	2.700599889	74.05	1.869525063	74	1.86923172	Postcranial measurements (Armstrong et al., 2011)	Silcox et al (2011)
Apatotheria	-	Apatemyidae	*Labidolemur kayi* (assumption set 4)	USNM 530208/530221	524.13	2.719439018	68.22	1.833911715	74	1.86923172	Postcranial measurements (Armstrong et al., 2011)	Silcox et al (2011)

Table S1. Data for bivariate plots in Figures 5 and 13, including endocranial volume, olfactory bulb volume, and body mass for *Anagale gobiensis*, stem lagomorphs, fossil rodents, plesiadapiforms, fossil euprimates, and apatemyids. Information on how body mass was estimated for each species is included.

Order	Family	Species	Specimen	Body mass (g)	Petrosal lobule volume (mm3)	Log Body mass	Log PL volume
-	Anagalidae	*Anagale gobiensis* (low body mass estimate)	AMNH 26079	1122.77	77.98	3.0502908	1.8919832
-	Anagalidae	*Anagale gobiensis* (high body mass estimate)	AMNH 26079	1464.67	77.98	3.1657398	1.8919832
Lagomorpha	Leporidae	*Brachylagus idahoensis*	AMNH 92869	339.56	153.04	2.5309165	2.184805
Lagomorpha	Leporidae	*Lepus americanus phaeonotus*	AMNH 97648	998.68	201.00	2.9994264	2.3031961
Lagomorpha	Leporidae	*Lepus arcticus*	AMNH 42139	4003.10	270.10	3.6023964	2.4315246
Lagomorpha	Leporidae	*Lepus americanus bairdii*	AMNH 99352	1396.22	231.02	3.1449539	2.3636496
Lagomorpha	Leporidae	*Oryctolagus cuniculus*	AMNH 34816	1796.07	207.03	3.2543233	2.3160333
Lagomorpha	Leporidae	*Poelagus marjorita*	AMNH 51052	2480.24	210.83	3.3944937	2.3239324
Lagomorpha	Leporidae	*Romerolagus diazi*	AMNH 148172	1027.79	142.54	3.0119044	2.1539368
Lagomorpha	Ochotonidae	*Ochotona pallasi*	AMNH 59712	223.85	59.32	2.3499571	1.7732011
Lagomorpha	Ochotonidae	*Ochotona princeps princeps*	AMNH 120698	202.92	74.74	2.3073249	1.8735531
Lagomorpha	Ochotonidae	*Ochotona princeps schisticeps*	AMNH 40547	155.10	71.80	2.1906118	1.8561244
Lagomorpha	Megalagidae	*Megalagus turgidus*	FMNH UC 1642	2325.01	162.59	3.3664248	2.2110938
Rodentia	Extant Aplodontiidae	*Aplodontia rufa*	AMNH 42389	1475.86	64.41	3.1690452	1.8089533
Rodentia	Fossil Aplodontiidae	*Altasciurus relictus*	USNM 437793	30.07	32.08	1.4781334	1.5062208
Rodentia	Fossil Aplodontiidae	*Mesogaulus paniensis*	AMNH F:AM 65511	266.48	46.27	2.4256646	1.6652995
Rodentia	Extant Sciuridae	*Callosciurus* sp.	USNM 294865	379.50	123.91	2.5792118	2.0931064
Rodentia	Extant Sciuridae	*Dremomys rufigenis*	USNM 488602	281.57	125.71	2.4495864	2.0993698
Rodentia	Extant Sciuridae	*Lariscus insignis*	USNM 488570	194.45	113.00	2.2888079	2.0530784
Rodentia	Extant Sciuridae	*Rhinosciurus laticaudatus*	USNM 488511	393.21	97.36	2.5946246	1.9883806
Rodentia	Extant Sciuridae	*Aeromys tephromelas*	USNM 481190	971.69	166.10	2.9875277	2.2203696
Rodentia	Extant Sciuridae	*Glaucomys volans*	AMNH 240290	63.30	33.73	1.8014037	1.5280163
Rodentia	Extant Sciuridae	*Hylopetes spadiceus*	USNM 488639	80.57	17.93	1.9061734	1.2535803
Rodentia	Extant Sciuridae	*Petaurista petaurista*	USNM 589079	2050.35	199.90	3.311828	2.3008128
Rodentia	Extant Sciuridae	*Pteromys buechneri*	USNM 172622	86.73	37.53	1.9381693	1.5743786
Rodentia	Extant Sciuridae	*Pteromyscus pulverulentus*	USNM 481178	248.25	49.50	2.3948893	1.6946052
Rodentia	Extant Sciuridae	*Ratufa affinis*	USNM 488104	783.80	234.90	2.8942053	2.370883
Rodentia	Extant Sciuridae	*Sciurus carolinensis*	AMNH 258346	437.91	163.26	2.6413849	2.2128798
Rodentia	Extant Sciuridae	*Sciurus granatensis*	USNM 441999	242.05	131.63	2.3839051	2.1193549
Rodentia	Extant Sciuridae	*Tamiasciurus hudsonicus*	USNM 549146	189.29	120.02	2.2771277	2.0792536
Rodentia	Extant Sciuridae	*Eutamias minimus*	USNM 298500	34.17	34.80	1.533645	1.5415792
Rodentia	Extant Sciuridae	*Funisciurus pyrropus*	USNM 294865	220.16	99.54	2.3427384	1.9979976
Rodentia	Extant Sciuridae	*Heliosciurus rufobrachium*	USNM 378091	394.39	113.61	2.5959259	2.0554166
Rodentia	Extant Sciuridae	*Paraxerus cepapi*	USNM 367956	182.66	44.66	2.2616435	1.6499187
Rodentia	Extant Sciuridae	*Protoxerus stangeri*	USNM 435027	544.05	183.74	2.7356388	2.2642037
Rodentia	Extant Sciuridae	*Xerus rutilus*	AMNH 179092	353.90	111.95	2.5488832	2.0490241
Rodentia	Extant Sciuridae	*Marmota marmota*	AMNH 146619	4546.97	127.40	3.6577223	2.1051694
Rodentia	Extant Sciuridae	*Cynomys ludovicianus*	AMNH114522	938.70	70.97	2.972525	1.8510748
Rodentia	Extant Sciuridae	*Urocitellus richardsonii*	AMNH 15062	245.78	55.33	2.3905463	1.7429607
Rodentia	Fossil Sciuridae	*Cedromus wilsoni*	USNM 256584	393.49	113.96	2.5949337	2.0567524
Rodentia	Fossil Sciuridae	*Protosciurus* cf. *rachelae*	YPM 14736	349.62	150.42	2.5435963	2.1773056
Rodentia	Ischyromyidae	*Ischyromys typus*	AMNH F:AM 144638	1109.01	116.58	3.0449355	2.0666241
Rodentia	Ischyromyidae	*Ischyromys typus*	ROMV 1007	1401.80	91.12	3.1466861	1.9596137
Rodentia	Ischyromyidae	*Paramys copei*	AMNH 4756	1029.89	89.99	3.0127908	1.9541943
Rodentia	Ischyromyidae	*Paramys delicatus*	AMNH 12506	2704.83	129.30	3.43214	2.1115985
Rodentia	Ischyromyidae	*Pseudotomus hians*	AMNH 5025	3153.50	142.40	3.4987928	2.15351
Rodentia	Ischyromyidae	*Pseudotomus horribilis*	USNM 17159	4472.67	173.80	3.6505669	2.2400498
Rodentia	Ischyromyidae	*Pseudotomus robustus*	USNM 17161	3911.71	74.80	3.5923667	1.8739016
Rodentia	Ischyromyidae	*Pseudotomus petersoni*	AMNH 2018	6644.56	65.80	3.8224662	1.8182259
Rodentia	Ischyromyidae	*Rapamys atramontis*	AMNH 128704	918.93	123.02	2.9632824	2.0899757
Rodentia	Ischyromyidae	*Rapamys atramontis*	AMNH 128706	1057.82	108.09	3.0244118	2.0337855
Rodentia	Ischyromyidae	*Reithroparamys delicatissimus*	AMNH 12561	843.33	148.86	2.9259975	2.172778
Primates	-	*Rooneyia viejaensis*	TMM 40688-7	381	60.53	2.580925	1.7819685
Primates	Adapoidea	*Adapis parisiensis*	NHM M 1345	1074	44.92	3.0310043	1.6524194
Primates	Adapoidea	*Notharctus tenebrosus*	AMNH 127167	2641	103.90	3.4217684	2.0166114
Primates	Adapoidea	*Notharctus tenebrosus*	USNM V 23277	2923	78.26	3.4658288	1.8935393
Primates	Adapoidea	*Smilodectes gracilis*	USNM V 17996	1303	111.35	3.1149444	2.0466863
Primates	Adapoidea	*Smilodectes gracilis*	USNM V 21815	1582	120.08	3.1992065	2.0794779
Primates	Adapoidea	*Smilodectes gracilis*	UM 32773 (=MPM 2612)	1547	122.63	3.1894903	2.0885932
Primates	Omomyoidea	*Microchoerus erinaceus*	UM-PRR1771	597	48.25	2.7759743	1.683536
Primates	Omomyoidea	*Necrolemur antiquus*	MaPhQ 289	144	25.59	2.1583625	1.4081314

Table S2. Data for the bivariate plot in Figure 11, including petrosal lobule volume and body mass for *Anagale gobiensis*, living and fossil lagomorphs, and living and fossil r

Group	Species	Body mass (g)	Brain mass (g)	Jerison's EQ	Eisenberg's EQ	Source
Anagalidae	*Anagale gobiensis* (low body mass estimate)	1122.77	7.4267	0.559656	0.74277404	This paper
Anagalidae	*Anagale gobiensis* (high body mass estimate)	1464.67	7.4267	0.468346	0.61012735	This paper
Stem lagomorph	*Megalagus turgidus*	2325.01	6.71693	0.310803	0.39200494	López-Torres et al. (2020)
Extant Lagomorpha	*Brachylagus idahoensis*	339.561082	4.90014	0.822835	1.18741999	López-Torres et al. (2020)
Extant Lagomorpha	*Lepus americanus phaeonotus*	998.681398	9.73476	0.793465	1.06175485	López-Torres et al. (2020)
Extant Lagomorpha	*Lepus americanus bairdii*	1396.21846	9.1093	0.593178	0.7753435	López-Torres et al. (2020)
Extant Lagomorpha	*Lepus arcticus*	4003.10484	15.191	0.488425	0.59304291	López-Torres et al. (2020)
Extant Lagomorpha	*Oryctolagus cuniculus*	1796.06978	8.91727	0.490517	0.62995199	López-Torres et al. (2020)
Extant Lagomorpha	*Romerolagus diazi*	1027.79098	5.73354	0.458422	0.61219303	López-Torres et al. (2020)
Extant Lagomorpha	*Poelagus marjorita marjorita*	2480.24151	11.2456	0.4983	0.6256518	López-Torres et al. (2020)
Extant Lagomorpha	*Ochotona pallasi*	223.84704	2.03624	0.452043	0.67164444	López-Torres et al. (2020)
Extant Lagomorpha	*Ochotona princeps princeps*	202.923758	2.16221	0.512629	0.76691336	López-Torres et al. (2020)
Extant Lagomorpha	*Ochotona princeps schisticeps*	155.100148	2.36176	0.670416	1.02201659	López-Torres et al. (2020)
Fossil Sciuroidea	*Altasciurus relictus*	30.07	0.91185	0.776951	1.32855846	Bertrand et al. (2019)
Fossil Sciuroidea	*Mesogaulus paniensis*	266.48	3.30	0.65	0.96	Bertrand et al. (2018)
Fossil Sciuroidea	*Protosciurus* cf. *rachelae*	349.62	4.3303	0.713063	1.02690931	Bertrand et al. (2019)
Fossil Sciuroidea	*Cedromus wilsoni*	268.89	3.43797	0.675003	0.99012925	Bertrand et al. (2019)
Ischyromyidae	*Paramys copei*	1029.89	7.16824	0.57235	0.76422646	Bertrand et al. (2019)
Ischyromyidae	*Paramys delicatus*	2913.82	11.967	0.47601	0.59096189	Bertrand et al. (2019)
Ischyromyidae	*Pseudotomus horribilis*	7466.70	14.465	0.306295	0.35602181	Bertrand et al. (2019)
Ischyromyidae	*Pseudotomus robustus*	5396.00	11.4886	0.30241	0.3595902	Bertrand et al. (2019)
Ischyromyidae	*Pseudotomus petersoni*	6644.56	16.2047	0.371028	0.43480043	Bertrand et al. (2019)
Ischyromyidae	*Pseudotomus hians*	3153.50	13.0277	0.491469	0.60678718	Bertrand et al. (2019)
Ischyromyidae	*Rapamys atramontis*	1307.61	6.7714	0.460741	0.605006	Bertrand et al. (2019)
Ischyromyidae	*Rapamys atramontis*	918.93	5.72045	0.493003	0.66355341	Bertrand et al. (2019)
Ischyromyidae	*Ischyromys typus*	1342.23	5.31245	0.355197	0.46556207	Bertrand et al. (2019)
Ischyromyidae	*Ischyromys typus*	1086.42	5.65195	0.43541	0.57920863	Bertrand et al. (2019)
Ischyromyidae	*Ischyromys typus*	1109.01	6.93039	0.526586	0.6994881	Bertrand et al. (2019)
Plesiadapiformes	*Microsyops annectens*	1710	5.61905	0.319429	0.41388806	Silcox et al. (2010)
Plesiadapiformes	*Ignacius graybullianus*	253	2.0381	0.416824	0.6140308	Silcox et al. (2009)
Plesiadapiformes	*Plesiadapis tricuspidens*	6372	4.9619	0.116843	0.13732804	Orliac et al. (2014)
Plesiadapiformes	*Plesiadapis cookei*	2200	4.7619	0.228653	0.28950948	Gingerich & Gunnell (2005)
Apatemyidae	*Labidolemur kayi* (low brain mass estimate)	74	0.47798	0.222762	0.35764366	Silcox et al. (2011)
Apatemyidae	*Labidolemur kayi* (high brain mass estimate)	74	0.57884	0.269769	0.43311371	Silcox et al. (2011)
Euprimates	*Notharctus tenebrosus*	2641	7.02857	0.298608	0.37327879	Harrington et al. (2016)
Euprimates	*Notharctus tenebrosus*	2923	7.67619	0.304691	0.3781876	Harrington et al. (2016)
Euprimates	*Notharctus tenebrosus*	2244	7.07619	0.3353	0.42395277	Harrington et al. (2016)
Euprimates	*Smilodectes gracilis*	1420	8.21905	0.529184	0.69088059	Harrington et al. (2016)
Euprimates	*Smilodectes gracilis*	1303	8.5619	0.583951	0.76698416	Harrington et al. (2016)
Euprimates	*Smilodectes gracilis*	1582	7.08571	0.42436	0.54985188	Harrington et al. (2016)
Euprimates	*Smilodectes gracilis*	1547	8.01905	0.487509	0.63266649	Harrington et al. (2016)
Euprimates	*Adapis parisiensis*	1074	8.39048	0.651377	0.86719808	Harrington et al. (2016)
Euprimates	*Rooneyia viejaensis*	381	6.88952	1.070997	1.53313215	Kirk et al. (2014)
Euprimates	*Microchoerus erinaceus*	597	4.05714	0.466806	0.64755128	Ramdarshan & Orliac (2016)
Euprimates	*Necrolemur antiquus*	144	2.36	0.70409	1.08482846	Harrington et al. (2020)
Extant Rodentia	*Acomys dimidiatus*	76	0.97	0.444064	0.7116141	Bertrand et al. (2019)
Extant Rodentia	*Acomys dimidiatus*	50.5	0.884	0.532189	0.87758969	Bertrand et al. (2019)
Extant Rodentia	*Aeromys tephromelas*	904.59	10.92	0.95071	1.28101056	Bertrand et al. (2019)
Extant Rodentia	*Allactaga elater*	80	1.9	0.840431	1.34196713	Bertrand et al. (2019)
Extant Rodentia	*Allactaga sibirica*	193	3.5	0.85815	1.28834004	Bertrand et al. (2019)
Extant Rodentia	*Allactaga sibirica*	106	2	0.732645	1.1470399	Bertrand et al. (2019)
Extant Rodentia	*Aplodontia rufa*	1475.86	7.52	0.471755	0.61424253	Bertrand et al. (2019)
Extant Rodentia	*Aplodontia rufa*	982.00	7.60	0.626495	0.83931688	Bertrand et al. (2019)
Extant Rodentia	*Aplodontia rufa*	870.00	8.40	0.750966	1.01463516	Bertrand et al. (2019)
Extant Rodentia	*Aplodontia rufa*	710.00	8.40	0.860508	1.17929641	Bertrand et al. (2019)
Extant Rodentia	*Aplodontia rufa*	985.00	8.80	0.723934	0.96964939	Bertrand et al. (2019)
Extant Rodentia	*Aplodontia rufa*	887.00	8.30	0.732467	0.98830156	Bertrand et al. (2019)
Extant Rodentia	*Apodemus agrarius*	28.5	0.632	0.5582	0.95809098	Bertrand et al. (2019)
Extant Rodentia	*Apodemus agrarius agrarius*	26.2	0.62	0.57936	1.00028465	Bertrand et al. (2019)
Extant Rodentia	*Apodemus flavicollis*	30	0.75	0.640042	1.09462762	Bertrand et al. (2019)
Extant Rodentia	*Apodemus flavicollis flavicollis*	33	0.8	0.640478	1.0880893	Bertrand et al. (2019)
Extant Rodentia	*Apodemus sylvaticus*	19.4	0.59	0.674285	1.18892265	Bertrand et al. (2019)
Extant Rodentia	*Apodemus sylvaticus*	22	0.564	0.592481	1.03552643	Bertrand et al. (2019)
Extant Rodentia	*Apodemus sylvaticus*	21.6	0.59	0.627461	1.09807273	Bertrand et al. (2019)
Extant Rodentia	*Apodemus sylvaticus sylvaticus*	19	0.6	0.695353	1.22785888	Bertrand et al. (2019)
Extant Rodentia	*Arvicola amphibius*	137.8	1.53	0.470125	0.7226398	Bertrand et al. (2019)
Extant Rodentia	*Arvicola amphibius*	131	1.5	0.476802	0.73550456	Bertrand et al. (2019)
Extant Rodentia	*Arvicola amphibius*	84.5	1.086	0.463078	0.73659833	Bertrand et al. (2019)
Extant Rodentia	*Atherurus africanus*	1600	17.2	1.02232	1.3235932	Bertrand et al. (2019)
Extant Rodentia	*Atherurus africanus*	3620	25.3	0.870171	1.06402308	Bertrand et al. (2019)
Extant Rodentia	*Atherurus africanus*	1925	17.8	0.934696	1.19458244	Bertrand et al. (2019)
Extant Rodentia	*Atherurus africanus*	2250	23	1.087888	1.37526896	Bertrand et al. (2019)
Extant Rodentia	*Atlantoxerus getulus*	251.00	3.75	0.771515	1.13716435	Bertrand et al. (2019)
Extant Rodentia	*Brachytarsomys albicauda*	300	2.47	0.450655	0.65599736	Bertrand et al. (2019)
Extant Rodentia	*Brachyuromys ramirohitra*	94	1.4	0.555842	0.87758318	Bertrand et al. (2019)
Extant Rodentia	*Callosciurus* sp.	437.35	6.67	0.945942	1.34110378	Bertrand et al. (2019)
Extant Rodentia	*Callospermophilus lateralis*	246.00	2.98	0.621223	0.91693369	Bertrand et al. (2019)
Extant Rodentia	*Callospermophilus lateralis*	217.00	3.10	0.701592	1.0446931	Bertrand et al. (2019)
Extant Rodentia	*Capromys pilorides*	7000	11	0.243218	0.28398474	Bertrand et al. (2019)
Extant Rodentia	*Castor canadensis*	20500	44	0.473583	0.51289644	Bertrand et al. (2019)
Extant Rodentia	*Castor canadensis*	18000	53	0.622389	0.68021951	Bertrand et al. (2019)
Extant Rodentia	*Castor canadensis*	14500	45	0.610822	0.67775864	Bertrand et al. (2019)
Extant Rodentia	*Castor canadensis*	22500	52	0.525847	0.56580027	Bertrand et al. (2019)
Extant Rodentia	*Castor canadensis*	8000	38	0.768302	0.88873416	Bertrand et al. (2019)
Extant Rodentia	*Castor canadensis*	9750	48	0.850016	0.96973415	Bertrand et al. (2019)
Extant Rodentia	*Castor canadensis*	12500	42	0.629707	0.70600983	Bertrand et al. (2019)
Extant Rodentia	*Castor canadensis*	16000	38	0.482883	0.53212012	Bertrand et al. (2019)
Extant Rodentia	*Castor canadensis*	5500	43	1.117491	1.32701226	Bertrand et al. (2019)
Extant Rodentia	*Castor canadensis*	20000	40	0.437712	0.47486774	Bertrand et al. (2019)
Extant Rodentia	*Castor canadensis*	4180	25.48	0.795848	0.96339379	Bertrand et al. (2019)
Extant Rodentia	*Castor canadensis*	5380	29.52	0.778594	0.92600288	Bertrand et al. (2019)
Extant Rodentia	*Castor canadensis*	14500	45	0.610822	0.67775864	Bertrand et al. (2019)
Extant Rodentia	*Castor fiber*	14300	41.4	0.56721	0.62997968	Bertrand et al. (2019)

Extant Rodentia	*Castor fiber*	16900	38.8	0.475298	0.52175958	Bertrand et al. (2019)
Extant Rodentia	*Castor fiber*	25000	45	0.424045	0.45290986	Bertrand et al. (2019)
Extant Rodentia	*Castor fiber*	23100	45.5	0.452075	0.48552702	Bertrand et al. (2019)
Extant Rodentia	*Castor fiber*	20000	39	0.426769	0.46299604	Bertrand et al. (2019)
Extant Rodentia	*Cavia aperea*	163	2.7	0.741339	1.12621111	Bertrand et al. (2019)
Extant Rodentia	*Cavia aperea*	260	3	0.602432	0.88575955	Bertrand et al. (2019)
Extant Rodentia	*Cavia aperea*	430	3.9	0.559061	0.7935473	Bertrand et al. (2019)
Extant Rodentia	*Cavia aperea*	647	5.46	0.595258	0.82110433	Bertrand et al. (2019)
Extant Rodentia	*Cavia aperea*	460	4.2	0.575467	0.81298656	Bertrand et al. (2019)
Extant Rodentia	*Cavia aperea*	792	4.7	0.447477	0.60857778	Bertrand et al. (2019)
Extant Rodentia	*Cavia aperea*	540	4.1	0.504544	0.70483481	Bertrand et al. (2019)
Extant Rodentia	*Cavia aperea f. porcellus*	485	4.57	0.604349	0.85063291	Bertrand et al. (2019)
Extant Rodentia	*Cavia porcellus*	520	5.4	0.681538	0.95461038	Bertrand et al. (2019)
Extant Rodentia	*Cavia porcellus*	650	5.8	0.630369	0.86925456	Bertrand et al. (2019)
Extant Rodentia	*Cavia porcellus*	348	6.4	1.05716	1.52295195	Bertrand et al. (2019)
Extant Rodentia	*Cavia porcellus*	648	4.4	0.479199	0.66094001	Bertrand et al. (2019)
Extant Rodentia	*Cavia porcellus*	493.1	3.8	0.496977	0.69869328	Bertrand et al. (2019)
Extant Rodentia	*Cavia porcellus*	361	4.1	0.660804	0.94951842	Bertrand et al. (2019)
Extant Rodentia	*Cavia porcellus*	324	3.8	0.658472	0.95335612	Bertrand et al. (2019)
Extant Rodentia	*Cavia porcellus*	214.94	3.32	0.757363	1.12849124	Bertrand et al. (2019)
Extant Rodentia	*Cavia porcellus*	214.57	3.28	0.749103	1.11631729	Bertrand et al. (2019)
Extant Rodentia	*Cavia porcellus*	432	4	0.571616	0.81110464	Bertrand et al. (2019)
Extant Rodentia	*Cavia porcellus*	456	4.23	0.582979	0.82410254	Bertrand et al. (2019)
Extant Rodentia	*Cavia porcellus*	675	4.54	0.481106	0.66167683	Bertrand et al. (2019)
Extant Rodentia	*Cavia porcellus*	971	4.28	0.355489	0.47662455	Bertrand et al. (2019)
Extant Rodentia	*Cavia porcellus*	900	4.94	0.431721	0.58191876	Bertrand et al. (2019)
Extant Rodentia	*Cavia porcellus*	500	5	0.647857	0.90992809	Bertrand et al. (2019)
Extant Rodentia	*Cavia porcellus*	700	4.73	0.489175	0.67106326	Bertrand et al. (2019)
Extant Rodentia	*Chaetodipus baileyi*	31.2	0.61905	0.514588	0.87765641	Bertrand et al. (2019)
Extant Rodentia	*Chaetodipus californicus*	26	0.57143	0.536721	0.92716396	Bertrand et al. (2019)
Extant Rodentia	*Chaetodipus fallax*	20.3	0.49524	0.549048	0.96503229	Bertrand et al. (2019)
Extant Rodentia	*Chaetodipus formosus*	15.3	0.40952	0.548725	0.98374461	Bertrand et al. (2019)
Extant Rodentia	*Chaetodipus hispidus*	35.2	0.62857	0.481936	0.81505691	Bertrand et al. (2019)
Extant Rodentia	*Chaetodipus penicillatus*	16.5	0.41905	0.533787	0.95191929	Bertrand et al. (2019)
Extant Rodentia	*Chaetodipus spinatus*	19.1	0.4381	0.505935	0.89305603	Bertrand et al. (2019)
Extant Rodentia	*Chinchilla chinchilla*	520	7.8	0.984444	1.37888167	Bertrand et al. (2019)
Extant Rodentia	*Chinchilla chinchilla*	425	6.4	0.924652	1.31355129	Bertrand et al. (2019)
Extant Rodentia	*Chinchilla chinchilla*	320	6.9	1.205639	1.74708074	Bertrand et al. (2019)
Extant Rodentia	*Chinchilla chinchilla*	470	8.9	1.201996	1.69555726	Bertrand et al. (2019)
Extant Rodentia	*Chinchilla chinchilla*	450	6	0.834291	1.18045343	Bertrand et al. (2019)
Extant Rodentia	*Chinchilla lanigera*	432	5.2	0.743101	1.05443604	Bertrand et al. (2019)
Extant Rodentia	*Chinchilla lanigera*	380	5.2	0.80978	1.15941349	Bertrand et al. (2019)
Extant Rodentia	*Chinchilla lanigera*	385	5.05	0.779563	1.11512951	Bertrand et al. (2019)
Extant Rodentia	*Chinchilla lanigera*	460	5.1	0.698781	0.98719796	Bertrand et al. (2019)
Extant Rodentia	*Chinchilla lanigera*	385	4.9	0.756408	1.08200685	Bertrand et al. (2019)
Extant Rodentia	*Chinchilla lanigera*	370	5.32	0.843403	1.20981015	Bertrand et al. (2019)
Extant Rodentia	*Chinchilla lanigera*	385	5.5	0.849029	1.21449748	Bertrand et al. (2019)
Extant Rodentia	*Chinchilla lanigera*	425	6.4	0.924652	1.31355129	Bertrand et al. (2019)
Extant Rodentia	*Chinchilla lanigera*	500	6	0.777428	1.0919137	Bertrand et al. (2019)
Extant Rodentia	*Colomys goslingi*	58.2	1.372	0.75106	1.22626963	Bertrand et al. (2019)
Extant Rodentia	*Cricetomys emini*	1000	6.6	0.53748	0.71914887	Bertrand et al. (2019)
Extant Rodentia	*Cricetomys emini*	80.50	2.70	1.189322	1.89823371	Bertrand et al. (2019)
Extant Rodentia	*Cricetulus griseus*	36	0.67	0.506024	0.85444836	Bertrand et al. (2019)
Extant Rodentia	*Cricetulus griseus*	23.18	0.628	0.637019	1.10930398	Bertrand et al. (2019)
Extant Rodentia	*Cricetus cricetus*	450	2.85	0.396288	0.56071538	Bertrand et al. (2019)
Extant Rodentia	*Cricetus cricetus*	297	2.2	0.404105	0.58865085	Bertrand et al. (2019)
Extant Rodentia	*Cuniculus paca*	5635	35.8	0.915383	1.08516654	Bertrand et al. (2019)
Extant Rodentia	*Cuniculus paca*	6125	33.5	0.810033	0.95468735	Bertrand et al. (2019)
Extant Rodentia	*Cuniculus paca*	3665	33.2	1.132471	1.38356067	Bertrand et al. (2019)
Extant Rodentia	*Cuniculus paca*	9000	37.3	0.696923	0.79954745	Bertrand et al. (2019)
Extant Rodentia	*Cuniculus paca*	5000	26.1	0.723018	0.86432599	Bertrand et al. (2019)
Extant Rodentia	*Cuniculus paca*	3627	21.85	0.750539	0.9176163	Bertrand et al. (2019)
Extant Rodentia	*Cuniculus paca*	4559	48	1.414547	1.70197277	Bertrand et al. (2019)
Extant Rodentia	*Cynomys ludovicianus*	939	6.88	0.584242	0.78518563	Bertrand et al. (2021)
Extant Rodentia	*Cynomys ludovicianus*	1200.00	6.40	0.461262	0.60934145	Bertrand et al. (2019)
Extant Rodentia	*Dasymys incomtus*	102.5	1.574	0.58971	0.92543077	Bertrand et al. (2019)
Extant Rodentia	*Dasyprocta leporina*	3600	21.6	0.745675	0.91214686	Bertrand et al. (2019)
Extant Rodentia	*Dasyprocta leporina*	2684	20	0.840552	1.04955646	Bertrand et al. (2019)
Extant Rodentia	*Dasyprocta leporina*	2390	18.4	0.835815	1.05215142	Bertrand et al. (2019)
Extant Rodentia	*Dasyprocta leporina*	2004	17	0.868953	1.10743815	Bertrand et al. (2019)
Extant Rodentia	*Dasyprocta leporina*	2880	18.5	0.741647	0.92150173	Bertrand et al. (2019)
Extant Rodentia	*Dasyprocta leporina*	2350	18	0.826943	1.04221461	Bertrand et al. (2019)
Extant Rodentia	*Dasyprocta leporina*	2550	17	0.739411	0.92658242	Bertrand et al. (2019)
Extant Rodentia	*Dasyprocta leporina*	3172	18.3	0.687665	0.84867109	Bertrand et al. (2019)
Extant Rodentia	*Dasyprocta leporina*	2371	19.8	0.904232	1.13891342	Bertrand et al. (2019)
Extant Rodentia	*Dasyprocta leporina*	2400	27	1.223041	1.53915485	Bertrand et al. (2019)
Extant Rodentia	*Dasyprocta leporina*	2370	19.8	0.904487	1.13926901	Bertrand et al. (2019)
Extant Rodentia	*Dasyprocta mexicana*	1527	17.8	1.091608	1.41792736	Bertrand et al. (2019)
Extant Rodentia	*Dasyprocta mexicana*	2300	20	0.932161	1.17659301	Bertrand et al. (2019)
Extant Rodentia	*Dasyprocta punctata*	3172	18.34	0.689168	0.8505261	Bertrand et al. (2019)
Extant Rodentia	*Dendromus mesomelas*	14	0.51	0.725242	1.30830891	Bertrand et al. (2019)
Extant Rodentia	*Desmodillus auricularis*	60	1.12	0.600725	0.97872564	Bertrand et al. (2019)
Extant Rodentia	*Dicrostonyx groenlandicus*	52.1	0.8983	0.529613	0.87143772	Bertrand et al. (2019)
Extant Rodentia	*Dipodomys deserti*	114.7	1.6	0.555944	0.86560134	Bertrand et al. (2019)
Extant Rodentia	*Dipodomys heermanni*	71.3	1.38095	0.659823	1.06210467	Bertrand et al. (2019)
Extant Rodentia	*Dipodomys merriami*	41	1.05714	0.731791	1.22447097	Bertrand et al. (2019)
Extant Rodentia	*Dipodomys microps*	65.7	1.12381	0.567208	0.91826748	Bertrand et al. (2019)
Extant Rodentia	*Dipodomys ordii*	60.2	1.39048	0.744137	1.21209601	Bertrand et al. (2019)
Extant Rodentia	*Dipodomys panamintinus*	74	1.46667	0.683542	1.09742492	Bertrand et al. (2019)
Extant Rodentia	*Dipodomys spectabilis*	146.6	1.98095	0.58396	0.89373706	Bertrand et al. (2019)
Extant Rodentia	*Dolichotis patagonum*	5500	15	0.389823	0.46291125	Bertrand et al. (2019)
Extant Rodentia	*Dolichotis patagonum*	5650	25.7	0.655963	0.77748522	Bertrand et al. (2019)
Extant Rodentia	*Dolichotis patagonum*	5650	25.66	0.654942	0.77627512	Bertrand et al. (2019)
Extant Rodentia	*Dolichotis patagonum*	7880	33.5	0.684212	0.79230113	Bertrand et al. (2019)
Extant Rodentia	*Dolichotis patagonum*	7500	32	0.675581	0.78501781	Bertrand et al. (2019)
Extant Rodentia	*Dolichotis patagonum*	5500	26	0.675693	0.8023795	Bertrand et al. (2019)

Extant Rodentia	*Dolichotis patagonum*	7200	30	0.650919	0.75852531	Bertrand et al. (2019)
Extant Rodentia	*Dremomys rufigenis*	418.43	5.59	0.815626	1.15993435	Bertrand et al. (2019)
Extant Rodentia	*Eliurus minor*	38	1.46	1.063449	1.78890741	Bertrand et al. (2019)
Extant Rodentia	*Eliurus myoxinus*	59	1.69	0.916716	1.49530947	Bertrand et al. (2019)
Extant Rodentia	*Epixerus ebii*	605.00	9.77	1.114296	1.54430811	Bertrand et al. (2019)
Extant Rodentia	*Erethizon dorsatum*	5160	27.9	0.756742	0.90264773	Bertrand et al. (2019)
Extant Rodentia	*Erethizon dorsatum*	3430	28.7	1.023419	1.2561431	Bertrand et al. (2019)
Extant Rodentia	*Erethizon dorsatum*	4980	25.1	0.697186	0.83367903	Bertrand et al. (2019)
Extant Rodentia	*Erethizon dorsatum*	4980	27.2	0.755517	0.90342907	Bertrand et al. (2019)
Extant Rodentia	*Erethizon dorsatum*	4640	27.1	0.789262	0.94846401	Bertrand et al. (2019)
Extant Rodentia	*Erethizon dorsatum*	6200	27.1	0.649958	0.76537507	Bertrand et al. (2019)
Extant Rodentia	*Erethizon dorsatum*	6640	24	0.549765	0.64429051	Bertrand et al. (2019)
Extant Rodentia	*Erethizon dorsatum*	2800	30.77	1.257044	1.56496786	Bertrand et al. (2019)
Extant Rodentia	*Erethizon dorsatum*	2725	21.22	0.882813	1.10115647	Bertrand et al. (2019)
Extant Rodentia	*Erethizon dorsatum*	3410	19.15	0.685555	0.84179319	Bertrand et al. (2019)
Extant Rodentia	*Erethizon dorsatum*	5000	24	0.664845	0.79478252	Bertrand et al. (2019)
Extant Rodentia	*Eutamias sibiricus*	110.00	2.60	0.929093	1.45083368	Bertrand et al. (2019)
Extant Rodentia	*Funisciurus anerythrus*	230.00	4.03	0.878238	1.30240885	Bertrand et al. (2019)
Extant Rodentia	*Funisciurus carruthersi*	107.50	4.00	1.45156	2.27034886	Bertrand et al. (2019)
Extant Rodentia	*Funisciurus carruthersi*	158.00	4.50	1.261627	1.92079554	Bertrand et al. (2019)
Extant Rodentia	*Funisciurus carruthersi*	195.50	3.25	0.790012	1.1849762	Bertrand et al. (2019)
Extant Rodentia	*Funisciurus carruthersi*	168.00	4.10	1.103177	1.67236033	Bertrand et al. (2019)
Extant Rodentia	*Funisciurus carruthersi*	195.00	4.65	1.132266	1.69864337	Bertrand et al. (2019)
Extant Rodentia	*Funisciurus isabella*	160.50	3.14	0.871917	1.32601361	Bertrand et al. (2019)
Extant Rodentia	*Funisciurus lemniscatus*	154.00	3.22	0.918137	1.4003511	Bertrand et al. (2019)
Extant Rodentia	*Funisciurus pyrropus*	258.75	4.47	0.899855	1.32350915	Bertrand et al. (2019)
Extant Rodentia	*Funisciurus pyrropus*	301.15	4.34	0.789315	1.14866046	Bertrand et al. (2019)
Extant Rodentia	*Funisciurus substriatus*	186.10	3.70	0.930784	1.40095071	Bertrand et al. (2019)
Extant Rodentia	*Galea spixii*	672	6.2	0.658981	0.90659495	Bertrand et al. (2019)
Extant Rodentia	*Geomys bursarius*	192.4	1.48571	0.365037	0.54814874	Bertrand et al. (2019)
Extant Rodentia	*Geomys pinetis*	313.5	2.30476	0.408287	0.59249563	Bertrand et al. (2019)
Extant Rodentia	*Gerbillus gerbillus*	95	3.4	1.340364	2.11464913	Bertrand et al. (2019)
Extant Rodentia	*Gerbillus nanus*	18	0.52	0.62487	1.10758371	Bertrand et al. (2019)
Extant Rodentia	*Gerbillus pyramidum*	79	1.14	0.508526	0.81271013	Bertrand et al. (2019)
Extant Rodentia	*Gerbillus pyramidum*	70	1.2	0.580476	0.93558568	Bertrand et al. (2019)
Extant Rodentia	*Gerbillus pyramidum*	72.3	1.08	0.511234	0.82212203	Bertrand et al. (2019)
Extant Rodentia	*Gerbillus pyramidum*	79	1.059	0.472394	0.75496494	Bertrand et al. (2019)
Extant Rodentia	*Gerbillus pyramidum*	57.9	1.004	0.551516	0.90079599	Bertrand et al. (2019)
Extant Rodentia	*Gerbillus pyramidum*	59.4	0.981	0.529725	0.86365821	Bertrand et al. (2019)
Extant Rodentia	*Glaucomys volans*	63.97	1.91	0.983817	1.59570287	Bertrand et al. (2019)
Extant Rodentia	*Glaucomys volans*	52.00	1.89	1.115728	1.83609099	Bertrand et al. (2019)
Extant Rodentia	*Glaucomys volans*	64.00	1.92	0.986233	1.59956877	Bertrand et al. (2019)
Extant Rodentia	*Glis glis*	118	1.4	0.477294	0.74166916	Bertrand et al. (2019)
Extant Rodentia	*Glis glis*	148	1.9	0.556541	0.85120624	Bertrand et al. (2019)
Extant Rodentia	*Grammomys dolichurus*	45	1.18	0.767447	1.27579124	Bertrand et al. (2019)
Extant Rodentia	*Graphiurus murinus*	17.7	0.551	0.66962	1.18830042	Bertrand et al. (2019)
Extant Rodentia	*Heliosciurus gambianus*	209.80	3.53	0.819207	1.22270988	Bertrand et al. (2019)
Extant Rodentia	*Heliosciurus rufobrachium*	354.98	5.79	0.943314	1.35705735	Bertrand et al. (2019)
Extant Rodentia	*Heliosciurus rufobrachium isabellinus*	280.90	4.84	0.922494	1.3490281	Bertrand et al. (2019)
Extant Rodentia	*Heliosciurus rufobrachium rufobrachium*	334.00	5.03	0.853794	1.23352259	Bertrand et al. (2019)
Extant Rodentia	*Heterocephalus glaber*	39	0.52	0.372228	0.62501495	Bertrand et al. (2019)
Extant Rodentia	*Heterogeomys cherriei*	405	3.19048	0.476079	0.67859969	Bertrand et al. (2019)
Extant Rodentia	*Heteromys desmarestianus*	77.1	1.07619	0.487957	0.78116679	Bertrand et al. (2019)
Extant Rodentia	*Heteromys pictus*	40.2	0.71429	0.501025	0.83949778	Bertrand et al. (2019)
Extant Rodentia	*Hoplomys gymnurus*	637	3.84762	0.423875	0.585334	Bertrand et al. (2019)
Extant Rodentia	*Hybomys univittatus*	56.8	1.149	0.63933	1.04562782	Bertrand et al. (2019)
Extant Rodentia	*Hydrochoerus hydrochaeris*	31000	85	0.693466	0.72960221	Bertrand et al. (2019)
Extant Rodentia	*Hydrochoerus hydrochaeris*	24130	61.4	0.59248	0.63438196	Bertrand et al. (2019)
Extant Rodentia	*Hydrochoerus hydrochaeris*	29500	76	0.640991	0.67673739	Bertrand et al. (2019)
Extant Rodentia	*Hydrochoerus hydrochaeris*	10000	55	0.957594	1.09052985	Bertrand et al. (2019)
Extant Rodentia	*Hydrochoerus hydrochaeris*	12000	53	0.816664	0.91824086	Bertrand et al. (2019)
Extant Rodentia	*Hydrochoerus hydrochaeris*	13000	53	0.774021	0.86543142	Bertrand et al. (2019)
Extant Rodentia	*Hydrochoerus hydrochaeris*	17000	61	0.7443	0.8167187	Bertrand et al. (2019)
Extant Rodentia	*Hydrochoerus hydrochaeris*	28000	52	0.454178	0.48126166	Bertrand et al. (2019)
Extant Rodentia	*Hydrochoerus hydrochaeris*	24031	61.4	0.594114	0.63631487	Bertrand et al. (2019)
Extant Rodentia	*Hydrochoerus hydrochaeris*	28500	75	0.647342	0.68509522	Bertrand et al. (2019)
Extant Rodentia	*Hydrochoerus hydrochaeris*	27670	52.21	0.459649	0.48746314	Bertrand et al. (2019)
Extant Rodentia	*Hydrochoerus hydrochaeris*	26700	75	0.676266	0.71898164	Bertrand et al. (2019)
Extant Rodentia	*Hydrochoerus hydrochaeris*	34300	73	0.556538	0.58140676	Bertrand et al. (2019)
Extant Rodentia	*Hydrochoerus hydrochaeris*	33000	75.5	0.590692	0.61875897	Bertrand et al. (2019)
Extant Rodentia	*Hydrochoerus hydrochaeris*	54000	82	0.461242	0.46678548	Bertrand et al. (2019)
Extant Rodentia	*Hydrochoerus hydrochaeris*	29500	76.02	0.641159	0.67691547	Bertrand et al. (2019)
Extant Rodentia	*Hydrochoerus hydrochaeris*	28000	75	0.655065	0.6941274	Bertrand et al. (2019)
Extant Rodentia	*Hydrochoerus hydrochaeris*	32500	71	0.561197	0.5884906	Bertrand et al. (2019)
Extant Rodentia	*Hylopetes spadiceus*	84.22	2.02	0.863155	1.37330095	Bertrand et al. (2019)
Extant Rodentia	*Hypogeomys antimena*	875	8	0.712465	0.96223001	Bertrand et al. (2019)
Extant Rodentia	*Hystrix brachyura*	22000	43	0.441432	0.47571905	Bertrand et al. (2019)
Extant Rodentia	*Hystrix cristata*	7036.5	36.5	0.804234	0.93869344	Bertrand et al. (2019)
Extant Rodentia	*Hystrix cristata*	15000	32	0.424607	0.47002106	Bertrand et al. (2019)
Extant Rodentia	*Hystrix cristata*	10000	37	0.6442	0.73362917	Bertrand et al. (2019)
Extant Rodentia	*Hystrix* hybrid	13500	37	0.526862	0.5875294	Bertrand et al. (2019)
Extant Rodentia	*Hystrix javanica*	23000	20	0.199293	0.21410473	Bertrand et al. (2019)
Extant Rodentia	*Hystrix* sp.	15000	37.5	0.497587	0.55080593	Bertrand et al. (2019)
Extant Rodentia	*Ictidomys tridecemlineatus*	200.00	2.20	0.526685	0.7887427	Bertrand et al. (2019)
Extant Rodentia	*Ictidomys tridecemlineatus*	115.00	2.40	0.832458	1.29589468	Bertrand et al. (2019)
Extant Rodentia	*Ictidomys tridecemlineatus*	139.00	2.16	0.660443	1.0145664	Bertrand et al. (2019)
Extant Rodentia	*Ictidomys tridecemlineatus*	153.00	2.30	0.657511	1.00330033	Bertrand et al. (2019)
Extant Rodentia	*Jaculus jaculus*	73	1.85	0.87009	1.39825918	Bertrand et al. (2019)
Extant Rodentia	*Jaculus orientalis*	140	2.64	0.802633	1.23237832	Bertrand et al. (2019)
Extant Rodentia	*Jaculus orientalis*	98	2.5	0.965244	1.51952406	Bertrand et al. (2019)
Extant Rodentia	*Lagidium viscacia*	2460	12.4	0.552477	0.69407208	Bertrand et al. (2019)
Extant Rodentia	*Lagidium viscacia*	2252	16	0.756341	0.95608003	Bertrand et al. (2019)
Extant Rodentia	*Lagidium viscacia*	2350	15.2	0.698308	0.88009233	Bertrand et al. (2019)
Extant Rodentia	*Lagidium viscacia*	3845	14.8	0.488877	0.59526903	Bertrand et al. (2019)
Extant Rodentia	*Lagostomus maximus*	6630	20	0.458601	0.5375079	Bertrand et al. (2019)
Extant Rodentia	*Lagostomus maximus*	6385	21	0.493833	0.5803301	Bertrand et al. (2019)

Extant Rodentia	*Lagostomus maximus*	5965	17.2	0.423339	0.49986368	Bertrand et al. (2019)
Extant Rodentia	*Lagostomus maximus*	3930	18	0.585933	0.71235567	Bertrand et al. (2019)
Extant Rodentia	*Lagostomus maximus*	3765	16.5	0.552765	0.67405095	Bertrand et al. (2019)
Extant Rodentia	*Lagostomus maximus*	2940	16.3	0.644486	0.79962332	Bertrand et al. (2019)
Extant Rodentia	*Lagostomus maximus*	7000	17	0.375882	0.43888551	Bertrand et al. (2019)
Extant Rodentia	*Lagostomus maximus*	1575	12.2	0.732826	0.94983263	Bertrand et al. (2019)
Extant Rodentia	*Lagostomus maximus*	1990	14.5	0.744655	0.94949262	Bertrand et al. (2019)
Extant Rodentia	*Lagostomus maximus*	1395	12	0.781871	1.02204778	Bertrand et al. (2019)
Extant Rodentia	*Lagostomus maximus*	1500	11.1	0.688907	0.8959635	Bertrand et al. (2019)
Extant Rodentia	*Lagostomus maximus*	1265	11.8	0.820919	1.08046297	Bertrand et al. (2019)
Extant Rodentia	*Lagostomus maximus*	1125	13.2	0.993392	1.31824439	Bertrand et al. (2019)
Extant Rodentia	*Lagostomus maximus*	1095	11.7	0.896597	1.19204948	Bertrand et al. (2019)
Extant Rodentia	*Lagostomus maximus*	1440	13	0.8292	1.0815086	Bertrand et al. (2019)
Extant Rodentia	*Lagostomus maximus*	1225	12.7	0.902758	1.19085226	Bertrand et al. (2019)
Extant Rodentia	*Lagostomus maximus*	1510	12.6	0.778529	1.01205117	Bertrand et al. (2019)
Extant Rodentia	*Lagostomus maximus*	1335	11.9	0.798534	1.04704583	Bertrand et al. (2019)
Extant Rodentia	*Lagostomus maximus*	1325	11.9	0.802567	1.05288777	Bertrand et al. (2019)
Extant Rodentia	*Lagostomus maximus*	1115	12.3	0.931214	1.236507	Bertrand et al. (2019)
Extant Rodentia	*Lagostomus maximus*	1075	11	0.85343	1.13612284	Bertrand et al. (2019)
Extant Rodentia	*Lagostomus maximus*	1030	11.2	0.894202	1.19396981	Bertrand et al. (2019)
Extant Rodentia	*Lagostomus maximus*	1125	11.2	0.842878	1.1185104	Bertrand et al. (2019)
Extant Rodentia	*Lagostomus maximus*	1230	11.7	0.829408	1.09378244	Bertrand et al. (2019)
Extant Rodentia	*Lagostomus maximus*	3854	8.8	0.290229	0.35333192	Bertrand et al. (2019)
Extant Rodentia	*Lagurus lagurus*	15	0.4	0.543122	0.97505099	Bertrand et al. (2019)
Extant Rodentia	*Lariscus insignis*	324.71	4.65	0.803933	1.16378115	Bertrand et al. (2019)
Extant Rodentia	*Lemmus lemmus*	21	0.7	0.75863	1.33024192	Bertrand et al. (2019)
Extant Rodentia	*Lemmus trimucronatus*	32	1.126	0.920252	1.56675928	Bertrand et al. (2019)
Extant Rodentia	*Lemmus trimucronatus*	48	1.312	0.817186	1.35235337	Bertrand et al. (2019)
Extant Rodentia	*Lemniscomys striatus*	53.3	1.02	0.592259	0.9729643	Bertrand et al. (2019)
Extant Rodentia	*Lemniscomys striatus*	53	1.007	0.586926	0.96458432	Bertrand et al. (2019)
Extant Rodentia	*Lemniscomys striatus*	53.4	1.014	0.588036	0.96590028	Bertrand et al. (2019)
Extant Rodentia	*Lemniscomys striatus*	57	0.99	0.549563	0.89859225	Bertrand et al. (2019)
Extant Rodentia	*Lophuromys sikapusi*	63.5	1.2	0.619643	1.00554974	Bertrand et al. (2019)
Extant Rodentia	*Lophuromys sikapusi*	70	1.13	0.546615	0.88100985	Bertrand et al. (2019)
Extant Rodentia	*Macrotarsomys bastardi*	28.5	0.8	0.706582	1.21277339	Bertrand et al. (2019)
Extant Rodentia	*Macrotarsomys ingens*	65	1.7	0.864203	1.40012853	Bertrand et al. (2019)
Extant Rodentia	*Malacomys longipes*	98	1.285	0.496136	0.78103537	Bertrand et al. (2019)
Extant Rodentia	*Malacothrix typicus*	124	0.5	0.164891	0.25533646	Bertrand et al. (2019)
Extant Rodentia	*Marmota bobak*	5333.00	11.97	0.31761	0.37797396	Bertrand et al. (2019)
Extant Rodentia	*Marmota marmota*	4547	14.47	0.427247	0.51415569	Bertrand et al. (2021)
Extant Rodentia	*Marmota marmota*	5000.00	16.00	0.44323	0.52985501	Bertrand et al. (2019)
Extant Rodentia	*Marmota marmota*	4050.00	17.00	0.542341	0.65797149	Bertrand et al. (2019)
Extant Rodentia	*Marmota marmota*	2950.00	17.00	0.670636	0.83187007	Bertrand et al. (2019)
Extant Rodentia	*Marmota marmota*	3500.00	17.00	0.598056	0.73301597	Bertrand et al. (2019)
Extant Rodentia	*Marmota sibirica*	1890.00	18.10	0.962206	1.2313222	Bertrand et al. (2019)
Extant Rodentia	*Mastomys coucha*	21.8	0.7132	0.753814	1.31834294	Bertrand et al. (2019)
Extant Rodentia	*Mastomys natalensis*	63	0.9	0.4672	0.75858696	Bertrand et al. (2019)
Extant Rodentia	*Meriones crassus*	122	1.36	0.453416	0.70292259	Bertrand et al. (2019)
Extant Rodentia	*Meriones libycus*	93	1.51	0.603826	0.95405725	Bertrand et al. (2019)
Extant Rodentia	*Meriones meridianus*	50	1.2	0.727261	1.20010242	Bertrand et al. (2019)
Extant Rodentia	*Meriones shawi*	140	1.48	0.449961	0.69087875	Bertrand et al. (2019)
Extant Rodentia	*Meriones unguiculatus*	50	1.3	0.787866	1.30011096	Bertrand et al. (2019)
Extant Rodentia	*Mesocricetus auratus*	100	1.4	0.53327	0.83830664	Bertrand et al. (2019)
Extant Rodentia	*Mesocricetus auratus*	125	1.12	0.367373	0.56856416	Bertrand et al. (2019)
Extant Rodentia	*Mesocricetus auratus*	87	1.32	0.551969	0.87620263	Bertrand et al. (2019)
Extant Rodentia	*Mesocricetus brandti*	80	1	0.442332	0.70629849	Bertrand et al. (2019)
Extant Rodentia	*Microdipodops megacephalus*	13.6	0.47619	0.690444	1.24806379	Bertrand et al. (2019)
Extant Rodentia	*Microdipodops pallidus*	12.9	0.50476	0.758246	1.37570417	Bertrand et al. (2019)
Extant Rodentia	*Micromys minutus*	5.5	0.267	0.710047	1.36746979	Bertrand et al. (2019)
Extant Rodentia	*Micromys minutus*	6.1	0.282	0.699676	1.33776522	Bertrand et al. (2019)
Extant Rodentia	*Micromys minutus*	5.95	0.278	0.701354	1.34331267	Bertrand et al. (2019)
Extant Rodentia	*Microtus agrestis*	42.5	0.9	0.608192	1.01510173	Bertrand et al. (2019)
Extant Rodentia	*Microtus agrestris*	30.5	0.532	0.449003	0.76701635	Bertrand et al. (2019)
Extant Rodentia	*Microtus arvalis arvalis*	20.5	0.4	0.440559	0.77381475	Bertrand et al. (2019)
Extant Rodentia	*Microtus oeconomus stimmingi*	45	0.68	0.442258	0.73520173	Bertrand et al. (2019)
Extant Rodentia	*Microtus pennsylvanicus*	23.7	0.6606	0.660201	1.14788839	Bertrand et al. (2019)
Extant Rodentia	*Microtus pennsylvanicus*	22.9	0.6464	0.661044	1.15212065	Bertrand et al. (2019)
Extant Rodentia	*Microtus pennsylvanicus*	25.2	0.7166	0.687317	1.18991317	Bertrand et al. (2019)
Extant Rodentia	*Microtus pennsylvanicus*	27.9	0.7394	0.662435	1.13869445	Bertrand et al. (2019)
Extant Rodentia	*Mus minutoides*	10.4	0.327	0.567485	1.04524464	Bertrand et al. (2019)
Extant Rodentia	*Mus minutoides*	5	0.26	0.737025	1.42892822	Bertrand et al. (2019)
Extant Rodentia	*Mus musculus*	18	0.43	0.516719	0.91588653	Bertrand et al. (2019)
Extant Rodentia	*Mus musculus*	24	0.45	0.445954	0.77469555	Bertrand et al. (2019)
Extant Rodentia	*Mus musculus*	20.85	0.43	0.468259	0.82149484	Bertrand et al. (2019)
Extant Rodentia	*Mus musculus*	16	0.36	0.468124	0.83662065	Bertrand et al. (2019)
Extant Rodentia	*Mus musculus*	24.32	0.475	0.46657	0.80975835	Bertrand et al. (2019)
Extant Rodentia	*Mus musculus*	24	0.5	0.495504	0.86077284	Bertrand et al. (2019)
Extant Rodentia	*Mus musculus*	18.92	0.424	0.492774	0.87040041	Bertrand et al. (2019)
Extant Rodentia	*Mus musculus domesticus*	12	0.36	0.567636	1.03510224	Bertrand et al. (2019)
Extant Rodentia	*Mus musculus musculus*	20	0.5	0.559885	0.98510535	Bertrand et al. (2019)
Extant Rodentia	*Mus triton*	8.4	0.36	0.720865	1.34775421	Bertrand et al. (2019)
Extant Rodentia	*Muscardinus avellanarius*	13	0.5	0.747217	1.35496099	Bertrand et al. (2019)
Extant Rodentia	*Myocastor coypus*	3300	23	0.841671	1.03586316	Bertrand et al. (2019)
Extant Rodentia	*Myocastor coypus*	3380	19	0.684224	0.84067883	Bertrand et al. (2019)
Extant Rodentia	*Myocastor coypus*	5000	23	0.637143	0.76166658	Bertrand et al. (2019)
Extant Rodentia	*Myocastor coypus*	5300	18.7	0.498191	0.59313333	Bertrand et al. (2019)
Extant Rodentia	*Myocastor coypus*	3300	21	0.768482	0.94578811	Bertrand et al. (2019)
Extant Rodentia	*Myocastor coypus*	7450	15.64	0.331674	0.38558131	Bertrand et al. (2019)
Extant Rodentia	*Myocastor coypus*	7530	15.6	0.328466	0.38156733	Bertrand et al. (2019)
Extant Rodentia	*Myocastor coypus*	8475	17.55	0.341383	0.39330422	Bertrand et al. (2019)
Extant Rodentia	*Myocastor coypus*	5510	17.43	0.452423	0.53718029	Bertrand et al. (2019)
Extant Rodentia	*Myocastor coypus*	3800	14.77	0.49175	0.59926029	Bertrand et al. (2019)
Extant Rodentia	*Myocastor coypus*	5700	18.35	0.465606	0.55152289	Bertrand et al. (2019)
Extant Rodentia	*Myocastor coypus*	5000	23	0.637143	0.76166658	Bertrand et al. (2019)
Extant Rodentia	*Myocastor coypus f domestica*	3500	18.4	0.647308	0.79338199	Bertrand et al. (2019)
Extant Rodentia	*Myodes glareolus*	35	0.593	0.456402	0.77218117	Bertrand et al. (2019)

Extant Rodentia	*Myodes glareolus*	20	0.7	0.783839	1.37914749	Bertrand et al. (2019)
Extant Rodentia	*Myoprocta pratti*	780	9.9	0.952249	1.29646279	Bertrand et al. (2019)
Extant Rodentia	*Mystromys albicaudatus*	130	1.47	0.469671	0.72489336	Bertrand et al. (2019)
Extant Rodentia	*Neotamias minimus*	37.05	1.45	1.073591	1.80917233	Bertrand et al. (2019)
Extant Rodentia	*Oenomys hypoxanthus*	92	1.15	0.463211	0.73243606	Bertrand et al. (2019)
Extant Rodentia	*Oenomys hypoxanthus*	92	1.166	0.469656	0.74262647	Bertrand et al. (2019)
Extant Rodentia	*Oenomys hypoxanthus*	92	1.162	0.468044	0.74007887	Bertrand et al. (2019)
Extant Rodentia	*Oenomys hypoxanthus*	178	1.48	0.383088	0.57839667	Bertrand et al. (2019)
Extant Rodentia	*Ondatra zibethicus*	1500	4.8	0.297906	0.38744367	Bertrand et al. (2019)
Extant Rodentia	*Ondatra zibethicus*	1500	7.6	0.471684	0.61345248	Bertrand et al. (2019)
Extant Rodentia	*Ondatra zibethicus*	1600	8.1	0.481441	0.62332006	Bertrand et al. (2019)
Extant Rodentia	*Ondatra zibethicus*	1032	5.7	0.454494	0.6067737	Bertrand et al. (2019)
Extant Rodentia	*Ondatra zibethicus*	900	5.33	0.465804	0.62785972	Bertrand et al. (2019)
Extant Rodentia	*Ondatra zibethicus*	900	5.33	0.465804	0.62785972	Bertrand et al. (2019)
Extant Rodentia	*Orthogeomys heterodus*	630	3.9619	0.439708	0.60766874	Bertrand et al. (2019)
Extant Rodentia	*Orthogeomys hispidus*	542.1	3.65714	0.448877	0.62689966	Bertrand et al. (2019)
Extant Rodentia	*Otomys irroratus*	57.7	0.97143	0.534862	0.87380724	Bertrand et al. (2019)
Extant Rodentia	*Otomys irroratus*	66	1.62	0.815153	1.31925081	Bertrand et al. (2019)
Extant Rodentia	*Paraxerus cepapi*	138.13	2.91	0.892084	1.37101409	Bertrand et al. (2019)
Extant Rodentia	*Paraxerus cepapi*	223.80	3.22	0.714727	1.06195425	Bertrand et al. (2019)
Extant Rodentia	*Paraxerus poensis*	100.00	2.73	1.041145	1.63669391	Bertrand et al. (2019)
Extant Rodentia	*Pelomys campanae*	91	1.23	0.499075	0.78974948	Bertrand et al. (2019)
Extant Rodentia	*Pelomys fallax*	121	1.46	0.489447	0.7592181	Bertrand et al. (2019)
Extant Rodentia	*Pelomys fallax*	110	1.406	0.502425	0.78456621	Bertrand et al. (2019)
Extant Rodentia	*Pelomys fallax*	111	1.412	0.501519	0.78265536	Bertrand et al. (2019)
Extant Rodentia	*Perognathus flavus*	8	0.28571	0.591126	1.10897111	Bertrand et al. (2019)
Extant Rodentia	*Perognathus longimembris*	8	0.29524	0.610831	1.14593682	Bertrand et al. (2019)
Extant Rodentia	*Perognathus parvus*	17.3	0.44762	0.552378	0.98181421	Bertrand et al. (2019)
Extant Rodentia	*Perognathus parvus*	17	0.58	0.724179	1.28875588	Bertrand et al. (2019)
Extant Rodentia	*Peromyscus californicus*	55	1.0292	0.585161	0.95919356	Bertrand et al. (2019)
Extant Rodentia	*Peromyscus californicus*	51.2	1.0295	0.614093	1.011676	Bertrand et al. (2019)
Extant Rodentia	*Peromyscus eremicus*	20.1	0.6506	0.726092	1.27709688	Bertrand et al. (2019)
Extant Rodentia	*Peromyscus eremicus*	20	0.6416	0.718444	1.26408718	Bertrand et al. (2019)
Extant Rodentia	*Peromyscus gossypinus*	27.2	0.68	0.619679	1.06709428	Bertrand et al. (2019)
Extant Rodentia	*Peromyscus leucopus*	25.5	0.63	0.599484	1.03699267	Bertrand et al. (2019)
Extant Rodentia	*Peromyscus leucopus*	19.7	0.6372	0.720779	1.26953778	Bertrand et al. (2019)
Extant Rodentia	*Peromyscus leucopus*	22.9	0.6221	0.636193	1.10880918	Bertrand et al. (2019)
Extant Rodentia	*Peromyscus maniculatus bairdii*	16.5	0.5182	0.660088	1.17715637	Bertrand et al. (2019)
Extant Rodentia	*Peromyscus maniculatus bairdii*	18	0.5188	0.623428	1.10502774	Bertrand et al. (2019)
Extant Rodentia	*Peromyscus maniculatus gracilis*	22.1	0.6885	0.721074	1.25987811	Bertrand et al. (2019)
Extant Rodentia	*Peromyscus maniculatus gracilis*	26	0.6909	0.648936	1.12101077	Bertrand et al. (2019)
Extant Rodentia	*Peromyscus polionotus*	13.5	0.4903	0.714426	1.2920811	Bertrand et al. (2019)
Extant Rodentia	*Peromyscus polionotus*	13.1	0.4867	0.723616	1.31146123	Bertrand et al. (2019)
Extant Rodentia	*Petaurista petaurista*	1096.65	11.73	0.898077	1.19389145	Bertrand et al. (2019)
Extant Rodentia	*Petinomys setosus*	41.86	1.44	0.983395	1.64307785	Bertrand et al. (2019)
Extant Rodentia	*Podomys floridanus*	36.5	0.8896	0.665698	1.12298233	Bertrand et al. (2019)
Extant Rodentia	*Podomys floridanus*	39.2	0.8917	0.636115	1.06773123	Bertrand et al. (2019)
Extant Rodentia	*Praomys jacksoni*	49	0.87	0.534449	0.88317959	Bertrand et al. (2019)
Extant Rodentia	*Protoxerus aubinni*	525.00	8.03	1.006816	1.40927342	Bertrand et al. (2019)
Extant Rodentia	*Protoxerus stangeri*	767.23	9.28	0.90281	1.23057362	Bertrand et al. (2019)
Extant Rodentia	*Protoxerus stangeri*	690.60	10.25	1.069449	1.46848724	Bertrand et al. (2019)
Extant Rodentia	*Pteromys buechneri*	106.37	2.22	0.81127	1.26982654	Bertrand et al. (2019)
Extant Rodentia	*Pteromys nitidus*	1600.00	11.80	0.701359	0.9080465	Bertrand et al. (2019)
Extant Rodentia	*Pteromyscus pulverulentus*	195.44	3.45	0.838463	1.25767647	Bertrand et al. (2019)
Extant Rodentia	*Rattus norvegicus*	274	2.18	0.422651	0.6191501	Bertrand et al. (2019)
Extant Rodentia	*Rattus norvegicus*	278	2.3	0.441608	0.64626339	Bertrand et al. (2019)
Extant Rodentia	*Rattus norvegicus*	197	1.61	0.389361	0.58370812	Bertrand et al. (2019)
Extant Rodentia	*Rattus norvegicus*	291	2.27	0.422704	0.61662328	Bertrand et al. (2019)
Extant Rodentia	*Rattus norvegicus*	305	2.36	0.425843	0.61916299	Bertrand et al. (2019)
Extant Rodentia	*Rattus norvegicus*	448	2.36	0.329135	0.46584468	Bertrand et al. (2019)
Extant Rodentia	*Rattus norvegicus domestica*	324	2.7	0.467862	0.67738461	Bertrand et al. (2019)
Extant Rodentia	*Rattus norvegicus norvegicus*	202	2.6	0.618311	0.92531202	Bertrand et al. (2019)
Extant Rodentia	*Rattus rattus*	160	2.24	0.622739	0.94727069	Bertrand et al. (2019)
Extant Rodentia	*Rattus rattus*	200	1.59	0.38065	0.57004586	Bertrand et al. (2019)
Extant Rodentia	*Rattus rattus*	150	1.92	0.557364	0.85166454	Bertrand et al. (2019)
Extant Rodentia	*Rattus rattus alexandrinus*	150	1.57	0.455761	0.69641319	Bertrand et al. (2019)
Extant Rodentia	*Rattus rattus rattus*	217	1.68	0.380803	0.56702727	Bertrand et al. (2019)
Extant Rodentia	*Ratufa affinis*	1074.27	11.73	0.910274	1.21185368	Bertrand et al. (2019)
Extant Rodentia	*Ratufa bicolor*	1440.00	12.00	0.765415	0.99831563	Bertrand et al. (2019)
Extant Rodentia	*Ratufa bicolor*	1400.00	12.00	0.779999	1.0193454	Bertrand et al. (2019)
Extant Rodentia	*Ratufa indica*	1935.00	11.40	0.596551	0.76214184	Bertrand et al. (2019)
Extant Rodentia	*Ratufa indica*	1010.00	11.60	0.938386	1.25468597	Bertrand et al. (2019)
Extant Rodentia	*Rhinosciurus laticaudatus*	507.38	4.17	0.535657	0.75157065	Bertrand et al. (2019)
Extant Rodentia	*Sciurus carolinensis*	592.55	7.67	0.886828	1.23084865	Bertrand et al. (2019)
Extant Rodentia	*Sciurus carolinesis*	469.00	7.58	1.025185	1.44635923	Bertrand et al. (2019)
Extant Rodentia	*Sciurus carolinesis*	466.00	7.48	1.016019	1.43407177	Bertrand et al. (2019)
Extant Rodentia	*Sciurus carolinesis*	535.00	7.53	0.932431	1.303431	Bertrand et al. (2019)
Extant Rodentia	*Sciurus granatensis*	336.99	6.02	1.01647	1.46763308	Bertrand et al. (2019)
Extant Rodentia	*Sciurus niger*	365.00	6.90	1.103905	1.5849926	Bertrand et al. (2019)
Extant Rodentia	*Sciurus niger*	365.00	6.50	1.03991	1.49310897	Bertrand et al. (2019)
Extant Rodentia	*Sciurus niger*	703.00	10.20	1.051862	1.44254078	Bertrand et al. (2019)
Extant Rodentia	*Sciurus niger*	770.00	10.50	1.01873	1.38822874	Bertrand et al. (2019)
Extant Rodentia	*Sciurus niger*	650.00	9.20	0.999896	1.37881758	Bertrand et al. (2019)
Extant Rodentia	*Sciurus niger*	580.00	8.95	1.049893	1.4593558	Bertrand et al. (2019)
Extant Rodentia	*Sciurus niger cinereus*	328.00	7.20	1.237416	1.79003169	Bertrand et al. (2019)
Extant Rodentia	*Sciurus vulgaris*	350.00	7.50	1.234112	1.77715693	Bertrand et al. (2019)
Extant Rodentia	*Sciurus vulgaris*	323.00	6.10	1.059212	1.53389219	Bertrand et al. (2019)
Extant Rodentia	*Sciurus vulgaris*	287.00	5.81	1.091978	1.59447751	Bertrand et al. (2019)
Extant Rodentia	*Sciurus vulgaris*	316.00	5.89	1.037872	1.50529536	Bertrand et al. (2019)
Extant Rodentia	*Sciurus vulgaris*	327.00	6.23	1.072901	1.55237835	Bertrand et al. (2019)
Extant Rodentia	*Sciurus vulgaris*	361.00	5.85	0.942855	1.35480068	Bertrand et al. (2019)
Extant Rodentia	*Sciurus vulgaris*	389.00	6.00	0.919822	1.31481126	Bertrand et al. (2019)
Extant Rodentia	*Sigmodon hispidus*	148	1.18	0.345641	0.52864388	Bertrand et al. (2019)
Extant Rodentia	*Spalax leucodon*	122	3	1.000182	1.55056454	Bertrand et al. (2019)
Extant Rodentia	*Spalax leucodon*	180	2.63	0.675681	1.01936323	Bertrand et al. (2019)
Extant Rodentia	*Spalax leucodon*	214	1.9	0.434705	0.64792133	Bertrand et al. (2019)

Extant Rodentia	*Spermophilus citellus*	290.00	2.58	0.481539	0.70261927	Bertrand et al. (2019)
Extant Rodentia	*Spermophilus suslicus*	224.00	2.30	0.510364	0.75826179	Bertrand et al. (2019)
Extant Rodentia	*Stochomys longicaudatus*	65	1.27	0.64561	1.04597837	Bertrand et al. (2019)
Extant Rodentia	*Tachyoryctes splendens*	282	2.1	0.399366	0.58386148	Bertrand et al. (2019)
Extant Rodentia	*Tachyoryctes splendens*	174	2.29	0.601847	0.910131	Bertrand et al. (2019)
Extant Rodentia	*Tachyoryctes splendens*	206	2.4	0.563299	0.84182994	Bertrand et al. (2019)
Extant Rodentia	*Tachyoryctes splendens*	218	2.24	0.506175	0.75346847	Bertrand et al. (2019)
Extant Rodentia	*Tamias striatus*	80.00	2.70	1.194297	1.90700593	Bertrand et al. (2019)
Extant Rodentia	*Tamias striatus*	97.00	2.90	1.127404	1.77607697	Bertrand et al. (2019)
Extant Rodentia	*Tamias striatus*	75.00	2.22	1.02537	1.64468415	Bertrand et al. (2019)
Extant Rodentia	*Tamias striatus*	62.00	2.31	1.212072	1.97023032	Bertrand et al. (2019)
Extant Rodentia	*Tamiasciurus hudsonicus*	256.61	4.90	0.99299	1.46134237	Bertrand et al. (2019)
Extant Rodentia	*Tamiasciurus hudsonicus*	125.00	4.80	1.574455	2.43670355	Bertrand et al. (2019)
Extant Rodentia	*Tamiasciurus hudsonicus*	159.00	4.10	1.144634	1.74190655	Bertrand et al. (2019)
Extant Rodentia	*Tamiasciurus hudsonicus*	248.00	5.02	1.040495	1.53491504	Bertrand et al. (2019)
Extant Rodentia	*Tamiasciurus hudsonicus*	183.00	4.71	1.196733	1.80335808	Bertrand et al. (2019)
Extant Rodentia	*Tamiasciurus hudsonicus*	169.00	4.21	1.12828	1.70970351	Bertrand et al. (2019)
Extant Rodentia	*Tamiasciurus hudsonicus*	183.00	3.97	1.008712	1.52002793	Bertrand et al. (2019)
Extant Rodentia	*Tamiasciurus hudsonicus*	159.00	4.80	1.340059	2.03930523	Bertrand et al. (2019)
Extant Rodentia	*Thamnomys venustus*	82.5	1.291	0.559398	0.89130263	Bertrand et al. (2019)
Extant Rodentia	*Thamnomys venustus*	82.5	1.284	0.556365	0.88646985	Bertrand et al. (2019)
Extant Rodentia	*Thamnomys venustus*	82.5	1.35	0.584963	0.93203606	Bertrand et al. (2019)
Extant Rodentia	*Thomomys bottae*	185.2	1.40952	0.355281	0.53492508	Bertrand et al. (2019)
Extant Rodentia	*Thomomys talpoides*	90.6	1.00952	0.410827	0.65030421	Bertrand et al. (2019)
Extant Rodentia	*Thryonomys gregorianus*	3500	13.15	0.462614	0.56700941	Bertrand et al. (2019)
Extant Rodentia	*Thryonomys gregorianus*	3500	13.15	0.462614	0.56700941	Bertrand et al. (2019)
Extant Rodentia	*Thryonomys swinderianus*	4500	12	0.356737	0.42961442	Bertrand et al. (2019)
Extant Rodentia	*Urocitellus columbianus*	482.00	3.52	0.467939	0.65891969	Bertrand et al. (2019)
Extant Rodentia	*Urocitellus columbianus*	529.00	3.57	0.4456	0.62338973	Bertrand et al. (2019)
Extant Rodentia	*Urocitellus parryii*	878.00	5.63	0.500249	0.6754564	Bertrand et al. (2019)
Extant Rodentia	*Urocitellus parryii*	958.00	5.74	0.481078	0.64561897	Bertrand et al. (2019)
Extant Rodentia	*Urocitellus parryii*	482.00	3.95	0.524851	0.73905857	Bertrand et al. (2019)
Extant Rodentia	*Urocitellus parryii*	756.00	4.98	0.48924	0.6675459	Bertrand et al. (2019)
Extant Rodentia	*Urocitellus richardsonii*	354.00	3.08	0.502342	0.72281254	Bertrand et al. (2019)
Extant Rodentia	*Urocitellus richardsonii*	361.00	3.31	0.534169	0.76755496	Bertrand et al. (2019)
Extant Rodentia	*Urocitellus richardsonii*	246	3.01	0.627154	0.92574645	Bertrand et al. (2021)
Extant Rodentia	*Xerus inauris*	638.00	6.41	0.705366	0.97394253	Bertrand et al. (2019)
Extant Rodentia	*Xerus rutilus*	354	5.72	0.933601	1.34337023	Bertrand et al. (2021)
Extant Rodentia	*Zapus hudsonius*	19.3	0.6961	0.798302	1.40810193	Bertrand et al. (2019)
Extant Rodentia	*Zapus hudsonius*	15.2	0.705	0.948796	1.70176556	Bertrand et al. (2019)
Extant Rodentia	*Zygogeomys trichopus*	545	3.62857	0.443781	0.6195511	Bertrand et al. (2019)

Table S3. Encephalization quotients, brain mass, and body mass for *Anagale gobiensis*, living and fossil lagomorphs, living and fossil rodents, plesiad

Group	Species	Specimen number	NS*/TS	OV/TV	PV2/TV	Source
Euprimates	*Notharctus tenebrosus*	AMNH 127167	30.88	2.1	1.41	Harrington et al. (2016); Bertrand et al. 2022
Euprimates	*Notharctus tenebrosus*	USNM V 23277	30.43	2.23	0.97	Harrington et al. (2016); Bertrand et al. 2022
Euprimates	*Notharctus tenebrosus*	USNM V 23278	29.42	1.51	NA	Harrington et al. (2016); Bertrand et al. 2022
Euprimates	*Smilodectes gracilis*	USNM V 17994	30.59	2.06	NA	Harrington et al. (2016); Bertrand et al. 2022
Euprimates	*Smilodectes gracilis*	USNM V 17996	30.85	1.67	1.24	Harrington et al. (2016); Bertrand et al. 2022
Euprimates	*Smilodectes gracilis*	USNM V 21815	31.37	1.24	1.61	Harrington et al. (2016); Bertrand et al. 2022
Euprimates	*Smilodectes gracilis*	UM 32773 (=MPM 2612)	32.84	1.54	1.46	Harrington et al. (2016); Bertrand et al. 2022
Euprimates	*Adapis parisiensis*	NHM M 1345	30.93	2.4	0.51	Harrington et al. (2016); Bertrand et al. 2022
Euprimates	*Rooneyia viejaensis*	TMM 40688-7	43.77	0.94	0.84	Kirk et al. (2014); Ramdarshan & Orliac (2016); Bertrand et al. 2022
Euprimates	*Microchoerus erinaceus*	UM-PRR 1771	41.34	0.96	1.13	Ramdarshan & Orliac (2016); Bertrand et al. 2022
Euprimates	*Necrolemur antiquus*	MaPhQ 289	NA	1.94	1.09	Harrington et al. (2020); Bertrand et al. 2022
Plesiadapiformes	*Microsyops annectens*	UW 12362	21.40	5.09	-	Silcox et al. (2010); Long et al. 2015
Plesiadapiformes	*Ignacius graybullianus*	USNM 421608	19.72	5.53	-	Silcox et al. (2009b); Long et al. 2015
Plesiadapiformes	*Plesiadapis cookei*	UM 87990	-	7.8	-	Gingerich & Gunnell (2005)
Plesiadapiformes	*Plesiadapis tricuspidens*	MNHN CR 125	19.93	4.9	-	Orliac et al. (2014)
Fossil Aplodontiic	*Altasciurus relictus*	USNM 437793	29.69	3.55	3.35	Bertrand et al. (2019; 2021)
Fossil Aplodontiic	*Mesogaulus paniensis*	AMNH F:AM 65511	26.49	3.29	1.33	Bertrand et al. (2018)
Fossil Sciuridae	*Protosciurus* cf. *rachelae*	YPM 14736	30.59	4.76	3.31	Bertrand et al. (2019)
Fossil Sciuridae	*Protosciurus* cf. *rachelae*	YPM 14737	30.95	3.65	2.96	Bertrand et al. (2019)
Fossil Sciuridae	*Cedromus wilsoni*	USNM 256584	29.59	2.96	3.16	Bertrand et al. (2019)
Ischyromyidae	*Paramys copei*	AMNH 4756	17.10	6.05	1.20	Bertrand et al. (2019)
Ischyromyidae	*Paramys delicatus*	AMNH 12506	16.25	4.74	1.03	Bertrand et al. (2019)
Ischyromyidae	*Pseudotomus horribilis*	USNM 17159	18.89	5.33	1.14	Bertrand et al. (2019)
Ischyromyidae	*Pseudotomus robustus*	USNM 17161	22.92	5.94	0.62	Bertrand et al. (2019)
Ischyromyidae	*Pseudotomus petersoni*	AMNH 2018	22.89	4.14	0.39	Bertrand et al. (2019)
Ischyromyidae	*Pseudotomus hians*	AMNH 5025	23.02	5.43	1.04	Bertrand et al. (2019)
Ischyromyidae	*Reithroparamys delicatissimus*	AMNH 12561	17.33	3.21	2.31	Bertrand et al. (2019; 2021)
Ischyromyidae	*Rapamys atramontis*	AMNH 128706	20.24	3.16	1.52	Bertrand et al. (2019)
Ischyromyidae	*Rapamys atramontis*	AMNH 128704	21.77	3.76	2.05	Bertrand et al. (2019)
Ischyromyidae	*Ischyromys typus*	ROMV 1007	21.18	3.23	1.63	Bertrand et al. (2019)
Ischyromyidae	*Ischyromys typus*	AMNH 12252	18.45	3.68	-	Bertrand et al. (2019)
Ischyromyidae	*Ischyromys typus*	AMNH F:AM 144638	23.03	3.15	1.60	Bertrand et al. (2019)
Extant Aplodontii	*Aplodontia rufa*	AMNH 42389	25.94	2.58	0.82	Bertrand et al. (2018)
Extant Sciuridae	*Sciurus carolinensis*	AMNH 42389	35.41	3.18	2.03	Bertrand et al. (2019)
Extant Sciuridae	*Sciurus granatensis*	AMNH 42389	35.39	2.69	2.08	Bertrand et al. (2019)
Extant Sciuridae	*Tamiasciurus hudsonicus*	USNM 549146	36.30	2.50	2.33	Bertrand et al. (2019)
Extant Sciuridae	*Eutamias minimus*	USNM 298500	34.93	3.36	2.29	Bertrand et al. (2019)
Extant Sciuridae	*Funisciurus pyrropus*	USNM 294865	36.44	3.22	2.19	Bertrand et al. (2019)
Extant Sciuridae	*Heliosciurus rufobrachium*	USNM 378091	35.85	2.45	1.87	Bertrand et al. (2019)
Extant Sciuridae	*Paraxerus cepapi*	USNM 367956	35.62	2.62	1.46	Bertrand et al. (2019)
Extant Sciuridae	*Protoxerus stangeri*	USNM 435027	38.02	2.31	1.89	Bertrand et al. (2019)
Extant Sciuridae	*Aeromys tephromelas*	USNM 481190	35.19	2.85	1.45	Bertrand et al. (2019)
Extant Sciuridae	*Glaucomys volans*	AMNH 240290	35.69	3.49	1.68	Bertrand et al. (2019)
Extant Sciuridae	*Petaurista petaurista*	USNM 589079	35.28	1.64	1.62	Bertrand et al. (2019)
Extant Sciuridae	*Hylopetes spadiceus*	USNM 488639	36.73	3.30	0.85	Bertrand et al. (2019)
Extant Sciuridae	*Petinomys setosus*	USNM 488674	35.76	3.10	-	Bertrand et al. (2019)
Extant Sciuridae	*Pteromyscus pulverulentus*	USNM 481178	33.82	2.81	1.37	Bertrand et al. (2019)
Extant Sciuridae	*Pteromys buechneri*	USNM 172622	34.11	1.75	1.61	Bertrand et al. (2019)
Extant Sciuridae	*Rhinosciurus laticaudatus*	USNM 488511	34.10	3.88	2.22	Bertrand et al. (2019)
Extant Sciuridae	*Callosciurus* sp.	USNM 294865	38.79	3.28	1.77	Bertrand et al. (2019)
Extant Sciuridae	*Lariscus insignis*	USNM 488570	33.88	4.73	2.32	Bertrand et al. (2019)
Extant Sciuridae	*Dremomys rufigenis*	USNM 488602	36.82	3.96	2.14	Bertrand et al. (2019)
Extant Sciuridae	*Ratufa affinis*	USNM 488104	37.09	1.64	1.91	Bertrand et al. (2019)
Extant Sciuridae	*Xerus rutilus*	AMNH 179092	38.52	3.28	1.87	Bertrand et al. (2021)
Extant Sciuridae	*Marmota marmota*	AMNH 146619	33.18	2.57	0.84	Bertrand et al. (2021)
Extant Sciuridae	*Cynomys ludovicianus*	AMNH114522	34.83	2.53	0.98	Bertrand et al. (2021)
Extant Sciuridae	*Urocitellus richardsonii*	AMNH 15062	36.57	3.35	1.75	Bertrand et al. (2021)
Leporidae	*Brachylagus idahoensis*	AMNH 92869	32.01	2.80	2.97	López-Torres et al. (2020)
Leporidae	*Lepus americanus phaeonotus*	AMNH 51052	35.11	3.58	1.97	López-Torres et al. (2020)
Leporidae	*Lepus arcticus*	AMNH 97648	41.98	2.55	1.69	López-Torres et al. (2020)
Leporidae	*Lepus americanus bairdii*	AMNH 42139	31.84	2.76	2.42	López-Torres et al. (2020)
Leporidae	*Oryctolagus cuniculus*	AMNH 99352	35.21	2.33	2.21	López-Torres et al. (2020)
Leporidae	*Poelagus marjorita*	AMNH 34816	33.23	3.04	1.79	López-Torres et al. (2020)
Leporidae	*Romerolagus diazi*	?	28.08	3.18	2.37	López-Torres et al. (2020)
Ochotonidae	*Ochotona pallasi*	AMNH 120698	33.71	2.71	2.77	López-Torres et al. (2020)
Ochotonidae	*Ochotona princeps princeps*	AMNH 59712	30.97	2.68	3.29	López-Torres et al. (2020)
Ochotonidae	*Ochotona princeps schisticeps*	AMNH 40547	31.84	2.49	2.90	López-Torres et al. (2020)
Stem lagomorph	*Megalagus turgidus*	FMNH UC 1642	18.98	3.97	2.31	López-Torres et al. (2020)
Apatemyide	*Labidolemur kayi* (low end of range)	USNM 530208/530221	-	12.18	-	Silcox et al. (2011)
Apatemyide	*Labidolemur kayi* (high end of range)	USNM 530208/530221	-	14.75	-	Silcox et al. (2011)
Anagalidae	*Anagale gobiensis*	AMNH 26079	10.98	7.15	1.01	This paper

Table S4. Data for boxplots in Figures 6, 10, 12. NS*, neocortical surface (calculation of NS varies among taxa; taxa coming from Bertrand et al. [2022] include the superior sagittal sinus,